

University of Montana

ScholarWorks at University of Montana

Graduate Student Theses, Dissertations, &
Professional Papers

Graduate School

2001

Magma mingling as a trigger of explosive silicic volcanism? A test of models involving the interaction of mafic and felsic magmas in the eastern Bearpaw Mountains MT

Stephen W. Moss
The University of Montana

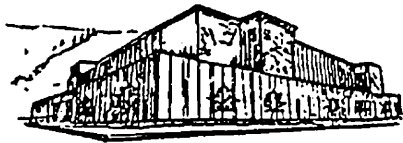
Follow this and additional works at: <https://scholarworks.umt.edu/etd>

Let us know how access to this document benefits you.

Recommended Citation

Moss, Stephen W., "Magma mingling as a trigger of explosive silicic volcanism? A test of models involving the interaction of mafic and felsic magmas in the eastern Bearpaw Mountains MT" (2001). *Graduate Student Theses, Dissertations, & Professional Papers*. 7146.
<https://scholarworks.umt.edu/etd/7146>

This Thesis is brought to you for free and open access by the Graduate School at ScholarWorks at University of Montana. It has been accepted for inclusion in Graduate Student Theses, Dissertations, & Professional Papers by an authorized administrator of ScholarWorks at University of Montana. For more information, please contact scholarworks@mso.umt.edu.



Maureen and Mike
MANSFIELD LIBRARY

The University of

Montana

Permission is granted by the author to reproduce this material in its entirety,
provided that this material is used for scholarly purposes and is properly cited in
published works and reports.

****Please check "Yes" or "No" and provide signature****

Yes, I grant permission

No, I do not grant permission

Author's Signature: Stephen W. Mos

Date: 5/22/01

Any copying for commercial purposes or financial gain may be undertaken only with
the author's explicit consent.

**Magma mingling as a trigger of explosive silicic volcanism?
A test of models involving the interaction of mafic and felsic magmas in the
eastern Bearpaw Mountains, MT.**

by

Stephen W. Moss

B.S., Wheaton College, Wheaton, IL.

presented in partial fulfillment of requirements

for the degree of

Master of Sciences

The University of Montana

May, 2001



Approved by;

Donald W. Anderson

Chairperson
[Signature]

Dean, Graduate School

5-22-01

Date

UMI Number: EP37947

All rights reserved

INFORMATION TO ALL USERS

The quality of this reproduction is dependent upon the quality of the copy submitted.

In the unlikely event that the author did not send a complete manuscript and there are missing pages, these will be noted. Also, if material had to be removed, a note will indicate the deletion.



UMI EP37947

Published by ProQuest LLC (2013). Copyright in the Dissertation held by the Author.


Microform Edition © ProQuest LLC.

All rights reserved. This work is protected against unauthorized copying under Title 17, United States Code



ProQuest LLC.
789 East Eisenhower Parkway
P.O. Box 1346
Ann Arbor, MI 48106 - 1346

Magma mingling as a trigger of explosive silicic volcanism? A test of models involving the interaction of mafic and felsic magmas in the eastern Bearpaw Mountains, MT.

Director: Don W. Hyndman 

Models proposed by Sparks et al. (1977), Murphy et al. (1999), Eichelberger (1980), and Feeley and Dungan (1997) cite extreme temperature contrast, volatile exsolution, and equilibrating densities as plausible mechanisms responsible for driving pluton-scale convection of interacting felsic and mafic magmas. These models are tested in the southeastern Bearpaw Mountains, MT., where abundant small mafic inclusions are distributed throughout well exposed quartz latite plutons. Latite co-exists with small (0.5-3cm) subspherical shonkinite inclusions showing many stages of disaggregation, cusped margin formation, and an outward decrease in grain size. Pluton-scale convection is evidenced by an even distribution of inclusions, compositional homogeneity, amphibole phenocryst alignment, heterogeneous reaction-rim thickness, and multiple reaction rims on amphiboles. Exsolved gas vesicles in inclusions of pyroclastic rocks, coeval shonkinite (~1000°C) and quartz latite (~750°C) magmas, resorbed pyroxenes, quartz, and biotite, and thin amphibole reaction rims around shonkinite inclusions all point to the injection of a hot, volatile-bearing shonkinite magma into a quartz latite magma host. At Deer Butte, phenocrysts of co-existing sanidine and plagioclase, along with anti-perthite xenocrysts all contain thin rims of sieved alkali feldspar, corresponding to a dramatic decrease in pressure from eruption. Shonkinite stringers trailing off inclusions of both tuff-breccia and plutonic samples point to a still-molten state of shonkinite magma during a rapid eruption. Biotite grains lacking reaction rims, and skeletal feldspar grains that grew rapidly around melt cores can also be seen in erupted samples.

Deer Butte and Suction Butte in the northern Rattlesnake Quadrangle are both interpreted to be quartz latite magma chambers that had partially crystallized before being intruded by an initially hot, dense shonkinite magma. As the shonkinite magma was released heat into the host quartz latite and crystallized, volatile phases exsolved, lowering the density of the shonkinite magma. The inclusions then rose buoyantly in the magma. Continued transfer of heat and volatiles rapidly initiated pluton-scale convection, effectively dis-aggregating and distributing the shonkinite magma to all parts of the pluton. The added volume and exsolved volatiles from the shonkinite magma sufficiently raised the vapor pressure within the magma chamber to drive explosive eruption of pyroclastic tuff and tuff-breccia.

Acknowledgements

Because He wants to be known, you said, embraced
In the way of creekbeds, canyons,
The caress of geologic times, the split instant of an age.
Eternity winks past like lightning bugs,
The lazy way time has of shining.
Forever is a strand of luminous moments.
And now sitting on a boulder by a river seems to take longer,
Seems a promise of divinity, of shaping, the most intimate
Knowledge that ever fell with turning leaves...

To the Artist whose work forever inspires both those who probe minutia and those who dream...please
receive this gift from your stubborn lover who refuses to punt paradox.

Don Hyndman
Ian Lange
Dick Field
The Office Queens
Fellow Grad Students
Diane Johnson and Scott Cornelius
Joel Moore
Jeff Greenberg

“The heavens are telling of the glory of God; And the firmament is declaring the work of His hands. Day
after day they pour forth speech...”
Psalm 19

Table of Contents

Abstract.....	ii
Acknowledgements	iii
List of Figures and Tables.....	v
Introduction:.....	1
Previous Studies:	1
Regional Geology of the Bearpaw Mountains and Central Montana Alkalic Province	5
Statement of the Problem	7
Models explained	10
Present Hypothesis	12
Methods	13
Field Work Findings:.....	14
Mineralogy, Petrology and Petrography of Quartz latite Plutons	15
Mineralogy, texture.....	15
Chemistry.....	15
Biotite	16
Quartz	16
Magnetite / titanomagnetite	17
Clinopyroxene	17
Feldspar phenocrysts.....	23
Amphibole Crystals at Suction Butte.....	36
Mafic Inclusions.....	44
Petrology and Petrography of Inclusions	44
Abundance and Distribution of Inclusions.....	50
Miarolitic Cavities.....	51
Convection	56
Hornblende Lineation	57
Cooling rates within plutons	60
Felsic Pyroclastic Rocks	61
Mineralogy, texture.....	61
Shonkinite Inclusions.....	62
Mineralogy of Pyroclastic Deposits.....	62
Discussion	66
Examination of models	66
Coeval, mingling magmas.....	74
Correlation between pyroclastic rocks and plutonic rocks	75
Pluton-scale Convection	75
Injection of hot, volatile-bearing mafic magma into relatively cool and dry magma.....	76
Rapid supersaturation and eruption of quartz latite magma	77
Conclusions.....	78
References.....	80

List of Figures and Tables

Figure

1. Geologic map of eastern Bearpaw Mountains.
- 2-1.1. Felsic inclusions at Deer Butte (photos).
- 2-1.2. Mineral textures at Deer Butte (photos).
3. Albite-orthoclase exsolution in plagioclase (photos).
4. Ternary plot of anti-perthite grains at Deer Butte.
5. Composite feldspar grains (photos and sketches).
6. Co-existing plagioclase and sanidine grains from Deer Butte.
 - a. Ternary diagram of system $\text{NaAlSi}_3\text{O}_8$, KAlSi_3O_8 , and $\text{CaAl}_2\text{Si}_2\text{O}_8$ (taken from Tuttle and Bowen, 1958).
 - b. Inferred crystallization history of Deer Butte pluton (drawing).
7. Eastern Bearpaw Mountains hastingsite (photos).
8. Experimental breakdown of amphibole in Mt. St. Helens dacite (taken from Rutherford and Hill, 1993).
 - a. Hastingsite dehydration and convection (drawing).
9. Shonkinite inclusions in thin section (photos).
10. Four different stages of inclusion disaggregation (photos).
11. Shonkinite inclusion textures (photos)
12. Pooled volatiles at Big Timber Butte (photos and drawing)
13. Mirolitic cavities (photos)
14. McCann Butte (photos)
15. Star Butte hornblende orientations (drawing)
16. Inclusions in pyroclastic rocks (photos)
17. Textures from pyroclastic latite

Table

1. Table of Models
2. Representative biotite analyses
3. Representative clinopyroxene analyses
4. Representative feldspar analyses
5. Representative hastingsite analyses
6. Representative reaction rim thicknesses
7. Representative analyses of shonkinite inclusions
8. Representative analyses of quartz latite

Introduction:

Various models proposed by Sparks et al. (1977), Murphy (2000), Feeley and Dungan (1996) and Eichelberger (1980) cite extreme temperature difference, volatile mobilization, and equilibrated densities as mechanisms responsible for driving pluton-scale convection of interacting felsic and mafic magmas (See Table 1). Many have also modelled the relationship of the movement and transfer of volatiles in a magma system with pressure-release eruption (Sparks, 1997, Huppert et al., 1982, L. Wilson et al. 1978). However, these models have not given volcanologists any confirmation of what driving forces prompt the mingling, mixing, and eruption of chemically distinct magmas because of insufficient correlating field evidence from the feeder plutons.

This project examines a group of well exposed quartz latite plutons and associated volcanic rocks in the southeastern Bearpaw Mountains in north-central Montana. It describes the petrology, geochemistry, and physical relationships of a dominant quartz latite magma with a volumetrically minor shonkinite magma in both intrusions and associated volcanic rocks. It also tests the existing models explaining the role of interacting mafic and felsic magmas in triggering explosive volcanic eruptions.

I suggest that evidence of coeval felsic and mafic magmas, small-scale heterogeneous thermal histories, and the abundance and distribution of inclusions and volatiles point to the introduction of a hot, volatile-bearing mafic magma into a felsic host pluton. I also suggest that this intruding mafic magma is directly responsible for the violent eruption of tuff and tuff-breccia deposits that are exposed in areas adjacent to the sub-volcanic chambers.

Previous Studies:

Pirsson and Weed first published a series of observational papers in 1896, based on a quick reconnaissance of the Bearpaw Mountains. They examined and described the igneous rock types and noted the alkalic chemistry of the rocks and the apparent co-existence of alkalic and sub-alkalic rock types. A regional examination of the Central Montana Alkalic Province was undertaken by Larsen (1940), relating the chemistry, petrology, and mineralogy of the various igneous intrusions seen throughout the region.

Table 1: Proposed Models

Model A (Sparks et al., 1977)	Model B (Eichelberger, 1980)	Model C (Feeley & Dungan, 1996)	Model D (Murphy et al., 2000)
<p>Magma mixing/mingling driven by extreme temperature difference; The introduction of a hot mafic magma into the base of a low-temp. felsic magma chamber starts both the exchange of volatiles and the rapid superheating and convection of the felsic magma. This results in the entrainment and physical mingling of some mafic magma with the felsic magma.</p> <p>*Note: There may or may not be some degree of chemical mixing along with the physical mingling.</p>	<p>Magma mingling driven by <i>density differences</i> between intruding magma and resident magma. A water-saturated mafic magma exsolving excess volatiles (because of cooling) can be lower in density than the more differentiated resident magma. The intruding magma is therefore <i>immediately buoyant</i> and ascends as either a laminar or an entraining turbulent plume, or as a collection of smaller inclusions.</p>	<p>Magma mixing that results in the development of a chemically hybrid boundary layer between the two distinct magmas. Subsequent entrainment and vigorous convection driven by temperature differences and exsolved free volatiles distributes chemically intermediate enclaves of 'mixed' magmas throughout the pluton.</p>	<p>Injection of mafic magma into the base of a partially crystallized felsic host magma as dikes and sills reheats and mobilizes felsic magma. As plumes of mafic magma in which gas has begun to exsolve ascend into the chamber, gas is released into the latite, and the host magma stirs, eventually pressurizing the magma chamber and setting the stage for violent pressure release.</p>
<p><u>Assumptions/Limitations/Constraints:</u> Magma mingling must have occurred rapidly; felsic magma became supersaturated with volatiles, perhaps leading to an eruption through fractures or fissures on the outside of the chamber due to increased pressure in the system. Turbulent flow is required.</p>	<p><u>Assumptions/Limitations/Constraints:</u> The density of the intruding mafic magma, a function of its mineralogy, temperature, and volatile content, must be < that of the quartz latite above; initial volatile content must be high enough to make density of mafic magma (almost like a foam) less than latite; heat transfer is only local.</p>	<p><u>Assumptions/Limitations/Constraints:</u> Whole-rock chemistry must show complete gradation of chemistry between theoretical end members.</p>	<p><u>Assumptions/Limitations/Constraints:</u> The intruding mafic magma must contain volatiles; host magma must have an initially rigid crystal framework which is intruded by dikes and injections of mafic magma.</p>

<p><u>Required supporting data:</u> widespread heterogeneous rocks where the magmas met, mingled, but did not completely chemically mix; mafic inclusions or entrainments in extrusive rocks of the same chemistry found distal to plutons (triggered eruption); different textures in inclusions of intrusive and extrusive rocks; chilled margins, complete crystallization of mafic inclusions before complete mixing; discontinuous or peritectic reactions, reaction halos, embayed minerals, and incompatible minerals.</p>	<p><u>Required supporting data:</u> Rounded mafic inclusions; disequilibrium textures; in addition to globular mafic inclusions, the presence of small pillowing plumes, or streaks of drawn-up mafic material; vesicular texture or other indicators of exsolving volatile content near the contact between the two magmas; inferred (based on density) high vesicularity in the mafic inclusions; textural clues (chilled margins, phenocrysts) suggesting partial crystallization of shonkinite prior to entrainment into latite; evidence of reheating close to contact between intruding shonkinite magma and overlying latite.</p>	<p><u>Required supporting data:</u> Intermediate chemistry inclusions distributed in the upper pluton of end member (shonkinite) intrusion; evidence of a hybrid layer; chemical zonation or layering within the pluton; equal to subequal ratio of mafic to felsic magmas.</p>	<p><u>Supporting data:</u> Phenocrysts in felsic host which have experienced varied crystallizing histories, heterogeneous magma composition; disequilibrium textures in phenocrysts (reaction rims, reverse/oscillatory zoning, resorption, etc.); both angular and rounded shonkinite inclusions; locally high mafic to felsic magma ratios.</p>
<p><u>Contradictory evidence:</u> If the inclusions were not end-member shonkinite, but were of an intermediate chemistry between latite and shonkinite; a lack of mafic inclusions in the extrusive equivalent of latite found adjacent to the plutons. If volatiles were not abundant enough to saturate the magma.</p>	<p><u>Contradictory evidence:</u> If the inclusions were angular, showing that they had chilled and solidified prior to being mingled into the latite magma.</p>	<p><u>Contradictory evidence:</u> If a contact between shonkinite and latite was found in a pluton containing the inclusions, without an intermediate composition horizon; if the inclusions were chemically incompatible with surrounding latite; small volume ratio of mafic to felsic magmas.</p>	<p><u>Contradictory evidence:</u> If phenocrysts experienced identical crystallization histories; thorough convection and mingling of shonkinite magma; exclusively rounded inclusions; evidence of shonkinite magma chilling in cooler latite magma (chilled margins, very fine-grain inclusions); homogeneous latite chemistry.</p>

Fisher's (1946) dissertation in the Bearpaws again was a reconnaissance of the alkalic igneous rocks of the northeastern Bearpaws area. The U.S. Geological Survey began a project in 1947, overseen by W.T. Pecora, that eventually yielded quadrangle-scale maps for the entire Bearpaw region. Comprehensive mapping by Hearn, Pecora, Schmidt and Bryant from 1957-1964 catalogued in detail most of the eastern Bearpaws. Of note is their recognition of the presence of abundant inclusions, which they repeatedly identified as pre-Cambrian xenoliths of pyroxenite, biotite gneiss, amphibolite, and local clastic sedimentary rocks from depth. Hearn (1976) compiled the geology (map scale 1:125,000) and structure of the Bearpaw Mountains (modified in Figure 1).

Radiometric age dating of the igneous centers of the Central Montana Alkalic Province are provided by Martin et al. (1980), who found the volcanoes of the Bearpaws to be of Eocene age. In many parts of the Central Montana Alkalic Province mafic and felsic rocks have a related origin. The contemporaneous, mutually intruding magmas show overlap and evidence of both mingling and mixing. Tureck-Schwartz (1992) and Tureck-Schwarz and Hyndman (1991) examined the relationship of alkalic and sub-alkalic mafic and felsic rocks in the Bearpaw Mountains and concluded that mafic alkalic magma (shonkinite) partially melted in the upper mantle, found its way into the epizonal crust, and melted surrounding country rocks to form a sub-alkalic quartz latite magma. Overlap, mingling and chemical mixing of shonkinite and quartz latite in shallow magma chambers explains many of the igneous textures seen in the Bearpaws today.

The role of volatiles associated with intruding mafic magmas in explosive volcanic activity was first explored by Sparks et al. (1977). Sparks et al. (1977) proposed that volatiles and heat introduced into felsic magma by entrained mafic inclusions was directly responsible for causing the magma chamber to convect. This convection could in turn pressurize the magma chamber, leading to eruption. Eichelberger (1980) provided a modification of Sparks et al.'s theory (1977) which instead focused on the density and viscosity contrast that would develop as felsic and mafic magmas mingled. A key difference in their models was in the timing of crystallization and volatile exsolution in the mafic magma. Eichelberger's model, however, only encompassed localized re-heating of a magma chamber due to the mafic magma intrusion, and not a pluton-scale phenomenon.

Interactions between mafic and felsic magmas has been dealt with extensively in the literature. Sparks and Marshall (1986) collected data which provided good constraints on the mechanical mixing of mafic and felsic magmas. Research by Bacon (1986) highlighted the limitations on the extent of chemical mixing between inclusions and a host magma. Feeley and Dungan (1996), and Clyne (1999) looked at the role of magmatic inclusions in producing a heterogeneous magma. Van der Laan and Wyllie (1992) did experimental work on interacting magmas to determine to what extent equilibration develops in magmas of different viscosity and temperature. Bacon & Metz (1984) saw mafic inclusions as a key to understanding the eruptive history of magma chambers, as mafic inclusions in plutonic rocks may record mingling of magmas with contrasting composition and physical properties.

Most recently, Murphy et al. (1999, 2000) examined the Soufriere Hills volcano at Montserrat in the West Indies for evidence of the intrusion of a mafic magma into a felsic reservoir. By examining the geothermometry, geochemistry, and textures in different phenocryst phases, Murphy et al. (1999, 2000) showed evidence for a reheating event of the magma chamber at Montserrat immediately before eruption. Devine et al. (1998b) showed evidence of rapid ascent rates of magma from depth at Montserrat by looking at the thickness of amphibole dehydration reaction rims. Barclay et al. (1998) and Devine et al. (1998a) studied phenocrysts and inclusions erupted from the volcano, concluding that the pre-eruptive andesite magma had crystallized extensively prior to being intruded by a mafic magma.

Regional Geology of the Bearpaw Mountains and Central Montana Alkalic Province

The Central Montana Alkalic Province is essentially a broad sea of Mesozoic sediments encompassing island-like late Cretaceous to Eocene alkalic igneous and volcanic centers. It is situated east of the Montana overthrust belt, generally between 107° and 112°30' west longitude, and 46° to 49° north latitude. Directly underneath a blanket of Tertiary gravels and glacial float in the central Montana corridor are local exposures of gently dipping and deformed sedimentary rocks, of Cretaceous through Paleozoic age. About 1300m of mostly terrigenous Cretaceous shales and sandstones overlie about 1000m of Mesozoic and Paleozoic shallow water carbonates. Most of these shallow marine and clastic sedimentary rocks lie on top of Precambrian crystalline basement rocks of the Wyoming craton.

Alkalic magmatic activity spanned from about 69-27 Ma with two main periods of activity from 69-60 Ma and 54-50 Ma (Marvin et. al., 1980). During the earlier period, felsic sub-silicic to silicic, alkalic to sub-alkalic magmas were emplaced in the eastern parts of the province; in the Little Rocky, Judith, and Moccasin ranges. Though not exposed on the surface, minor mafic dikes and shonkinite inclusions indicate mafic alkalic rocks exist beneath all three ranges (Hearn 1989; Tureck-Schwartz and Zieg, 1989).

During the later period of magmatism in early Eocene time, rocks of the Sweetgrass Hills, and the Bearpaw, Highwood, Little Belt, Castle and Crazy mountains were emplaced and extruded. Activity in several minor centers also occurred during this period. Both mafic and felsic rocks exist in all these ranges, and felsic sub-alkalic rocks are present in most centers. Magmatism in one large volcanic center, the Adel Mountains, and two smaller intrusive centers, the Moccasin and Judith Mountains, overlap the two main periods of magmatic activity outlined above; they were emplaced between 69-53 Ma (Marvin et. al., 1980; Hearn, 1989).

There is no apparent geographic migration of igneous activity in the ranges of the Central Montana alkalic province to suggest progressive rifting or movement relative to a hot spot or hot spots. Their occurrence is believed to have been the indirect result of low-angle subduction of oceanic crust underneath the old cratonic margin to the west.

The Eocene Bearpaw Mountains of north-central Montana form an east-west arch south of Havre, MT. Intrusive alkalic igneous bodies comprise most of the arch core, and are commonly preserved as well-exposed domes that are resistant to erosion. Quartz latite, shonkinite, monzonite, nepheline syenite, syenite and phonolite are among the most abundant intrusive igneous rocks. Flanking this core on both the north and south are large volcanic fields of interbedded felsic and mafic volcanic flows and pyroclastic deposits (Figure 1). Their present position reflects modification by gravity slump faulting that resulted from volcanic loading which caused the failure of surrounding Mesozoic sediments. Notably, the absence of extrusive rocks on the eastern flank of the Bearpaws was caused by the most recent continental glaciation which removed a significant thickness of strata from the area.

A model of magma mixing best explains the relationships and association of alkalic and sub-alkalic rocks in the Bearpaw Mountains and accounts for the chemical and mineralogical gradation between the suites as discovered by Tureck-Schwarz (1992). Magma mixing implies that the two end-members,

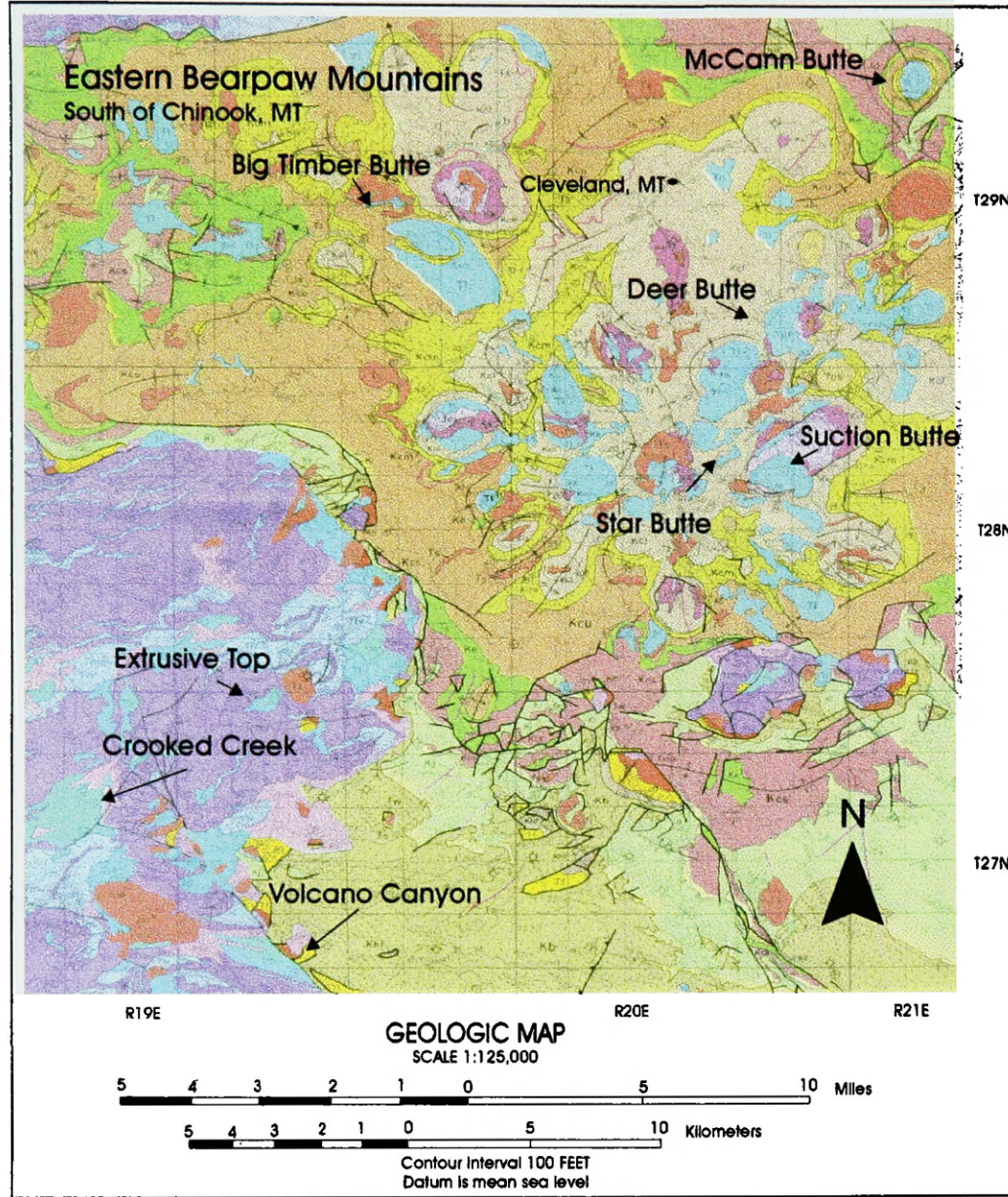
shonkinite and quartz latite, existed in the liquid phase in the same place and at the same time. This contrasts with assimilation which requires that one end member is shonkinite magma and the other solid crustal rock, and fractional crystallization in which various magmas and/or cumulates are derived from a single magma.

“Shonkinite is the parent mafic magma in the Bearpaw igneous complex; upper mantle peridotite inclusions in shonkinitic rocks supports a mantle source. Heat from the shonkinite magma melted the granitoid crustal rocks to form separate felsic magma: quartz latite. Quartz latite and shonkinite magmas mixed and mingled in variable proportions prior to eruption and shallow emplacement, and produced rocks showing a complete compositional range from shonkinite to quartz latite. Variation in major and minor elements show straight-line trends between the shonkinite and quartz latite fields, supporting bulk mixing of variable proportions of shonkinite and quartz latite. The alternate hypothesis, that quartz latite formed through differentiation of shonkinite, is not supported by the variation diagrams: graphical removal of any reasonable proportions of the mafic minerals from shonkinite produces trends away and not towards the quartz latite field (with the exception of CaO)” (Tureck-Schwarz, 1992).

Statement of the Problem

In order to model volcanic processes, we need to understand the dynamics of eruption and the mechanical properties of magma. In the last 25 years, several authors have proposed the role of a late stage intrusion of volatile-rich magma in generating explosive silicic volcanism. Sparks et al. (1977), Eichelberger (1980), and others have laid down some foundational models which have formed the basis for many others. The need for improved analogues that accurately mimic existing models of magma systems has recently been addressed by Van der Laan (1993), Oldenburg (1989), Murphy et al. (2000), and Sparks et al. (1998), but there remains a shortage of *field sites* that provide tests for any of these ideas.

A series of shallowly emplaced, porphyritic quartz-quartz latite plutons in the eastern-southeastern Bearpaw Mountains contains evenly distributed, very fine-grained, rounded to sub-angular mafic inclusions from 1-3cm in diameter, as noted by Tureck-Schwartz (1992), Schmidt (1961, 1964) and Hearn et al. (1964, 1976). These can be observed throughout the entire exposed intrusive body, a fairly unusual phenomenon suggestive of vigorous pluton-scale mingling of two chemically distinct magmas.



- Tlv** **FELSIC VOLCANIC FLOWS** - Flows and flow breccias of porphyritic latite and quartz latite; light gray, gray, brown; green calcianite alteration is common; phenocrysts of potassium feldspar, plagioclase, augite, hornblende and biotite; quartz in groundmass only; interlayered with mafic and felsic pyroclastic rocks; extrusive equivalent of porphyritic latite; maximum thickness about 6000 feet.
 - Tlp** **FELSIC PYROCLASTIC ROCKS** - Agglomerate, tuff-breccia, lapilli tuff, tuff, waterlaid volcanic sediments, and coarse mudflow deposits; contains more than 50 percent fragments of felsic volcanic rocks; inclusions of biotite pyroxenite and Precambrian basement rocks are locally abundant; commonly forms lowermost volcanic unit; particularly in northwestern part; in part deposited in local early collapse basins; fossil plants and fish indicate middle Eocene age; maximum thickness about 3000 feet.
 - Tmt** **MAFIC VOLCANIC FLOWS** - Flows and flow breccias of phonolite and mafic phonolite; brown, red and purple; phenocrysts of olivine, augite, biotite, anoclime, and rare leucite in groundmass of augite, potassium feldspar and anoclime; nepheline, anoclime and calcite are common alteration products; interlayered with felsic flow and felsic and mafic pyroclastic rocks; as mapped includes some mafic pyroclastic rocks; extrusive equivalent of shonkinitic, syenite, and possibly of monzonite; maximum thickness about 6000 feet.
 - Tmp** **MAFIC PYROCLASTIC ROCKS** - Agglomerate, tuff-breccia, lapilli tuff, tuff, waterlaid volcanic sediments and mudflow deposits; contains more than 50 percent fragments of mafic volcanic rocks; inclusions of biotite pyroxenite and Precambrian basement rocks are locally abundant; commonly forms lowermost volcanic unit, particularly in the southeastern part; in part deposited in local early collapse basins; fossil plants and fish indicate middle Eocene age; maximum thickness about 3000 feet.
 - Tps** **PORPHYRYTIC POTASSIC SYENITE** - Dikes, sills, plugs and stocks; light gray to green; fine- to coarse grained, as mapped includes a wide variety of subalkalic-alkalic rocks (pseudoleucite-sodalite tingedite, nepheline tingedite, aegirine-nepheline syenite, etc. restricted to the central and western Bearpaw Mountains) and alkalic rocks (porphyritic syenite, the only variety of this rock type in the eastern Bearpaw Mountains); fine-grained varieties typically have phenocrysts of tabular zoned potassium feldspar, aegirine with or without pseudoleucite, nepheline, and sodalite, in a fine grained green or gray groundmass; rock type associated with most sulfide deposits; plug in Rocky Bay stock contains carbonatic vein-dikes; cut by mafic anoclime phonolite in western Bearpaw Mountains; in eastern Bearpaw Mountains, generally the youngest rock type, with exception of one dike of porphyritic latite.
 - TI** **PORPHYRYTIC LATITE** - Dikes, sills, plugs and stocks; light gray to brown; fine- grained felsic porphyritic rocks; most contain less than 20 percent mafic minerals; phenocrysts of augite ubiquitous; phenocrysts of potassium feldspar, plagioclase, biotite, and hornblende in varying amount characterize separate varieties; groundmass of feldspar, augite and quartz; may represent several episodes of intrusion, post-dates most but not all shonkinitic-syenite intrusions.
 - Ts** **SHONKINITE AND SYENITE** - Dikes, sills, laccoliths, plugs and stocks; gray to black; fine to coarse grained, porphyritic and equi-granular; mafic mineral content of shonkinitic more than 40%, mafic syenite 20-40%, and syenite less than 20 percent; includes subalkalic-alkalic and alkalic varieties; contains augite, biotite and dominantly potassic feldspar, with or without olivine, plagioclase, nepheline, pseudoleucite, apatite, and anoclime or interstitial quartz; many varieties weather to biotite rich soil with no outcrop; represent several episodes of intrusion, and is the earliest intrusive rock in the eastern Bearpaw Mountains.
 - Tw TT** **WASATCHFORT UNION FORMATIONS** - Assorted non-marine shales, sandstones and siltstones of lower Eocene through Paleocene age.
 - KK** **CRETACEOUS SEDIMENTS** - Marine and non-marine variable sediments. Occur as trace lenses in center of volcanic cluster, as well as extensive sedimentary units throughout the region. County rocks into which most of the Tertiary igneous rocks intruded. Includes Kh, Kb, K, Kc, Ke, Kc, Kc, Kc, Kam, Kal, and Kk.
 - Je** **ELLIS GROUP (Upper and Middle Jurassic)** - Total thickness 280-550 feet. Includes Swift, Rierdon, and Piper formations.
- Approximate southeastern limit of glacial deposits
- Contour, queried where intersected or approximately labeled
- Fault, normal, queried where intersected or approximately
- Fault, reverse or thrust, queried where intersected or approximately
- Anticline axis showing plunge
- Synclinal axis showing plunge
- 30 Strike and dip of beds
- 90 Strike and dip of vertical beds
- 60 Strike and dip of low layering
- 0 Horizontal beds and flows

Fig. 1: Eastern half of Bearpaw Mountains volcanic arch. The cluster of latite buttes seen in the east-central part of the map were the focus of this study. The plutons and pyroclastic deposits referenced in this study are noted on the map. Slightly modified from Hearn (1976).

Comprehensive mapping by Hearn et al (1976), and Schmidt and Pecora et al (1961, 1964) yielded a catalog similar to that compiled by Tureck-Schwartz (1992) of the acidic and basic rocks in the southeast Bearpaw Mountains, briefly noting the presence of small mafic inclusions. Importantly, they also point out the presence of these same inclusions in extrusive rocks that appear to be chemically equivalent to the quartz latite porphyritic plutons.

At the time of mapping, Hearn et al. (1976, 1941) and Schmidt et al. (1964, 1961) believed the inclusions to be chunks of pC biotite pyroxenite, gabbro, hornblendite, gamet gneiss, and mica schist. However, chemical analysis and textural analyses by Tureck-Schwartz (1992) and that presented in the present paper have since revealed otherwise for most mafic inclusions in quartz latite plutons and their extrusive equivalents. The distribution, size, and chemistry of the inclusions point to the possibility that the plutons are snapshots of magma chambers undergoing pluton-scale convection.

All of the models explaining the injection of mafic magma into felsic magma as a possible trigger for explosive eruption have been constructed based upon evidence seen in volcanic rocks. The difficulty of observing the chambers of active volcanoes, such as the Soufriere Hills site, is an obvious barrier in our ability to further test any of the models. However, by providing frozen views of developing magma chambers and their pyroclastic equivalents, this field area in the Bearpaw Mountains provides a window into the evolution of an eruptive magma needed to better determine the dynamics of movement and material transfer within plutons that leads to eruption. It should provide a key link between the modeling and reality. I test the plutons and pyroclastic deposits in the Bearpaw Mountains to determine which of the following models was responsible for initiating explosive silicic volcanism:

- a) Magma mingling resulting from volatile exchange and temperature contrast (Sparks et al., 1977)
- b) Equilibrating densities of two associated magmas (Eichelberger, 1980)
- c) Entrainment of a hybrid mixture of the two magmas (modified from Feeley & Dungan, 1996)
- d) Remobilization of partially crystallized host magma by intruding mafic magma (Murphy et al, 2000)

See Table 1 for a summary of supporting data, constraints, and contradictory evidence.

In addition, I examined the relationships between pyroclastic and intrusive quartz latite in the the present field area to see:

- a) The extent of crystallization of the quartz latite host prior to eruption.
- b) The role of volatiles in the violent release of magma.
- c) The role of shonkinite magma in causing an eruption.

This project contributes to our knowledge of intrusive and eruptive processes by advancing our understanding of magma interaction, plutonic convection, and possibly the triggering of eruptions. I provide data to test models by Sparks et al. (1977), Eichelberger (1980), Murphy et al. (2000), and Feely and Dungan (1996), and test work on the physical behavior of interacting felsic and mafic magmas (Sparks and Marshall, 1986). This project tests these models by evaluating the processes proposed for pluton-scale convection and subsequent eruption. I determine the parameters that control development of a magma system in which a hotter and denser mafic magma intruded into the base of a felsic magma chamber.

Models explained

Various models have been proposed regarding the role of a secondary intrusion of a hot mafic magma into the base of a cooling felsic magma in triggering explosive silicic volcanism. Each of these models represent scenarios involving manipulation of the following variables:

- Volume ratio of mafic magma to felsic magma
- Extent of cooling of silicic host prior to intrusion
- Initial volatile content of felsic magma
- Initial volatile content of mafic magma
- Initial and final density of mafic magma
- Extent of crystallization and degassing of both felsic and mafic magmas prior to eruption
- Time interval between intrusion of mafic or felsic magma and eruption

Sparks et al.'s (1977) model recognizes the exchange of heat and volatiles from the mafic magma into the felsic magma as the primary driving force in initiating pluton-scale convection and subsequent eruption. Key evidence favoring this model would include the following:

- a) Chilled margins, complete crystallization, or other quench textures of mafic inclusions before complete mixing.
- b) Disequilibrium textures: embayed crystals, incompatible minerals, reaction halos.
- c) Inclusions with evident volatile saturation in extrusive rocks.
- d) Evenly distributed inclusions of mafic rocks in the felsic plutons.
- e) Relatively small volume of mafic magma relative to felsic magma

A similar model proposed by Eichelberger (1980) recognizes that a saturated mafic magma containing excess volatiles can attain lower density than the more differentiated resident magma, and is therefore immediately buoyant and capable of rising as a vesiculated magma in the form of blebs and droplets throughout the magma chamber. Key evidence for this model would include the following:

- a) Rounded mafic inclusions with abundant vesicles in both plutonic and pyroclastic rocks.
- b) Textures (chilled margins, resorption) suggesting extensive crystallization of mafic magma prior to being entrained into relatively cooler felsic magma.
- c) Relatively small volume of mafic magma relative to felsic magma

Feeley and Dungan (1996) propose another model based on a field site in Tatara-San Pedro, Chile, in which magma mixing results in the development of a hybrid boundary layer between an overlying felsic magma and an underlying mafic magma. This hybrid layer is then entrained into the pluton as inclusions or blebs. Temperature difference and exsolved free volatiles mobilize the resident felsic magma into convection. Some evidence that would support a scenario like this includes:

- a) Inclusions with an intermediate chemistry between two end member magmas distributed in shallower areas than the location of shonkinite intrusion.
- b) A hybrid contact layer between the two magmas.

- c) Chemical zonation or layering within the pluton.

Murphy et al. (2000) suggest that the recent explosions seen at Soufriere Hills Volcano in Montserrat were the result of mafic magma being injected into the base of a partially crystallized felsic host as dikes and sills, reheating and mobilizing the resident magma to convection and subsequent eruption. In this model, volatiles and heat are transferred from the mafic magma to the felsic magma in a process similar to Sparks et al. (1977). Evidence that would support this model includes:

- a) Phenocrysts in felsic host which have experienced varied crystallizing histories.
- b) Heterogeneous magma composition.
- c) Dis-equilibrium textures in phenocrysts (reaction rims, reverse/oscillatory zoning, resorption, etc.).
- d) Pooled volatiles at the top of magma chamber.
- e) Both angular and rounded inclusions from forcibly injected mafic magma.

Present Hypothesis

Sparks et al.'s model (1977) proposes that the decrease in density of a hot mafic magma that has intruded or forcibly injected into the base of felsic magma is not the result of crystallization and thermal effects alone, but is also largely due to the presence of exsolved free volatiles. As the intruding, denser mafic magma loses heat and begins to partially crystallize, it becomes saturated with respect to its fluid phases, causing exsolution of gas bubbles within the mafic magma, and the equilibration of densities between the two magmas. This then allows the mafic magma to rise into the felsic magma of the pluton in small plumes, from which small inclusions are entrained, and gas and heat is transferred to the felsic magma. These inclusions are then brought into a vigorous convection stream initiated by the exchange of the heat and less dense volatiles from mafic to felsic magmas. The introduction of volatiles released from the mafic magma plumes into the felsic magma quickly supersaturates the chamber in volatiles, setting the stage for pressure-release and subsequent eruption. I believe this model presents the most likely scenario for distributing the blebs and droplets of mafic magma throughout the quartz latite plutons, and directly lead to violent eruption.

Methods

The focus of this research was to evaluate what parameters or conditions (eg: temperature; density; chemistry; volatile abundance, distribution and content; viscosity) were responsible for initiating and driving dispersal of the mafic magma, convection, and subsequent eruption from the magma chamber. How are the mafic inclusions distributed? What created this condition within the plutons? Was there convection in the magma chamber, and was it directly or indirectly responsible for triggering an eruption? The answer to these questions was then compared with one or more of the mechanisms suggested by Sparks et al.(1977), Eichelberger (1980), Feeley & Dungan (1996) and Murphy et al. (2000).

- a) Field measurements were conducted of the % abundance by volume, size, shape, and distribution of mafic inclusions, by point counting to test the plausibility and scale of convection, dynamics of their entrainment, and density of the mafic inclusions.
- b) Whole-rock chemistry was analyzed to assess chemical relationship between two magmas, and/or their extrusive equivalents to determine the extents of mingling and chemical mixing both within the magma chamber and in the extrusive rocks.
- c) Mineralogy of the mafic and felsic rocks was analyzed using the Electron Microprobe at Washington State University in Pullman, WA. The data was used to infer extent of chemical mixing (if any), conditions of crystallization (temperature and pressure), and to compare mineral compositions of quartz latite plutons with volcanic rocks.
- d) The % abundance and distribution of volatiles/vesicles/miarolitic cavities was measured by point counting in thin section and hand sample. This helped to evaluate the extent of laminar/turbulent convective flow within plutons that may be driven by the difference in temperature between the two magmas, the abundance of volatiles within the mafic magma, and the contrast in viscosity between the two magmas.
- e) Looked for clues in the textural relationship between the mafic inclusions and quartz latite in hand sample and thin sections which point to the timing and sequence of crystallization and other events leading to convection, possible eruption, the magnitude of temperature difference between two magmas, and the role of volatiles in the system. Clues included disequilibrium textures,

phenocryst phases, peritectic reactions, reaction minerals, reaction halos, embayed or resorbed mineral grains, chilled margins, angularity of inclusions, mafic and felsic members observed in cross cutting relationships, small pillowing plumes, brecciation, and veining.

- f) Looked for evidence of a triggered eruptive event, in the form of whole-rock chemistry, electron microprobe chemistry, textural and/or structural equivalency in extrusive pyroclastic rocks as seen in thin sections and hand samples.
- g) Calculated plausible rates of cooling for the pluton using the procedures of Jaeger (1959) regarding the size and shape of the pluton, and by thin section inspection to see what phases had crystallized as phenocrysts, resorption minerals, rims, or chilled margins of the inclusions.

Field Work Findings:

A total of 15 plutonic buttes were examined in the eastern Bearpaw Mountains for evidence outlined above to test the proposed models. Although all of the buttes contained at least a small volume of mafic inclusions (between 0.05 and 4 %), poor exposure and severe weathering limited this study to 5 buttes and nearby volcanic tuffs and tuff-breccias. The quartz latite buttes of the southeast Bearpaw Mountains were previously categorized by Hearn et al. (1964), and Schmidt (1964, 1961) according to their dominant phenocryst mineral species. They identified six different groups of Tertiary quartz latite: hornblende and biotite (Tlhb), feldspar and biotite (T!fb), hornblende (Tlh), biotite (Tlb), hornblende and feldspar (Tlhf), and biotite, hornblende and feldspar (Tlbhf).

Suction Butte (Tlhb, SW 12 T28N, R20E, Figure 1) and Deer Butte (T!fb, Sections 34, 35, T28N, R20E, Figure 1), because of their excellent exposure, are used here to assess the distribution of mafic inclusions. Deer Butte samples were used for whole-rock analyses. McCann and Big Timber Buttes were both used for counting miarolitic cavities and for determining their distribution. Hornblende alignment data were obtained from Star Butte. Thin sections were made from a total of 7 buttes and 3 pyroclastic quartz latite outcrops. Textural evidence was collected from several of the other buttes as well. The extrusive pyroclastic quartz latite equivalents were studied in the northern Rattlesnake Quadrangle, at T26, 27N, R19E in the Maddux Quadrangle, an area west and southwest from the cluster of plutonic buttes.

Mineralogy, Petrology and Petrography of Quartz latite Plutons

Mineralogy, texture

A cluster of erosion-resistant hypabyssal quartz latite buttes occur in the southeast Bearpaw Mountains in T28,29N and R19-21E. Although well exposed, the weathering and alteration of many of the buttes into large talus slopes limited the coverage in this study. Five buttes of slightly variable composition were incorporated into this study.

The intrusive quartz latite plutons of the northern Rattlesnake Quadrangle (Hearn, 1962) are typically a light gray color, massive, fine-grained, and porphyritic. Most of the intrusions are ellipsoidal plutons, and some laccolithic bodies. The plutons contain euhedral to anhedral phenocrysts of plagioclase and potassium feldspar, and smaller proportions of resorbed salite, biotite, and/or hastingsite amphibole. The very fine-grained groundmass is composed of plagioclase, potassium feldspar, quartz, and lesser analcime, apatite, magnetite, iddingsite, and altered mafic minerals. Total mafic mineral content ranges between 10-15% by volume.

Nearly all bodies of quartz latite contain abundant small (1-3% by volume), rounded to sub-rounded, fine-grained, evenly distributed mafic inclusions. Crustal xenoliths are also ubiquitous, but much less abundant (<0.5% by volume), including gneiss, limestone, granite, pyroxenite and amphibolite. At Deer Butte (Tlfb), feldspar-rich felsic inclusions were found near the margin of the pluton. The edges of the felsic inclusions are rounded, and are surrounded by a thin halo that is rich in pyroxene and biotite (Figure 2-1).

Chemistry

Polished thin sections from Deer Butte (Tlfb) and Suction Butte (Tlhb) were analyzed using the Electron Beam Microprobe at Washington State University. Feldspar, hornblende, augite, and biotite were analyzed for 9 major elements. Deer Butte contains phlogopite, plagioclase (An₂₅-An₂₇), sanidine, orthoclase, salite (locally), titano-magnetite, magnetite, quartz, and accessory analcime, iddingsite, sphene and apatite. Suction Butte contains hastingsite, phlogopite, salite, orthoclase, titano-magnetite, and accessory sphene, analcime, iddingsite, and apatite.

The chemistry, texture, and habit of biotite, quartz, magnetite, clinopyroxene, and feldspars are described in the following sections. Interpretations of texture and occurrence are made for each mineral phase regarding the pressure, temperature, and compositional conditions in which they formed.

Biotite

Biotite forms subhedral to anhedral books and laths in Deer Butte and Suction Butte. Biotite grains in Deer Butte samples were Mg-rich (19-23% Mg) (Table 2). Titanomagnetite is commonly part of an alteration assemblage on biotite rims, and forms euhedral grains in the resorbed interior of many biotite grains. Biotite makes up an estimated 20% of Deer Butte, and 15% of Suction Butte. Biotite grains are resorbed, and commonly included within feldspar phenocrysts in both Deer Butte and Suction Butte (Figure 2-1.2b, f).

The resorption of biotite is either from pressure-relief melting or reheating of the quartz latite melt. Since a minimum amount of water is needed in a melt to crystallize stable biotite, the breakdown of biotite into titanomagnetite is likely due to a transition in the quartz latite melt from water-saturated to water-undersaturated conditions.

Quartz

Interstitial quartz grains form up to 10% of the quartz latite at Deer Butte, Suction Butte, McCann Butte, and Big Timber butte. Quartz grains occur as phenocrysts and at the edges of feldspar phenocrysts, but also interstitially in the groundmass as blebs, streaks, and stringers. Many quartz phenocrysts are strongly embayed and resorbed (Figure 2-1.2a). Clusters of small melt inclusions occur in many quartz grains.

Resorption of quartz at Deer Butte is either the result of pressure-relief melting or a temperature increase. The presence of melt inclusions in the interior of quartz phenocrysts suggests the possibility that the quartz crystallized at depth, only to be resorbed as the quartz latite magma ascended. However, if the quartz crystallized at shallow depths in the emplaced pluton, resorption from pressure-relief melting would only be plausible if the chamber were subject to eruption. The cause of rounded edges and embayments on quartz grains is indeterminable, as temperature and pressure constraints on the quartz latite melt are not good.

Magnetite / titanomagnetite

Minor titanomagnetite and magnetite can be seen at Deer Butte and Suction Butte. At Suction Butte, titanomagnetite occurs as small euhedral grains in the groundmass, surrounding amphibole phenocrysts as fine-grained reaction-rims, and magnetite alters the interior of the amphibole phenocrysts (up to 10%). There are commonly multiple zones of titanomagnetite reaction rims in the amphibole grains at Suction Butte (Figure 7). At Deer Butte, magnetite occurs as a minor part of the fine-grained groundmass, and locally alters biotite (up to 5%). The composition of titanomagnetite and magnetite grains is listed in Appendix VI.

Titanomagnetite reaction rims form after amphibole if surrounding melt becomes water-undersaturated (Rutherford and Hill, 1993). Multiple titanomagnetite reaction rims on amphibole grains at Suction Butte suggest the amphibole grains experienced changes in water pressure of the surrounding melt over time. These changes might result from the exsolution of gas as magma ascends to lower pressures, the introduction of a new high temperature or low H₂O magma into the magma chamber, or the fluxing of a magma with a CO₂-rich fluid.

Clinopyroxene

The lack of groundmass pyroxene, the compositional similarity of pyroxenes to those in shonkinite, and the occurrence of both un-resorbed and resorbed pyroxene grains in the quartz latite plutons suggest they are xenocrysts coming from the shonkinite magma. This is based on the following observations of clinopyroxene salite grains:

Most of the salite grains in Deer Butte quartz latite are strongly resorbed, and are locally mantled or pseudomorphed by biotite. Reverse, normal, and oscillatory zoning are all present in salite from Deer Butte (see representative analyses, Table 3). Fe/Mg ratios range from 0.20-1.08. Ten 2V-angle measurements were taken from clinopyroxene crystals in both the quartz latite and the shonkinite inclusions. A mean 2V angle of +54° was consistently measured for crystals adjacent to and within mafic inclusions, values similar to those expected for salite, an intermediate clinopyroxene between diopside and hedenbergite (ferrosalite). Salite crystals locally comprise up to an estimated 10% of Deer Butte, but are

rare in Suction Butte, having mostly been pseudomorphed by calcite, sericite, and Fe-oxide (<1%).

Resorbed salite is also incorporated poikilitically into many sanidine and plagioclase phenocrysts.

Salite grains are either xenocrysts separating from the shonkinite melt before it chilled against the cooler quartz latite, or represent the earliest crystallizing phase which has resorbed due to pressure-release or a temperature increase.

Clinopyroxene grains could have crystallized at depth as early cumulates. However, there is no clinopyroxene in the groundmass of the quartz latite, suggesting that the salite phenocrysts are not in equilibrium with the groundmass melt. Also, there is strong similarity in composition between clinopyroxene grains dispersed in the latite with those in the shonkinite. Salite grains found in both rock types are notably higher in Ca and lower in Al than would be expected for pyroxenes growing in granitic magma, suggests that the salite grains are xenocrysts that separated from the shonkinite magma during forcible injection into the quartz latite.

Assuming the salite grains are xenocrysts from shonkinite, intrusion of the shonkinite must have pre-dated or occurred simultaneously with the growth of sanidine and plagioclase phenocrysts. If resorption resulted from pressure relief as magma rose from depth, then all pyroxene grains would show resorption. Resorbed salite grains are more abundant in deeper levels of the Deer Butte pluton, but both resorbed and unresorbed clinopyroxene grains are ubiquitous in all parts of the pluton, commonly in the same thin section (Figure 2-1.2d-e). As the quartz latite is the lower temperature melt of the two, movement of individual grains from shonkinite into quartz latite would not resorb the phenocrysts at all, making it unlikely that the resorption of some salite crystals is due to intermingling. Therefore, the resorption is likely caused by either a localized (cm scale) increase in temperature from an independent source, convective cycling of some salite grains to hotter, deeper parts of the pluton, or by a significant contrast in composition between the salite grains and the quartz latite melt, leading to incorporation of Ca and Mg back into the melt. Thorough convective recycling could have prevented differential density settling, and instead distributed both resorbed and unresorbed clinopyroxene grains to all parts of the pluton. Resorption of the salite grains led to localized (probably cm scale) enrichment of Ca in the melt. This might explain the subtle variability in Ca and Mg contents in the whole-rock chemistry of the quartz latite (Table 8, Appendix 1).

Table 2: Representative Biotite Analyses from Deer Butte

Type# of anal.	Rev(2)	Rev(1)	Rev(2)	Rev(1)	Rev(1)	Rev(1)	Nor(1)	Nor(1)	Nor(1)	gm1	gm2	gm3	gm4	
Sample #/locat	DB-1aC	DB-1aI	DB-1aR	DB-9C	DB-9I	DB-9R	DB-1bC	DB-1bI	DB-1bR	DB-1c	DB-1d	DB-9a	DB-9b	
SiO ₂	39.23	39.71	40.60	37.85	39.63	39.32	40.37	39.99	39.61	SiO ₂	39.08	39.27	39.88	39.16
TiO ₂	0.79	0.66	0.61	1.06	1.45	0.80	0.66	0.57	0.63	TiO ₂	1.00	0.81	0.64	0.89
Al ₂ O ₃	11.79	12.32	12.30	13.10	12.26	13.04	12.49	12.75	12.64	Al ₂ O ₃	13.57	12.81	13.12	13.95
FeO*	7.41	7.06	5.17	8.49	8.51	6.08	5.80	5.13	8.38	FeO*	9.28	8.68	5.11	5.34
MnO	0.00	0.05	0.02	0.04	0.06	0.00	0.01	0.05	0.02	MnO	0.09	0.05	0.03	0.03
MgO	21.36	21.96	23.71	19.89	20.72	22.44	22.78	22.14	21.34	MgO	20.23	21.42	23.30	22.85
CaO	0.00	0.00	0.01	0.01	0.55	0.01	0.01	0.00	0.00	CaO	0.00	0.00	0.00	0.00
Na ₂ O	0.53	0.60	0.67	0.64	0.68	0.72	0.70	0.71	0.66	Na ₂ O	0.62	0.70	0.58	0.68
K ₂ O	9.43	9.59	9.64	9.38	8.72	9.64	9.51	9.56	9.53	K ₂ O	9.41	9.42	9.76	9.52
Total	90.53	91.96	92.74	90.46	92.57	92.06	92.33	91.89	92.81	F	3.64	4.07	3.65	3.95
Fe/Mg	0.35	0.32	0.22	0.43	0.41	0.27	0.25	0.27	0.39	Cl	0.06	0.08	0.01	0.01
										Total	96.98	97.31	96.09	96.38
										Fe/Mg	0.46	0.40	0.22	0.23

DB-1, 9 represent different hand samples; a,b, c, d represent different grains from same hand sample

C = core, I = intermediate, R = rim gm = Groundmass, Rev = Reverse, Nor = Normal

*Total iron expressed as FeO

Analyses of groundmass using F, Cl standards

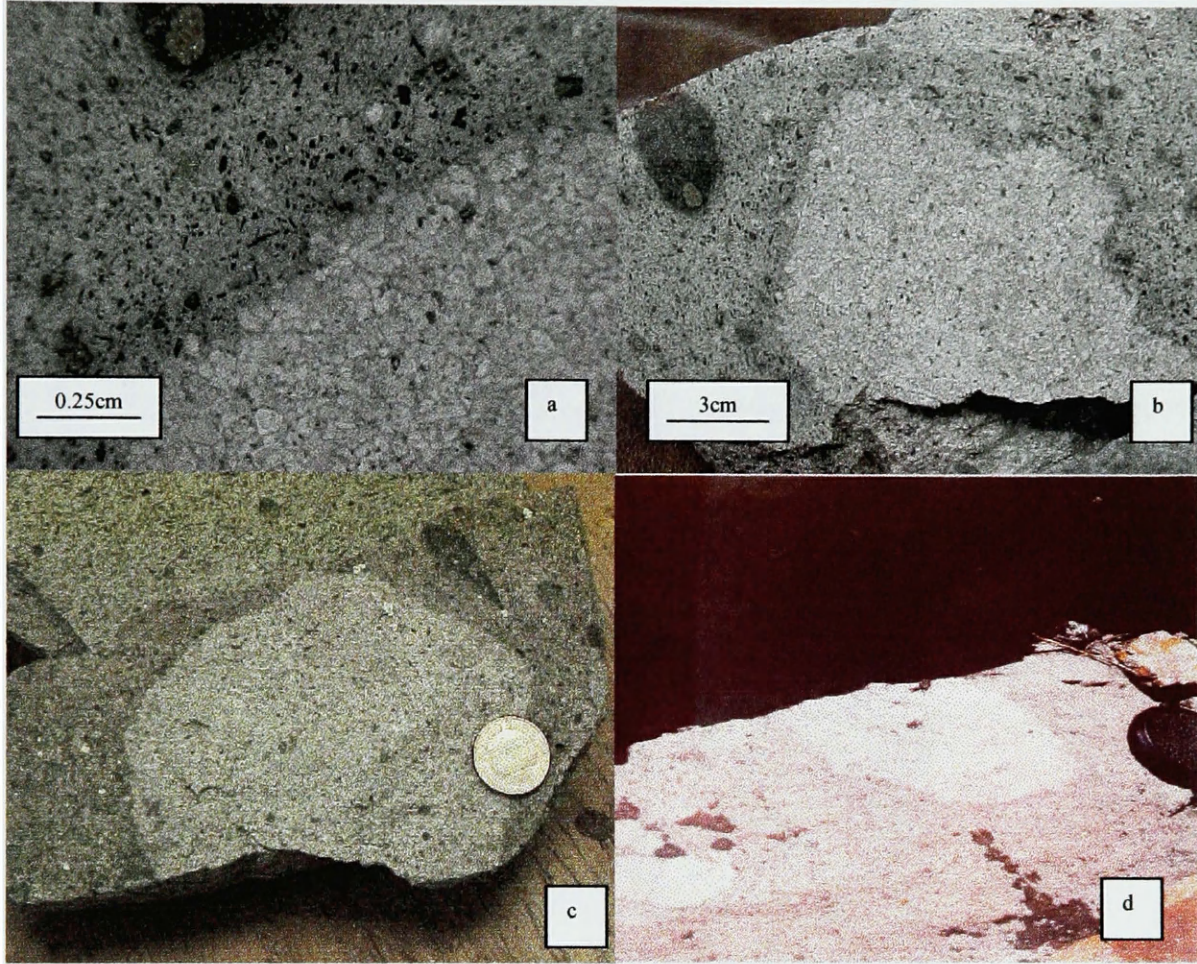


Figure 2-1.1: Felsic inclusions at Deer Butte: (a) close-up look at zoned feldspars on cut surface of felsic inclusion. Felsic inclusion has significantly larger grain size than surrounding quartz latite. Note the dark halo surrounding the inclusion; (b) same felsic inclusion as (a) with rounded edges next to small shonkinite inclusion. Surrounding quartz latite is contaminated with pyroxenes from the shonkinite; (c) felsic inclusion with tear-shaped mafic inclusion nearby. Penny (1.5cm in diameter) for scale; (d) large felsic inclusion in bedrock of Deer Butte. Lens cap (5cm in diameter) for scale.

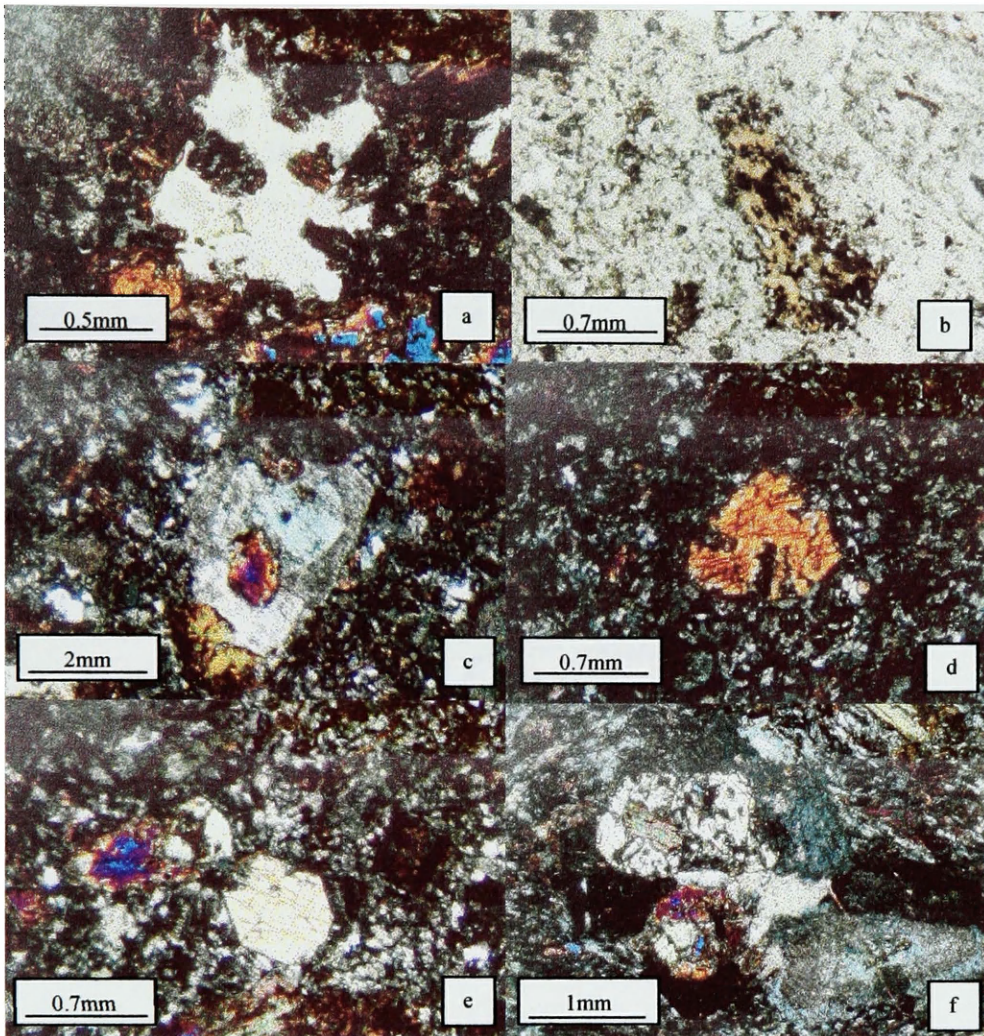


Figure 2-1.2a: Deer Butte phenocrysts: (a) resorbed quartz grain; (b) resorbed and altered biotite grain; (c) salite grain included in sanidine phenocryst; (d) resorbed salite grain showing embayments; (e) un-resorbed and resorbed salite grains adjacent to each other; (f) xenolith clotted with shonkinite with salite and biotite enclosed by feldspar.

Table 3: Representative average calite analyses from Deer Butte

Type(# of anal) Sample # / loc.	Rev(3) DB-5C	Rev(2) DB-5R	Osc(1) DB-1C	Osc(2) DB-1I	Osc(2) DB-1R	Osc(1) DB-9C	Osc(2) DB-9I	Osc(2) DB-9R	Nor(2) DB-5C	Nor(2) DB-5R	Nor(2) DB-1C	Nor(3) DB-1R
SiO ₂	52.98	54.23	52.16	53.11	52.02	53.73	55.59	52.77	53.34	53.75	54.68	54.20
TiO ₂	0.54	0.13	0.11	0.13	0.13	0.06	0.04	0.17	0.11	0.04	0.22	0.16
Al ₂ O ₃	1.78	1.32	1.52	1.64	1.72	1.03	0.58	1.92	1.19	1.23	0.95	1.21
FeO*	7.03	6.14	11.53	11.52	11.59	6.76	6.20	9.97	5.41	7.36	3.68	9.89
MnO	0.21	0.19	0.50	0.41	0.58	0.26	0.28	0.33	0.28	0.29	0.12	0.48
MgO	14.57	15.34	10.75	11.02	10.91	14.34	15.28	12.47	15.43	13.54	17.05	12.13
CaO	23.06	23.24	20.27	20.98	21.61	21.76	22.51	22.71	23.26	22.43	23.76	21.45
Na ₂ O	0.46	0.39	2.07	1.96	1.36	1.08	0.97	0.83	0.62	1.28	0.23	1.80
K ₂ O	0.00	0.00	0.00	0.00	0.00	0.03	0.00	0.00	0.00	0.00	0.00	0.00
Total	100.45	100.43	98.90	100.77	99.92	99.07	101.46	101.17	99.64	99.92	100.68	100.87

DB-1,5,9 represent different hand samples; a, b, c, d, represent different grains from same sample

Rev = Reverse; Osc = Oscillatory; Nor = Normal

*Total iron expressed as FeO

C = core; I = intermediate; R = rim

Individual grains separated by vertical dividing lines

Feldspar phenocrysts

The large feldspar grains at Deer Butte also show a complex cooling history, and are interpreted to include both xenocrysts from granite and gneiss basement rocks, and feldspars that crystallized from the quartz latite. Three types of feldspar grains are evident: smaller plagioclase grains (<2mm) which have exsolved into patches and blebs of albite and orthoclase, and large homogeneous sanidine and plagioclase grains (2-4mm) which are in equilibrium with each other (Table 4). These three grain types occur in a variety of relationships with each other, and are described below:

Small plagioclase grains show patches which are alternatively end member albite and orthoclase, and a thorough exsolution in thin section which gives grains a dusty appearance from core to rim. These anti-perthite grains are up to 2mm in length, and are commonly enclosed by, or attached to the periphery of the larger sanidine and plagioclase phenocrysts (Figure 3). However, many of the anti-perthite grains also appear to be independent of the larger plagioclase and sanidine phenocrysts.

Such thorough exsolution suggests (Tuttle and Bowen, 1958, p.157) that an initially crystallizing Ca-poor plagioclase reached a temperature below the solvus (< 660° C), where with continued cooling, the exsolving orthoclase and albite phases became more pure, forming end-member albite and orthoclase (Figure 4). Exsolution to this extent could only have taken place in conditions of elevated pressure and temperature such that exsolution proceeded very slowly, at a depth much greater than that which the plutons were finally emplaced. These anti-perthite grains show disequilibrium with the larger sanidine and plagioclase phenocrysts.

Most of the anti-perthite crystals are surrounded by streaks and pods of glass, and are enclosed by larger sanidine and plagioclase phenocrysts. Biotite grains also locally form between the two phenocryst types. Rounded grain shape and embayments on many enclosed anti-perthite grains also suggest a state of disequilibrium, such that the melt surrounding the anti-perthite experienced a sudden change in pressure or temperature causing the crystallization of homogenous sanidine or plagioclase.

Table 4: Representative Feldspar Analyses from Deer Butte

Phenocryst / Rim type feldspar (# of analyses)	Coexisting feldspars		Exsolution pair		Alkali Rims
	Plag(9)	Sanidine(4)	Albite(7)	Orthocl(5)	Alkali feld(6)
SiO ₂	64.58	65.72	67.77	63.94	67.03
TiO ₂	0.00	0.00	0.00	0.00	0.00
Al ₂ O ₃	21.80	19.37	19.68	19.56	18.77
FeO*	0.14	0.18	0.11	0.06	0.08
MnO	0.00	0.00	0.01	0.00	0.02
MgO	0.00	0.00	0.01	0.04	0.00
CaO	3.11	0.43	0.29	0.03	0.35
Na ₂ O	8.89	5.60	10.95	0.67	7.99
K ₂ O	1.41	7.57	0.70	15.04	4.32
Total	99.93	98.86	99.52	99.34	98.56
Na+Ca+K	13.4	13.6	11.9	15.7	12.7
Ca%	23.2	3.2	2.4	0.2	2.8
Na%	66.3	41.1	91.9	4.3	63.3
K%	10.5	55.7	5.7	95.6	33.9

Plagioclase composition ranged from An₂₂-An₂₅

Alkali feldspar rim composition ranged from Ab₅₅Or₄₅-Ab₇₁Or₂₉

*Total iron expressed as FeO

(#) Parentheses indicate number of analyses from 4 grains in 4 different thin section

Element % represents mean of (#) analyses

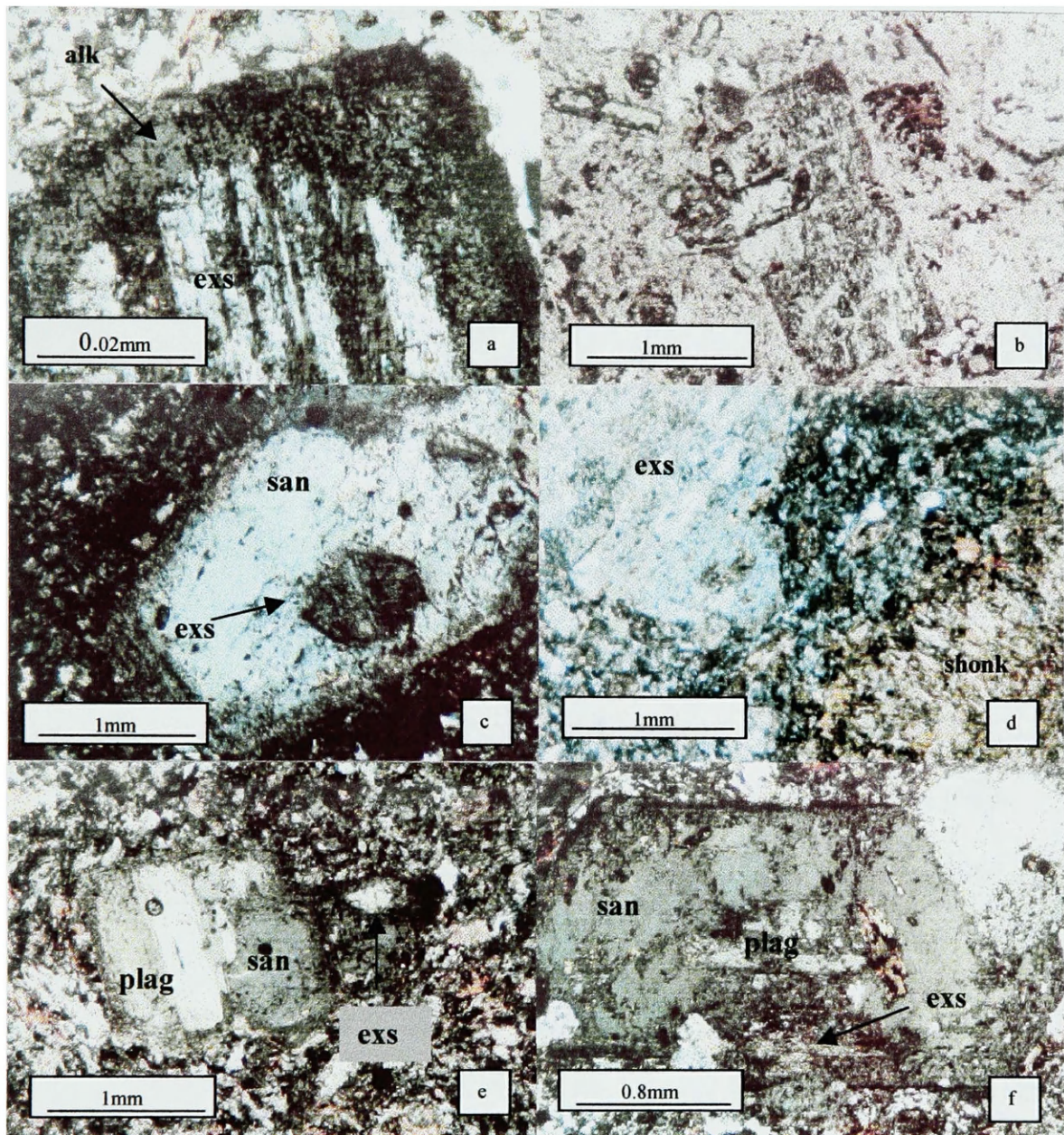


Figure 3: Albite – orthoclase exsolution in plagioclase: (a) rounded, anti-perthite grain (= exs) surrounded by sieved alkali feldspar rim (crossed polars) (= alk); (b) albite and orthoclase exsolution in plagioclase phenocryst (plane light); (c) anti-perthite (arrow) surrounded by homogenous sanidine grain (= san); (d) anti-perthite adjacent to fine-grained shonkinite inclusion (= shonk); (e) glomeroporphyritic plagioclase, sanidine and grain; (f) sanidine grain enclosing plagioclase core and anti-perthite grain.

Deer Butte Feldspar Compositions

Albite/Orthoclase exsolution pairs, alkali feldspar rims

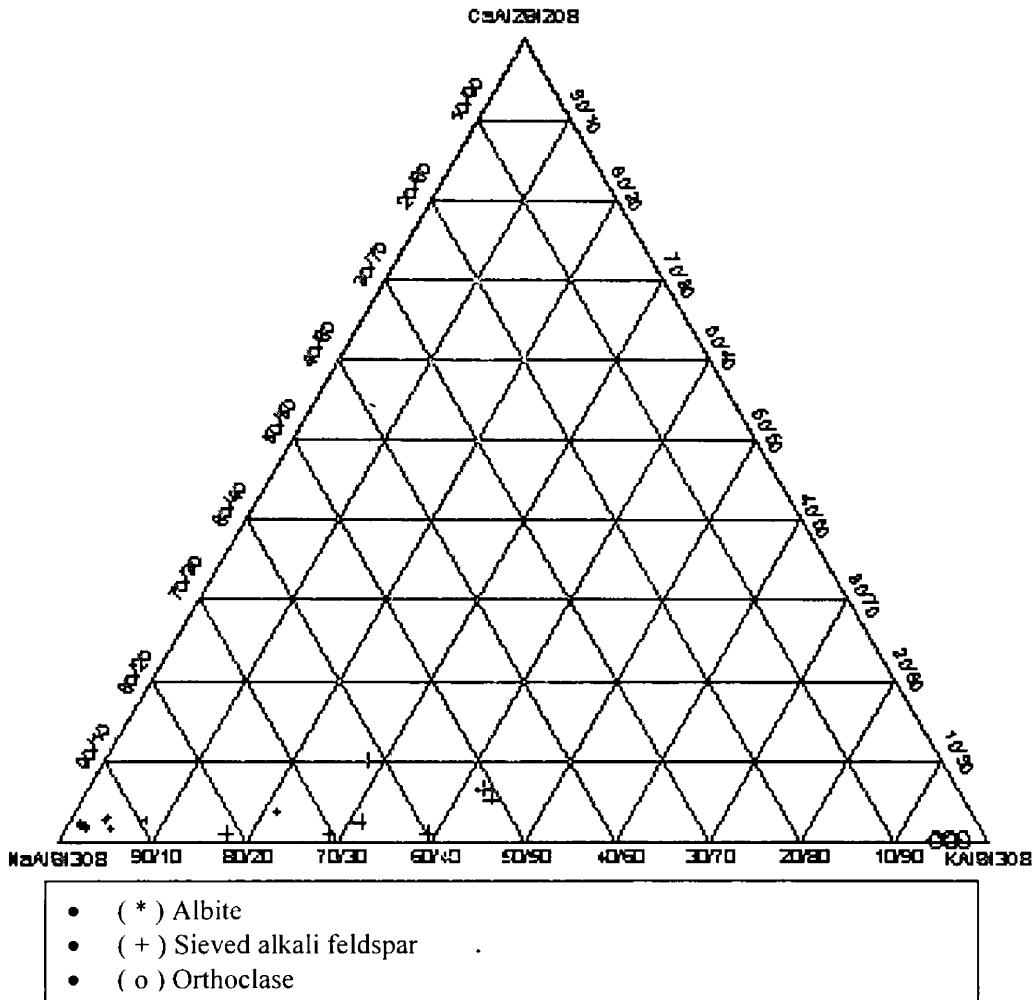


Figure 4: Ternary plot of anti-perthite grains at Deer Butte. Electron microprobe analysis was conducted from core to rim on 7 anti-perthite grains. Circles (O) indicate orthoclase patches, dots (*) indicate albite patches, and plus signs (+) indicate sieved alkali feldspar rims from all types of feldspar phenocrysts.

The rounded shape, extent of exsolution, and local occurrence of anti-perthite crystals independent of larger sanidine or plagioclase all support the contention that these are really xenocrysts from basement rocks. Basement rock inclusions have been observed throughout the Bearpaw Mountains, within nearly all types of intrusive bodies, including those in the present study. The partial melting of the basement rocks at depth that formed the quartz latite magma likely entrained xenocrysts of anti-perthite feldspar. These xenocrysts moved with the quartz latite melt until it pooled at its current shallow depth.

Coexisting unzoned and unexsolved plagioclase and sanidine make up second and third groups of phenocrysts (Figure 5). Euhedral phenocrysts of sanidine occur in glomero-porphyritic clusters with plagioclase and exsolved plagioclase, and as isolated, unzoned phenocrysts (1-4mm). Sanidine ($2V < 20^\circ$) also grows around strongly resorbed and unzoned plagioclase, and locally around exsolved plagioclase, salite, and biotite phenocrysts. Plagioclase grains are large (1-3mm), unzoned, and locally enclose sanidine, exsolved plagioclase, salite, and biotite. Cores of sanidine +/- plagioclase locally include small, glassy and irregular blebs, suggestive of either rapid crystal growth around pods of melt or pressure-relief melting of the phenocrysts.

If the plagioclase system were in perfect equilibrium, crystals would react continuously with the host melt to ultimately produce unzoned plagioclase with the same composition as the original melt. Instead, the plagioclase ($An_{22}-An_{25}$) cores surrounded by sanidine feature embayment textures, suggesting the composition of the liquid crossed over the plagioclase / sanidine solidus from the plagioclase stability field to the sanidine stability field, starting but not finishing the resorption of remnant plagioclase (Figure 6a).

Resorption of the plagioclase core is not due to a temperature increase, as the surrounding feldspar is depleted in Ca relative to the core. Nor is a change in magma chemistry responsible, as the plagioclase does not become Ca-enriched near the rims, but is instead normally zoned towards Na. Resorbed salite xenocrysts are, however, poikilitically enclosed in the outer portions of sanidine grains, suggesting a possible change in local magma enrichment in Ca and Mg at an earlier stage. Instead, the resorption of plagioclase is likely due to the expected crystallization path described by Tuttle and Bowen (1958) for a feldspar system in equilibrium whose initial chemistry was above the solvus (Figure 6a):

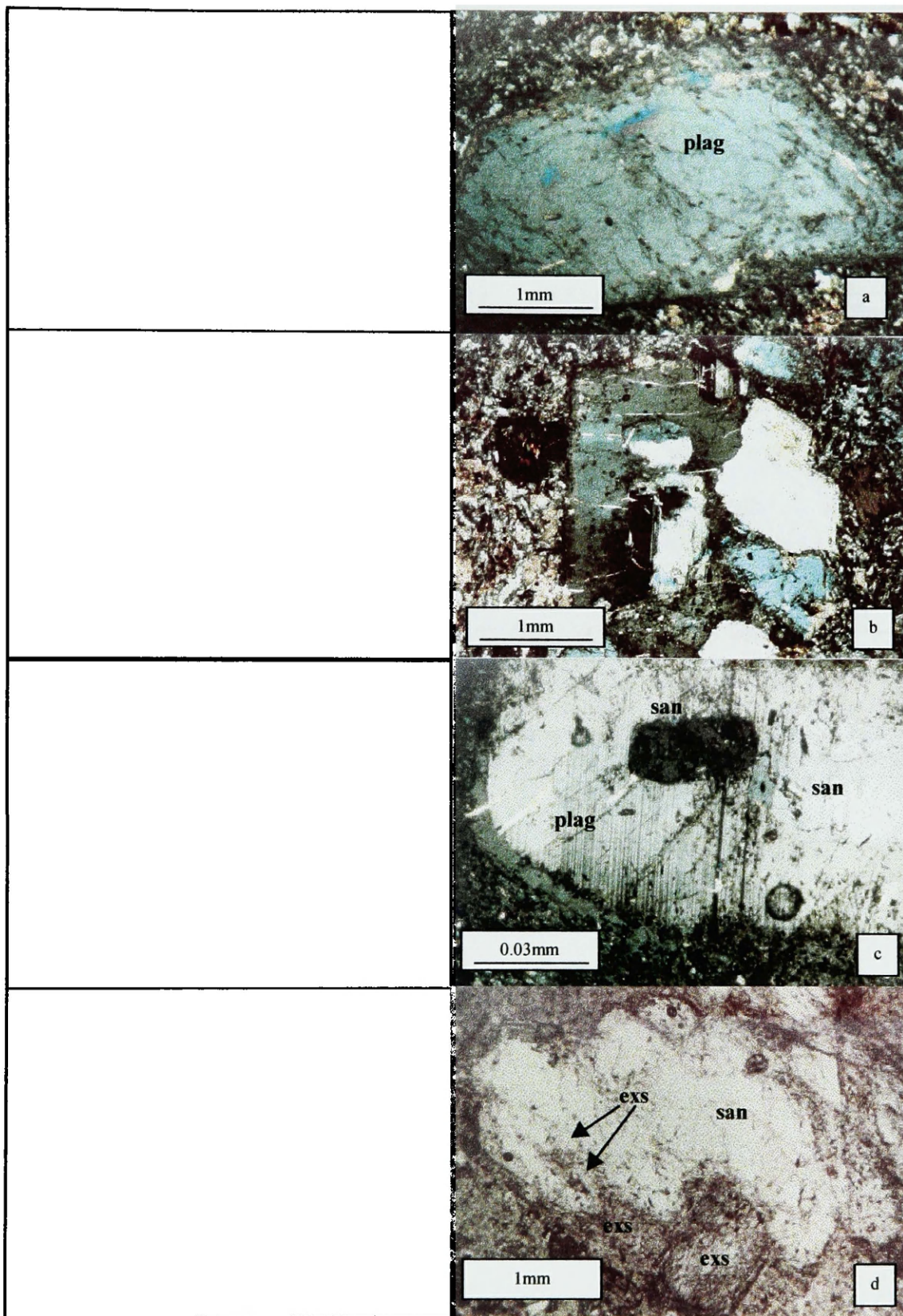


Figure 5: Photographs and drawings of composite feldspar grains: (a) homogeneous plagioclase grain (= **plag**); (b) plagioclase, anti-perthite (= **exs**), enclosed by sanidine (= **san**), rimmed by sieved alkali feldspar (= **alkali**); (c) two sanidine grains overgrown by large unzoned plagioclase, which is surrounded by a thin sanidine rim, followed by sieved alkali feldspar (crossed polars); (d) large sanidine grain enclosing smaller anti-perthite grains (plane light).

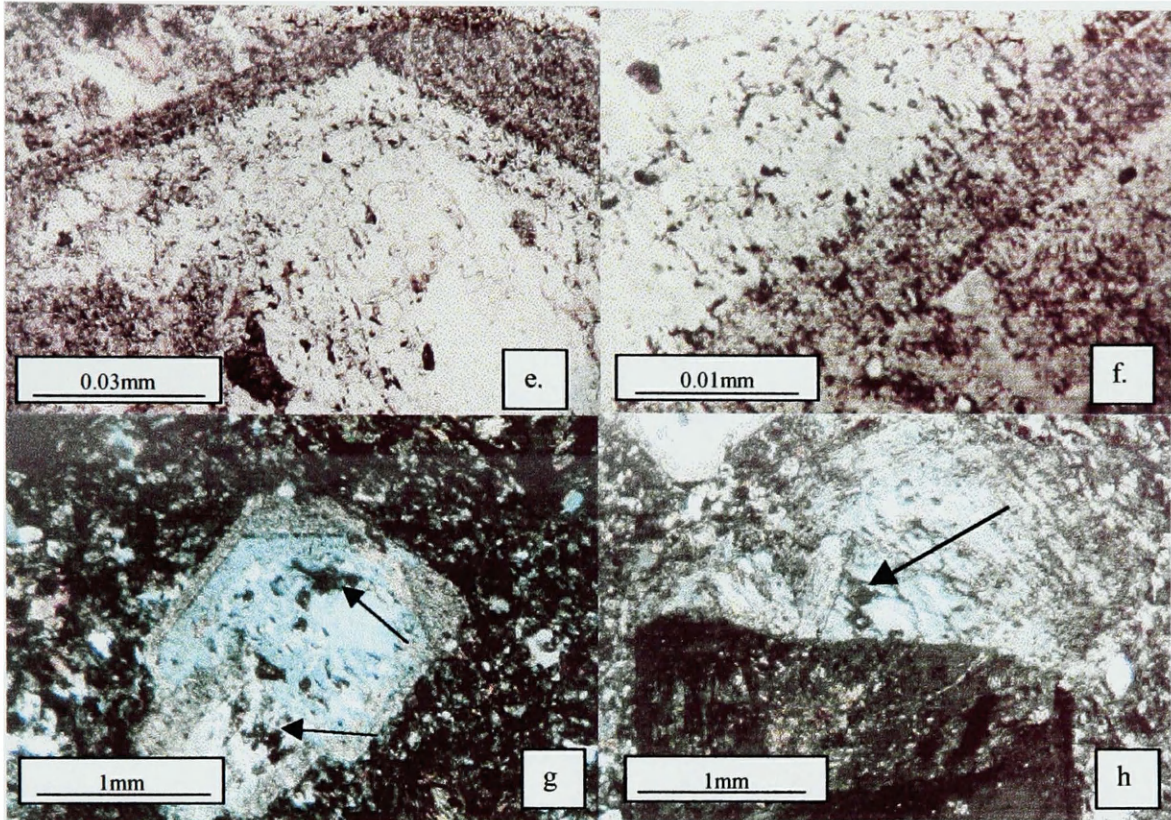


Figure 5(cont.): Dusty sieve texture in alkali feldspar rims of feldspars at Deer Butte: (e) plagioclase phenocryst with alkali feldspar rim showing dusty sieve texture. Ca-rich pods of melt formed in the alkali feldspar, as tiny blebs and streaks that align perpendicular to the edge of the grain; (f) close-up view of sieved alkali feldspar rim; (g) overall view of same grain as in (e) and (f), revealing melt-inclusion cores (arrows) similar to those observed in the feldspars of equivalent pyroclastic samples; (h) large plagioclase phenocryst showing melt-inclusion core.

Deer Butte Feldspar Compositions

Plagioclase vs Sanidine

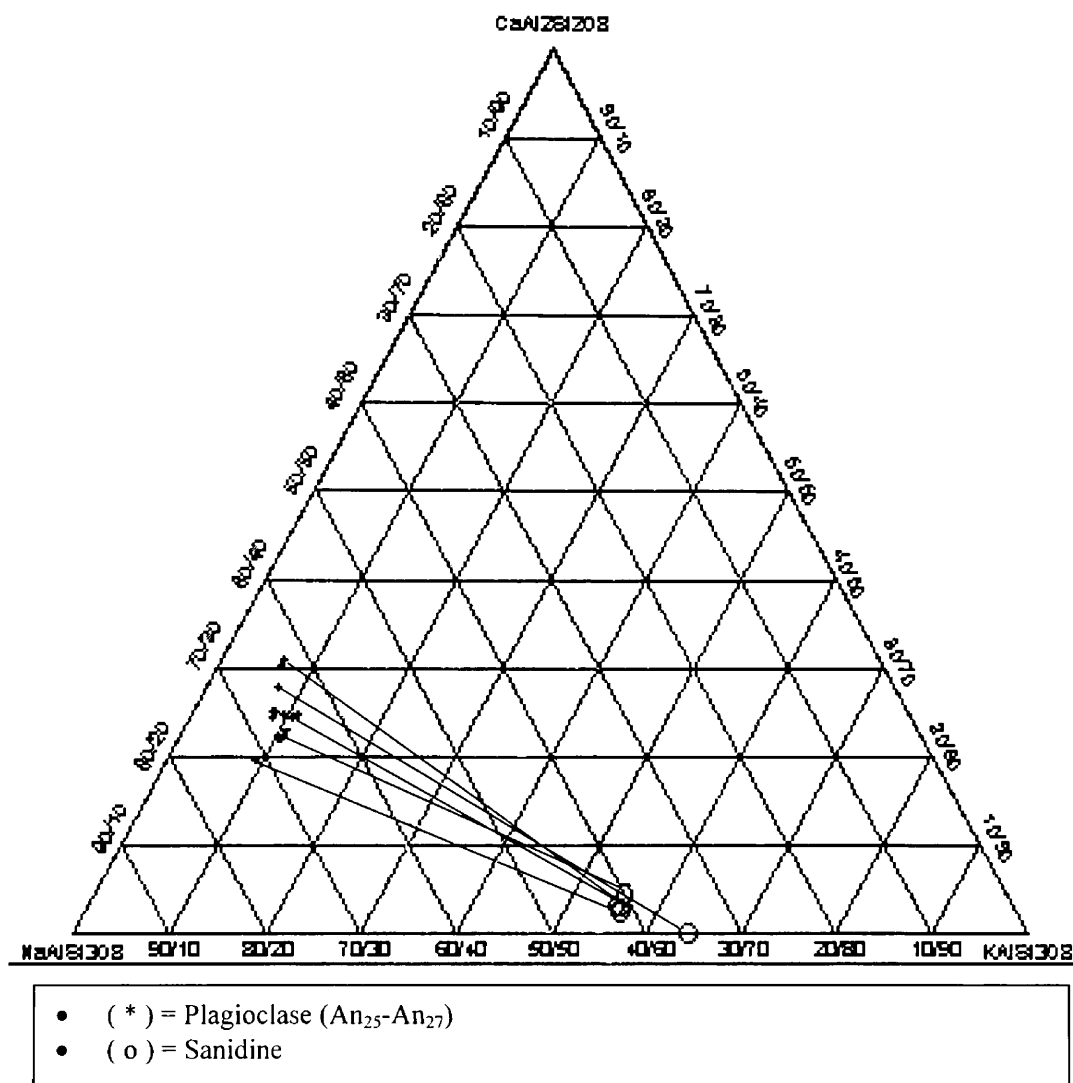


Figure 6: Co-existing plagioclase and sanidine grains from Deer Butte. Plagioclase content ranges from An₂₅-An₂₇. Dots (*) indicate plagioclase grains, and circles (o) indicate sanidine grains.

Assuming the initial composition of the magma is at X (Figure 6a), plagioclase of composition more calcic than G' is the first feldspar to crystallize, moving the liquid towards the point G_L along the solidus field boundary $D-K_L$. At this temperature, alkali feldspar richer in potassium (G) begins to separate, and the liquid changes composition along the solidus to A_L , at which temperature the mixture consists of an alkali feldspar (A), liquid (A_L), and a trace of plagioclase crystals having the composition (A'). During crystallization from G_L to A_L , the plagioclase reacts with the liquid continuously and changes composition from G' to A' , and the potassium feldspar crystals move from G to A . Continued crystallization would eventually yield an alkali feldspar A and liquid A_L . However, coexisting plagioclase and sanidine (Figure 6) at Deer Butte generally correspond to G' and G , respectively, suggesting this process was prevented from reaching completion. Coexisting plagioclase and sanidine, and remnant plagioclase cores in the phenocrysts of Deer Butte, then, suggest that the above process was prevented from reaching completion by a decrease in the pressure and/or an increase in temperature within the magma chamber.

However, relationships between sanidine and plagioclase vary locally within Deer Butte. Plagioclase surrounds some sanidine, and sanidine encloses and resorbs some plagioclase. Localized reheating likely gave rise to a variety of melt conditions surrounding feldspar phenocrysts in different parts of the magma chamber, resulting in some areas of the chamber crystallizing sanidine first, while other areas crystallized plagioclase first. These sanidine and plagioclase phenocrysts are interpreted to have crystallized at depth, incorporating and nucleating around the anti-perthite feldspar grains.

All feldspar phenocrysts and clusters of phenocrysts are rimmed by alkali feldspar of varying thicknesses, the composition of which is denoted by small plus signs (+) in Figure 4. The alkali feldspar plots at what would be the expected composition if the plagioclase and sanidine the crystals were given enough time to react with the remaining liquid. The alkali feldspar rim shows a sieve-like texture that transitions sharply into the phenocryst, extending only within the alkali feldspar rim (Figure 5). Included within the sieved alkali feldspar rim are tiny, unidentifiable inclusions.

The alkali feldspar rims with inclusions of unknown material are interpreted to be the result of rapid crystal growth around exsolved plagioclase, sanidine, and plagioclase phenocrysts, presumably at a relatively shallow depth. The sharp contact between the two phenocryst types and the alkali feldspar rims

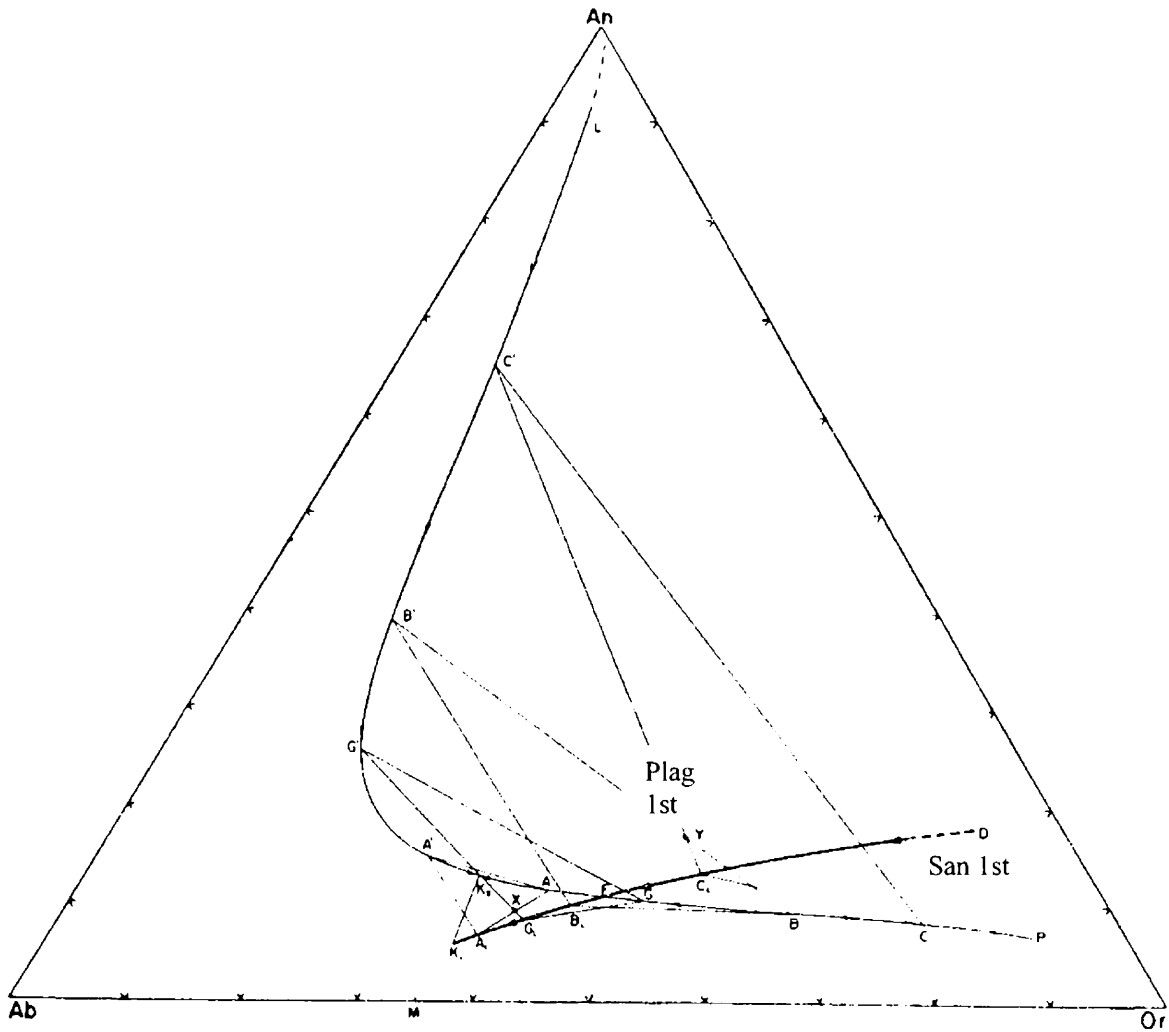


Figure 6a: Ternary diagram showing the system $\text{NaAlSi}_3\text{O}_8$, KAlSi_3O_8 , $\text{CaAl}_2\text{Si}_2\text{O}_8$. Shows the approximate compositions of liquids co-existing in equilibrium with two feldspars. The temperatures represented by this diagram are relatively high and are believed to be comparable to those existing in trachytic lavas. Arrows indicate direction of falling temperatures. The field boundary has been located by examining analyses of extrusive rocks in which the feldspar phenocrysts have also been analyzed and by noting the composition of two analyzed feldspars co-existing in extrusive rocks, in which the rock or the groundmass has also been analyzed. $D-K_L$ represents cotectic separating plagioclase first and sanidine first fields. Tie-lines connect co-existing plagioclase and sanidine. (Taken from Tuttle & Bowen, 1958)

point to a state of disequilibrium between the feldspars and surrounding melt, a condition prompted by either pressure-release or a rapid increase in temperature. Although the rims contain abundant glass inclusions and the cores contain glass only locally, both alkali feldspar rims and the sanidine/plagioclase phenocryst interiors contain pods and lenses of glass. This suggests that the sanidine and plagioclase phenocrysts underwent pressure-relief melting only after the growth of alkali feldspar rims. Rapid crystal growth, therefore, was followed by the sieving of the alkali feldspar rims into pods of melt and the melting of the feldspar cores.

There are two possible causes of the dusty sieve texture and of the formation of pods of glass in the alkali feldspar rim. One explanation of the sieve texture is the re-heating of a given feldspar to a point above its equilibrium solidus temperature but below its liquidus. Recrystallization then occurs, rapidly producing a very fine-grained inter-growth of Ca-enriched alkali feldspar with trapped glass, similar to the situation described for the feldspars of the Soufriere Hills volcano (Murphy et al., 2000). However, if this were the case there should be evidence that corrosion was accompanied by a change in the composition of the magma. If the sieving were the result of a rapid increase in the temperature of the melt, only the rims would melt, and would have shown reverse zoning.

Another explanation is that sieving resulted from the rapid decrease of pressure as magma and volatiles erupt or as magma rises rapidly toward the surface. As pods of glass can be seen in both phenocrysts *and* rapidly grown alkali feldspar rims, the simplest explanation is that pressure-relief melting took place after the alkali feldspar rim had crystallized, presumably at a shallow depth. Therefore, the pressure-release was not the result of magma ascending, but was instead the result of a drastic drop in pressure of the melt at a static depth, probably caused by eruption.

A composite history of feldspar crystallization is therefore inferred as follows and summarized in Figure 6b:

- a) Plagioclase in basement rock (granite) at great depth and pressure exsolved into end-member albite and orthoclase.
- b) Partial melting of the basement rock entrained the anti-perthite grains within a new quartz latite melt.
- c) Plagioclase in the quartz latite crystallized very slowly at significant depth and pressure.

- d) Plagioclase crystallization gave way to the crystallization of coexisting sanidine as liquid composition moved across cotectic $D-K_L$ (Figure 6a).
- e) Plagioclase is partially resorbed as it reacts with the liquid, leaving an alkali feldspar (sanidine) and liquid.
- f) Plagioclase and sanidine crystals in the quartz latite magma rise to shallower levels and are emplaced into a shallower magma chamber.
- g) Rapid growth of thin alkali feldspar rim around plagioclase, sanidine, and anti-perthite feldspar phenocrysts. Rims enclose tiny bits of unknown material from the quartz latite melt as they grow.
- h) Sieving of outer portion of alkali feldspar rims and melting of plagioclase and sanidine cores as pressure rapidly drops during an eruptive release of volatiles and magma.

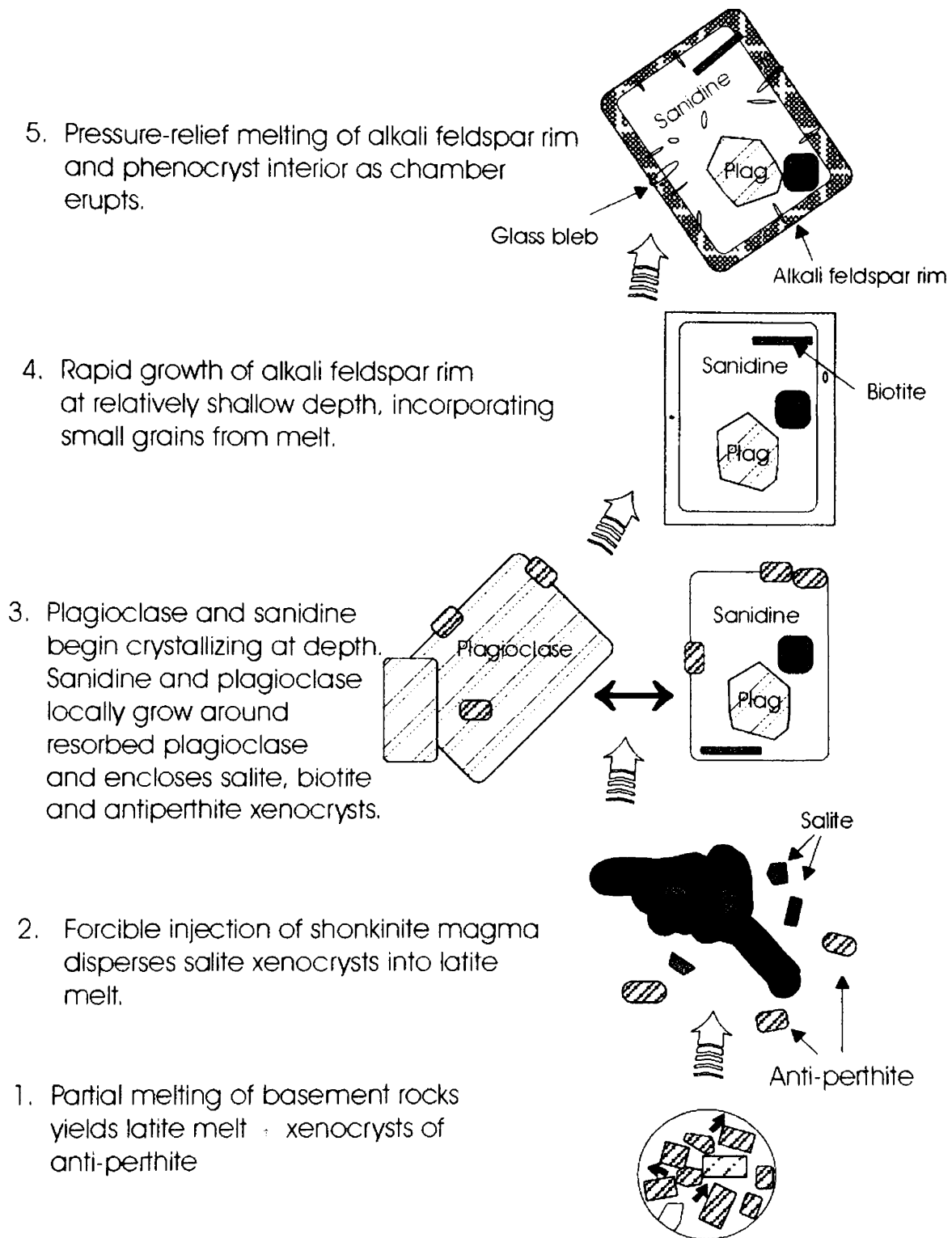


Figure 6b: Inferred crystallization history of Deer Butte pluton showing timing of shonkinite intrusion into cooling quartz latite magma chamber and its effects upon growth and incorporation of mineral grains.

Amphibole Crystals at Suction Butte

Amphibole grains at Suction Butte record a transition from pressures at which $\geq 4\%$ by weight water is dissolved in the quartz latite melt to lower pressures at which the water saturates the quartz latite melt and exsolves, breaking down and reacting into a fine-grained Fe-oxide rim. This transition is interpreted to reflect the convection of amphibole grains throughout the Suction Butte pluton. Conclusions are based on the following observations:

Suction Butte amphibole crystals show a mean chemistry of hastingsite (Deer, Howie, and Zussman, 1963; Appendix VI). Hastingsite comprises an estimated 15% of Suction Butte. Normal, reverse, and oscillatory zoning are all evident (See Representative analyses, Table 5). Many hastingsite grains at Suction Butte show resorption in their rims. Amphibole is only stable at temperatures less than 880°C (Barclay et al., 1998; Rutherford and Hill, 1993). Local reverse zoning and melting could be the result of local variation in pressure-temperature conditions within the magma chamber, pressure-relief melting as the magma ascended, or a heating event that raised the temperature in the quartz latite melt above 880°C .

Also, titanomagnetite reaction rims commonly surround amphibole, typically forming several distinct zones within an individual grain (Figure 7). Hornblende and biotite are only stable in hydrous melts, and hence can only grow if pressures are sufficient to keep enough water in solution. Previous work (MacGregor, 1938; Jakes and White, 1972; Garcia and Jacobsen, 1979) agrees that if a melt loses its dissolved water because of decompression, amphibole is no longer stable and breaks down, forming rims consisting of plagioclase, clinopyroxene, and titanomagnetite, or an assemblage representative of the composition of the whole melt. Other possible explanations of the reaction rims are the introduction of a new higher-temperature or low H_2O magma into the magma chamber, or the fluxing of a magma with a CO_2 -rich fluid (Rutherford and Hill, 1993).

Garcia and Jacobsen (1979) categorized two types of amphibole breakdown rims: a 'black' type, and a 'gabbroic' type. They regarded the gabbroic type to be caused by an $f_{\text{H}_2\text{O}}$ decrease in the magma reservoir, while the black type is produced from oxidation and dehydrogenation during or after extrusion. The gabbroic rims occur only on amphiboles in contact with melt, whereas the black rims cut through amphibole crystals in the erupted dacite, showing a reaction that does not require the presence of melt.

Table 5: Representative average hastingsite (amphibole) analyses from Suction Butte

Type(# of anal) Sample # / loc.	N(2) SB-2aC	N(1) SB-2aI	N(2) SB-2aR	O(2) SB-9C	O(1) SB-9I	O(2) SB-9R	O(2) SB-11C	O(1) SB-11I	O(2) SB-11R	O(1) SB-2bC	O(2) SB-2bI	O(1) SB-2bR
SiO ₂	40.09	39.62	38.95	38.40	38.09	38.98	39.89	41.28	40.10	41.15	41.04	40.35
TiO ₂	1.86	1.90	1.94	2.01	2.05	1.99	1.94	1.91	1.87	1.94	1.86	1.92
Al ₂ O ₃	11.91	12.17	12.04	11.60	11.26	11.92	11.80	11.43	11.59	11.51	11.35	11.64
FeO	17.75	18.35	21.06	21.32	20.90	20.87	19.40	17.31	19.05	18.11	16.70	19.75
MnO	0.28	0.32	0.48	0.49	0.55	0.48	0.45	0.39	0.42	0.40	0.34	0.45
MgO	9.64	9.41	7.45	7.53	7.29	7.45	8.82	10.47	8.90	10.03	11.04	9.13
CaO	11.42	11.51	11.30	11.38	11.50	11.40	11.26	11.55	11.37	11.31	11.68	11.05
Na ₂ O	2.12	2.11	2.23	2.13	2.02	2.18	2.14	2.31	2.24	2.15	2.29	2.17
K ₂ O	1.73	1.76	1.55	1.67	1.67	1.69	1.76	1.52	1.63	1.50	1.48	1.55
Total	96.80	97.16	97.00	96.55	95.33	96.97	97.46	98.15	97.18	98.11	97.78	98.01
Fe/Mg	1.84	1.95	2.85	2.83	2.87	2.80	2.20	1.65	2.14	1.81	1.51	2.16

SB-2,9,11 represent different thin sections; a, b represent different grains in the thin sections

N = Normal; O = Oscillatory

*Total iron expressed as FeO

C = core; I = Intermediate; R = rim

Individual grains separated by vertical dividing lines

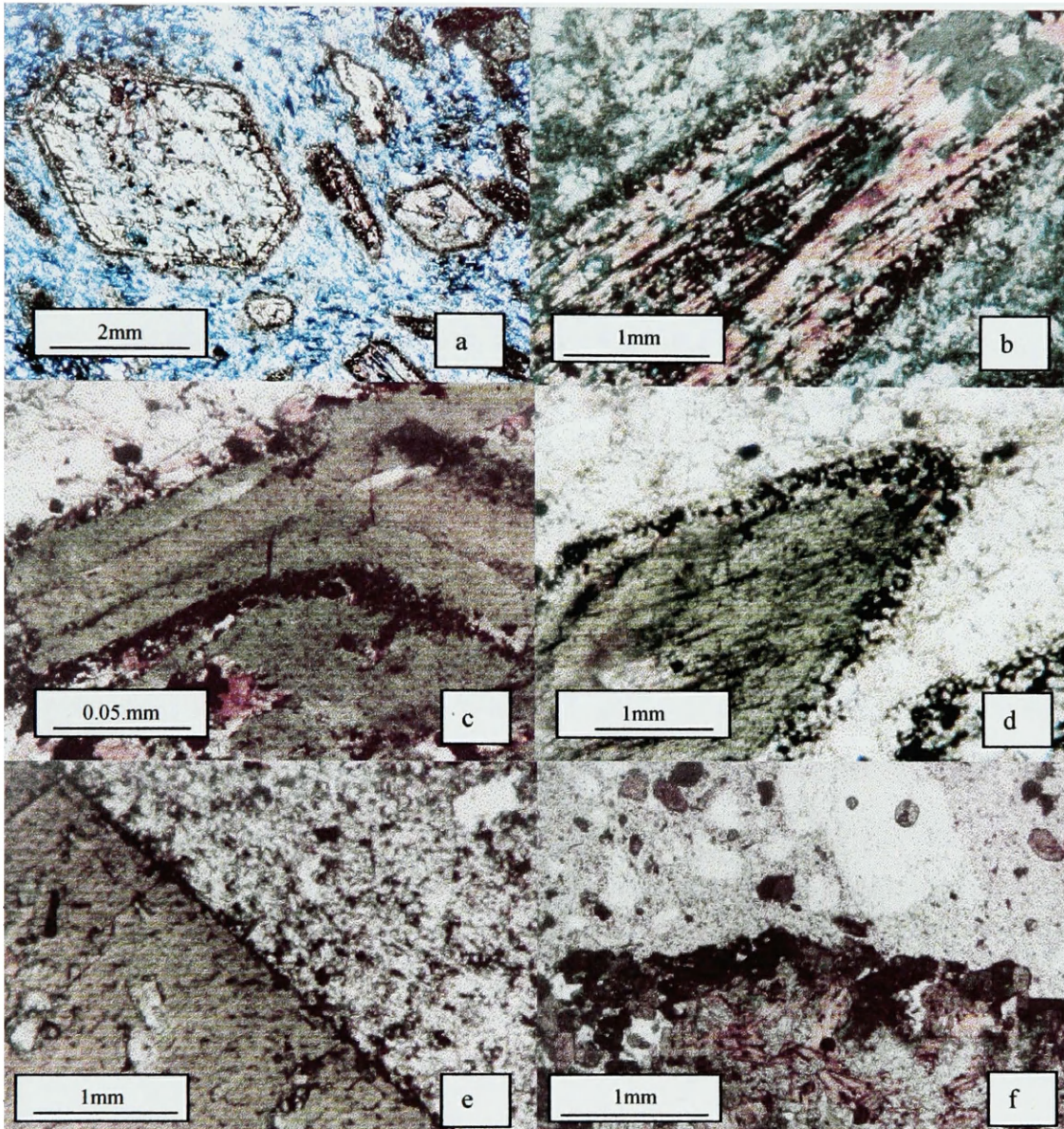


Figure 7: Eastern Bearpaws hastingite: (a) hastingite grains showing multiple horizons of very fine-grained titanomagnetite-plagioclase-iddingsite reaction rims at Suction Butte. Resorbed hastingite grain in upper right corner; (b-c) close-up look at two distinct reaction rims on hastingite grains from Suction Butte. Note the resorption and alteration within the hastingite cores; (d-e) variations in reaction rim thickness from samples 4 meters apart at Suction Butte; (f) hastingite reaction rim on shonkinite inclusion at McCann Butte.

Although the rims on amphiboles at Suction Butte lack clinopyroxene and hence are not gabbroic in the true sense of the word, titanomagnetite and minor plagioclase *are* present, and, importantly, reflect the composition of the initial melt. The reaction rims are only present on the crystals in contact with melt, are found in plutonic rocks, and do not cut through amphibole grains, all of which suggest that they are the result of an f_{H_2O} decrease in the magma reservoir and can be considered equivalent of the 'gabbroic' type of Garcia and Jacobsen (1979).

Constant T and P and isothermal decompression experiments by Rutherford and Hill (1993) established a relationship between the thickness of the reaction rim surrounding amphiboles and the rate of ascent experienced in a magma chamber. They showed that during a 900°C constant-rate decompression from 8km (2.2 kbars) to the surface, no reaction rim develops on amphiboles in 4 days, a 10µm rim develops in 10 days, and a 35µm rim develops in 20 days (Figure 8, taken from Rutherford and Hill, 1993).

The presence of stable amphibole in the core of the amphibole phenocrysts at Suction Butte allows the inference that as the grains were crystallizing the minimum amount of dissolved water in the initial melt was at least 4% at 890°C (Rutherford and Hill, 1993; Barclay, 1998). Melt with this water content that experienced a steady adiabatic decrease in pressure would achieve water saturation and subsequent reaction and dehydration of amphiboles at 1.6kbars (160 Mpa) of pressure (Rutherford and Hill, 1993). The occurrence and thickness of reaction rims can therefore provide a constraint on the how the prevailing water pressure conditions in the magma chamber have changed.

The oldest rocks found contacting the plutons are Jurassic limestones of the Ellis Group. Assuming this unit to be the oldest rock lying on top of the plutons, the total sedimentary overburden at the time of pluton intrusion ranges from 2.5km to 3.5km for the top and base of the Ellis Group. If the plutonic body extends 2km below the upper contact with country rock, the estimated maximum total overburden and lithostatic pressure experienced by magma in the quartz latite plutons, all other factors equal, would be 5.5 km and ~1.7 kb, respectively. Therefore, the Suction Butte pluton likely straddles the pressure stability limit (1.6 kbars) of amphibole.

The narrow width of the titanomagnetite reaction rims on the hastingsite of Suction Butte indicates that the amphiboles did not stay for long (days) outside their stability field (Rutherford and Hill, 1993). Reaction rim thicknesses were measured on 10 grains from each of 8 different thin sections from

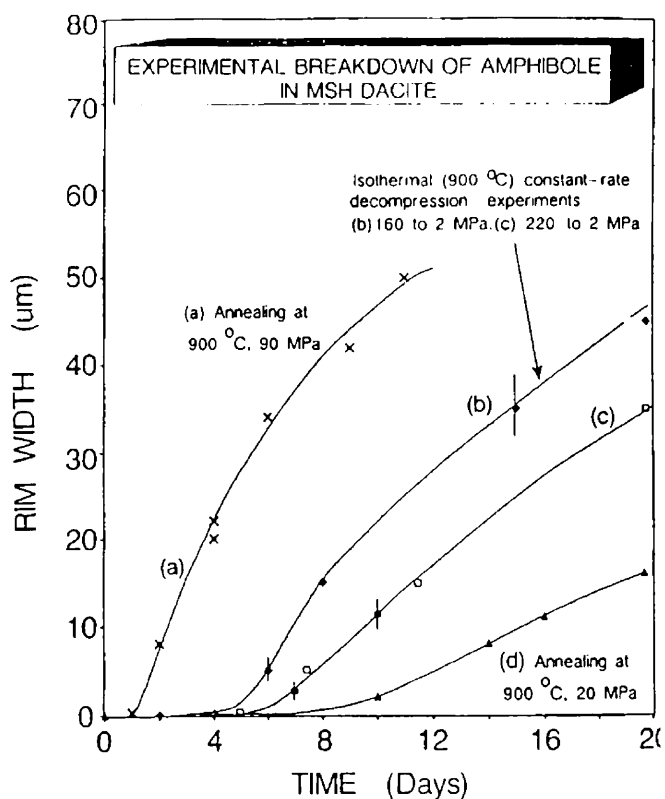


Figure 8: Amphibole reaction rim width versus time for experiments on Mount St. Helens (MSH) dacite. Curves a and d are for constant P and T annealing experiments where the time is the annealing time following an emplacement time of 1-12 hours (no breakdown would occur during this emplacement according to curve b). Curve b is for an isothermal 900°C decompression from 160 to 2 Mpa (~1.6kbars to 2kbars), or, to the surface; the decompression time is the time following a 12 hour annealing at 1.6kbars. Curve c shows the breakdown as a function of time for a constant-rate decompression beginning in the deep Mount St. Helens source region at 220 Mpa; it is based on two experiments (closed symbols) and extrapolation of the curve b data (open symbols) to 2.2kbars, assuming that no breakdown would occur during the 2.2 to 1.6 kbar part of the ascent because hornblende is stable in this pressure range (from Rutherford and Hill, 1993).

Suction Butte. Rims were chosen for thickness measurement based on the large size of the amphibole, rim sharpness, and consistency of rim thickness throughout the grain, all of which served to ensure grain faces being measured were vertical and perpendicular to the surface of the thin section. Values ranged from 0-70 μm , with standard deviations of 5.2-15 for each of the thin sections. The mean thickness of amphibole rims in the pluton was 34.5 μm , and the standard deviation among the thin sections was 13.2. Variation was seen at slightly larger than hand-sample scale, as one thin section showed a mean thickness of 11.2 μm , whereas a thin section from 1m away had a mean rim thickness of 52.0 μm . (see Representative rim thicknesses, Table 6).

If the amphibole grains cooled statically with the rest of the pluton at pressures below 1.6kb, continued saturation and dehydration of the magma would have destroyed the amphibole in entirety. However, the thickness of the reaction rims suggest the amphibole grains were in the presence of a water-saturated (exsolved) magma at a temperature above the solidus for a very short time. Assuming the results that Rutherford and Hill obtained from the Mt. St. Helens dacite can be extrapolated qualitatively to Suction Butte, the observed rim thicknesses correspond to a time of less than 20 days outside the amphibole stability field (Figure 8). As evidenced by the large standard deviations of rim thickness *within* each thin section, and the significant difference in rim thickness *between* thin sections, the Suction Butte magma body likely experienced thorough churning and mixing. Assuming the pluton straddles the pressure stability limit of amphiboles, quartz latite magmas with different residence times at pressures <1.6 kbars (Devine et al., 1998a) probably mingled within the magma chamber.

Also, previous reaction rims which have been overgrown by further amphibole crystallization are locally observed (Figure 7a-c). This suggest that these grains grew in an environment in which $f_{\text{H}_2\text{O}}$ has changed through time (Figure 8a), oscillating between water-saturated and water-undersaturated conditions.

Decreases in dissolved water concentration are the result of a decrease in pressure as magma rises and water exsolves. On the other hand, increases in $f_{\text{H}_2\text{O}}$ could be the result of either replenishment by under-saturated quartz latite magma from depth or the release of H_2O and other volatiles into the quartz latite host by an intruding mafic magma. Grains that experience a successive increase and decrease in water pressure could also be the result of the convective cycling of crystals within the magma chamber, so that at different heights within the pluton the crystal experienced different conditions of $f_{\text{H}_2\text{O}}$.

Experimental studies have shown that shallowly emplaced granites contain relatively less dissolved water than granites emplaced at depth (Holtz, 2001; Hamilton et al., 1964; Burnham and Jahns, 1962). The relatively low pressures (<2.0 kbars) into which the quartz latite in the eastern Bearpaw Mountains was emplaced correspond to *less than 4%* water by weight that can be dissolved in the melt. Therefore, it is unlikely the addition of under-saturated quartz latite magma from depth was a source for additional dissolved water, as the entire Suction Butte exposure contained abundant amphibole crystals that could only grow in magmas with *more than 4 %* dissolved water. However, mafic magma intruded into a felsic host would cool and begin crystallizing immediately, therefore causing exsolution of water and other volatiles. If these volatiles moved into a dry felsic magma, they might again at first dissolve, and thereby increase the f_{H_2O} . However, since the Suction Butte pluton was emplaced at pressures close to 1.6 kbars, the probability of water initially dissolving into even a dry melt at such pressures is low. The most likely scenario, however, is that individual grains experienced different water-pressure conditions because they were in a pluton undergoing convection, moving above and below depths corresponding to 1.6 kbars of lithostatic pressure.

Assuming the growth rate of amphibole correlates with the experimentally-derived breakdown rate of amphibole, the amount of fresh amphibole growth in-between titanomagnetite reaction rims indicates how much time elapsed while the grain re-entered water-undersaturated conditions. If the magma chamber at Suction Butte straddles the pressure stability limit of amphiboles (1.6kbars), the total thickness of fresh amphibole growth between reaction rims then provides a constraint on the time for one convective cycle within the pluton and therefore the relative flow velocity (Figure 8a). The total thickness between reaction rim horizons in the amphibole grains of Figure 7a and 7c is 40 μ m and 50 μ m respectively. This corresponds to times on the order of several weeks for individual grains to make one complete cycle within the pluton.

Of note is the presence of an amphibole rind around some of the shonkinite inclusions. Amphibole crystals that rim the shonkinite inclusions are themselves rimmed with titano-magnetite where in contact with the melt; this is similar to the phenocryst phase in the quartz latite. This suggests that the shonkinite was present within the quartz latite magma prior to when the amphiboles experienced a melt dehydration, as H₂O was exsolved from the magma. It also shows that at least some of the shonkinite

Hastingsite dehydration and convection

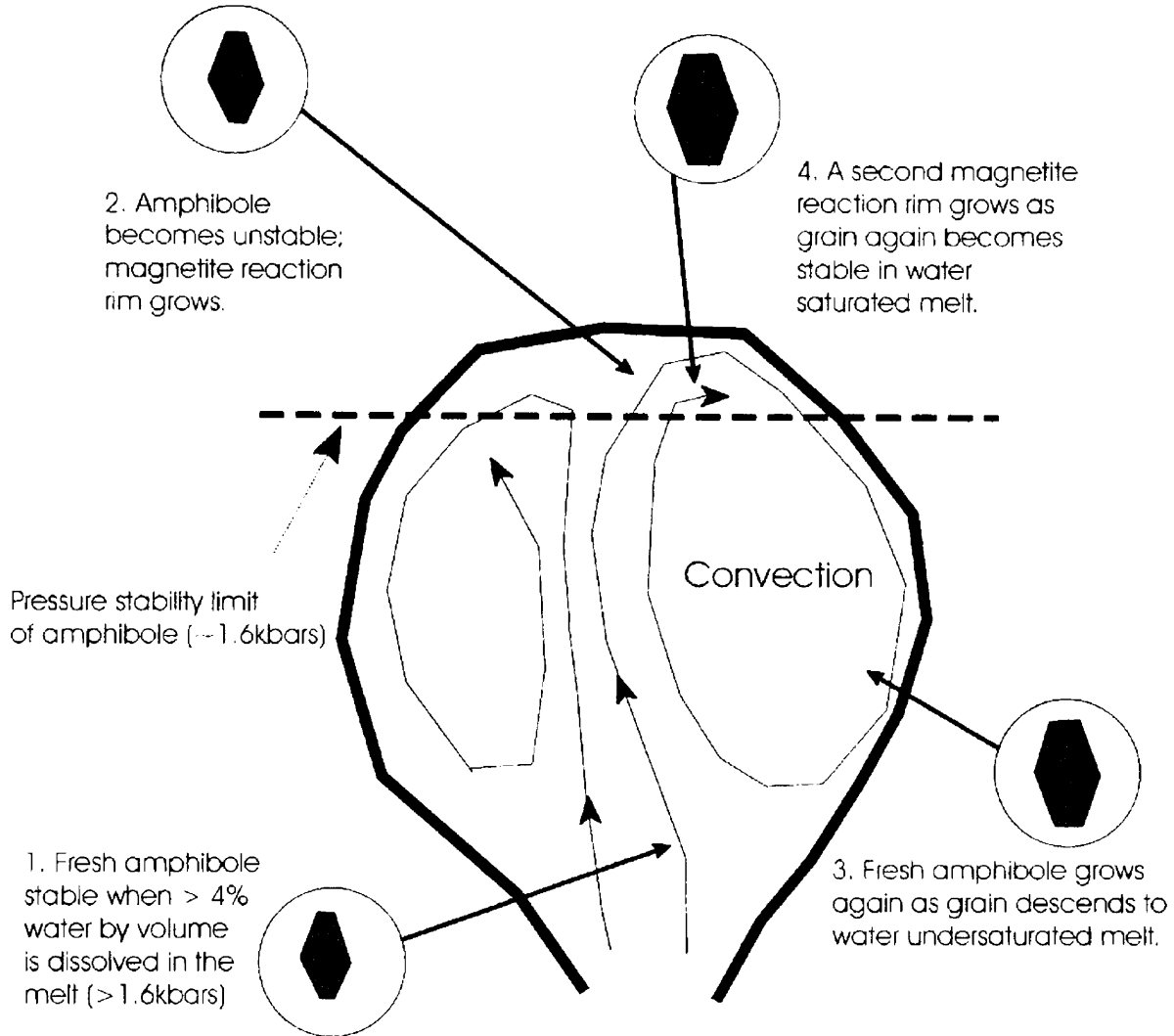


Figure 8a: Drawing of inferred convection cycle and movement of amphibole grains at Suction Butte. Amphibole grains at Suction Butte record a transition from crystallizing in a water under-saturated melt (<4%) to a water-saturated melt, breaking down and reacting into a fine-grained Fe-oxide rim. Assuming the water content for amphibole to be stable is 4% (Rutherford and Hill, 1993), melt starts degassing at depths which correspond to the amphibole pressure stability limit at about 1.6kb. Narrow reaction rims suggest amphiboles did not stay for long (days) outside their stability field. Melt with this water content that experienced a steady adiabatic decrease in pressure would achieve water saturation, and subsequent reaction and dehydration of amphiboles at 1.6kbars of pressure (160Mpa). Amphibole grains at Suction Butte experience a successive increase and decrease in water pressure, resulting from the convective cycling of crystals within the magma chamber, so that at different heights within the pluton the crystal experienced different conditions of f_{H_2O} .

inclusions at Suction Butte cycled convectively through low pressures at the top of the magma chamber in the same manner interpreted for the independent amphibole crystals.

I conclude that the formation of titanomagnetite reaction rims around amphibole grains at Suction Butte records both a drop in pressure of the surrounding melt, and a rapid convective motion within the magma chamber. Individual amphibole grains repeatedly crossed the pressure stability limits for amphibole in the quartz latite magma.

Mafic Inclusions

Petrology and Petrography of Inclusions

The quartz latite plutons all contain abundant small (0.5-10cm), rounded to sub-rounded, very fine-grained, cusped, and evenly distributed mafic inclusions. The total mafic mineral content of the inclusions ranges from 50-75%. Many of the exposed inclusions are severely weathered, and range in color from medium gray to mixed black and white to black. Dominant phenocrysts that are visible in hand specimens are clinopyroxene, sanidine, biotite, and pseudomorphed olivine.

Mafic inclusions were examined both in thin sections and using X-ray fluorescence (XRF) whole-rock analyses. Due to severe weathering, alteration, and their typically small size (<3cm in diameter), only five inclusions were analyzed using XRF. Results compare well to data obtained by Tureck-Schwarz for shonkinite throughout the Bearpaws (Appendix I). See Table 7 for representative results.

Variations in inclusion chemistry can be seen in Al (8.3-12.6%), Mg (9.25-17.52%), and total alkali (3.6-7.4%) contents normalized to 100%. Two of the five samples had values for Al, Mg, and total alkalis that did not fit into the range of values identified as Bearpaw Mountains 'shonkinite' by Tureck-Schwarz (1992). However, data from Nash (1971) from shonkinite of the Shonkin Sag in central Montana provides a range of values that does incorporate those found in this study. These two samples can be considered either pyroxenite or shonkinite, but have Al values that are much higher than the normal range for pyroxenite of the Central Montana high-Potassium Province. Therefore, the two samples will also be considered "shonkinite" for the purposes of this study.

Table 7: Representative whole-rock analyses (inclusions)

Sample	from Deer Butte				
	MOS DB R	MOS DB 2	MOS DB 6	MOS DB 11	MOS DB I
Date	14-Oct-96	14-Oct-96	14-Oct-96	14-Oct-96	14-Oct-96
Rock	Shonkinite	Shonkinite	Shonkinite	Shonkinite	Shonkinite
Normalized Results (Weight %):					
SiO ₂	50.78	47.36	50.30	50.79	52.42
Al ₂ O ₃	9.29	12.16	8.36	11.77	12.67
TiO ₂	0.682	2.087	0.692	0.842	0.740
FeO*	10.94	13.85	11.60	9.67	9.42
MnO	0.152	0.204	0.153	0.166	0.164
CaO	6.92	7.94	6.92	9.13	7.09
MgO	16.10	9.71	17.52	9.49	9.25
K ₂ O	3.02	3.58	2.63	4.83	4.86
Na ₂ O	1.34	1.84	1.01	2.25	2.63
P ₂ O ₅	†0.77	†1.27	†0.82	†1.07	†0.76
K+Na	4.362	5.420	3.638	7.081	7.494
Total	100.00	100.00	100.00	100.00	100.00
Trace Elements (ppm):					
Ni	602	245	699	126	162
Cr	912	576	959	407	751
Sc	19	32	17	24	25
V	157	236	136	173	156
Ba	1720	1464	1537	†2952	†3712
Rb	121	129	111	165	162
Sr	441	321	373	752	973
Zr	112	379	103	149	129
Y	16	54	16	29	23
Nb	13.6	19.7	15.3	11.5	10.1
Ga	17	20	18	20	17
Cu	6	5	6	73	53
Zn	141	183	149	121	120
Pb	26	33	29	30	48
La	50	54	52	51	38
Ce	70	112	71	101	74
Th	10	4	8	2	0

*Major elements are normalized on a volatile-free basis, with total Fe expressed as FeO.
 "†" denotes values >120% of highest standards for P₂O₅ and Ba.

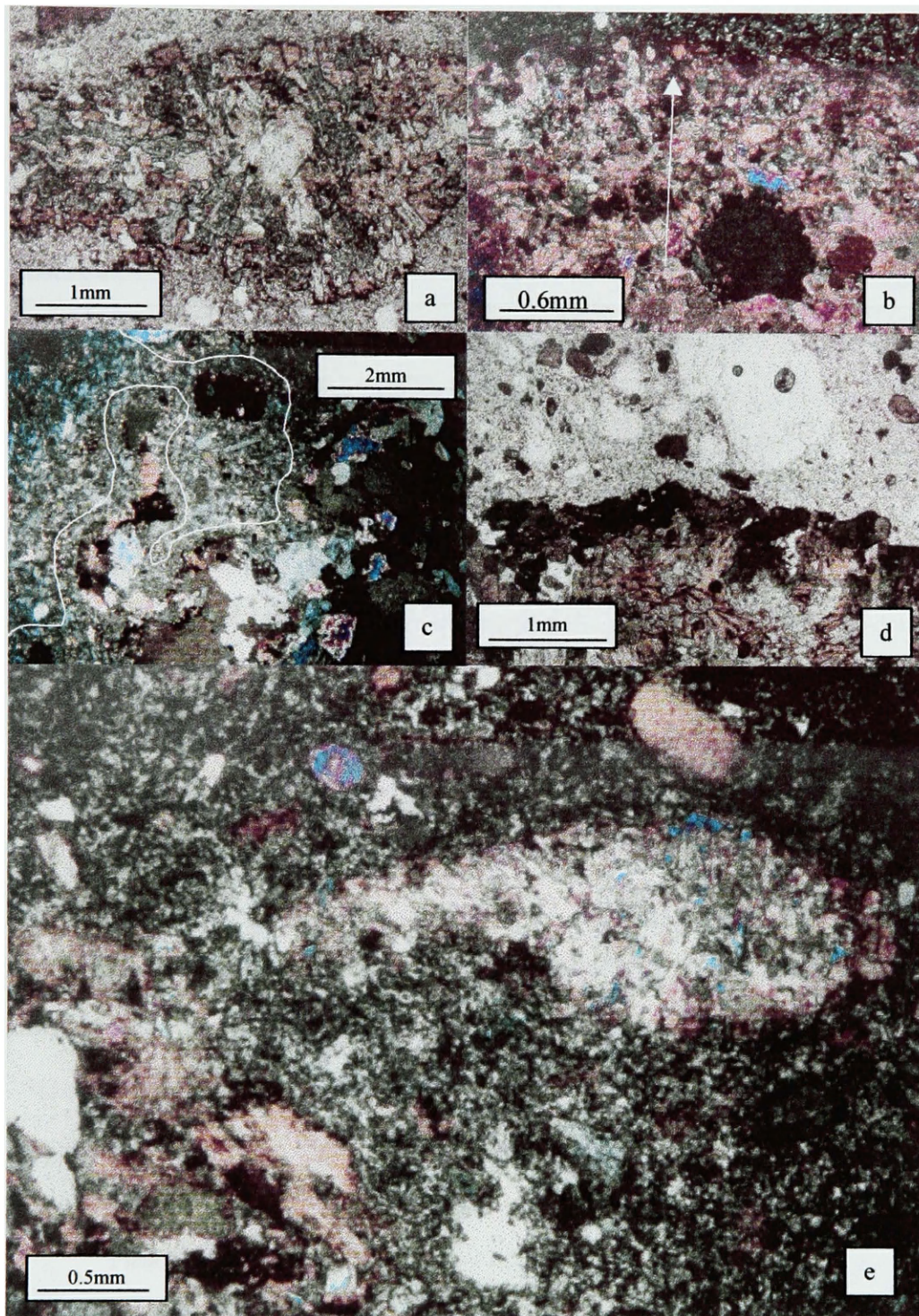


Figure 9: Shonkinite inclusions: (a) uniformly fine-grained shonkinite inclusion from Deer Butte; (b) shonkinite inclusion with decreasing grain size from core to rim. Arrow points from core to rim. Note the cusped margin at contact with surrounding latite at top of photo; (c) inclusion trailing off into host quartz latite. White line traces inclusion; (d) hastingsite rim surrounding shonkinite inclusion at McCann Butte; (e) tear-shaped, uniformly fine-grained drop of shonkinite pulling away from larger inclusion. Note the cusped margins of the inclusion.

Mineralogy of inclusions

Examination of 12 shonkinite inclusions in thin section shows them to contain salite clinopyroxene (25%), biotite (up to 30%), K-feldspar (up to 30%), titanomagnetite (up to 15%), analcime (up to 2%), iddingsite (up to 3%), aegerine-augite (up to 3%), and trace pseudoleucite. Biotite and hastingsite commonly form fine-grained reaction rims around inclusions (Figure 9). Larger inclusions have larger grain size, suggesting less rapid chilling. Larger inclusions tend to have larger crystals as you move inward from the inclusion border, whereas smaller inclusions are uniformly fine-grained (Figure 9). Trails of pyroxene, hastingsite, and biotite crystals are commonly seen trailing off or pinching out into the quartz latite (Figure 9). Titanomagnetite forms as much as 15% of the inclusions, and is most commonly associated with hastingsite rims and biotite.

Petrographic analyses of the mafic inclusions found within the quartz latite-dome bodies show textures which point to a state of disequilibrium between the inclusions and their host. The majority of the inclusions in the buttes are fine-grained mafic blobs whose sub-spherical, elliptical or even strung-out geometry suggests that the quartz latite and mafic magmas coexisted in a partly liquid state (Figure 9). Hand samples and petrographic examples show different stages of break-up within the less viscous mafic inclusions. Textures of several inclusions suggest the additional process of mechanical separation or disaggregation of inclusions following initial chilling (Figure 10). Definitive evidence for this process consists of all stages of inclusion disaggregation at both outcrop and thin-section scales. Four different stages of breakup can be identified, and are chronicled in the photographs below (Figure 10). In places, the breakup of the inclusions resembles something more like brecciation, which is likely due to the significant viscosity difference between the quartz latite and shonkinite magmas (Figure 10).

Fine-grained margins, and grain size that decreases from the center on many of the larger inclusions suggests that the mafic magma chilled only upon entering the quartz latite magma (Figure 9). Extreme temperature difference between the latite (~750°) and shonkinite (~1000°) caused the borders of larger inclusions to chill, while smaller inclusions crystallized completely as uniformly fine-grained masses (Figure 9). Phenocryst and microphenocryst-laden streaks are observed trailing off inclusions in many thin sections and in outcrop (Figure 9, 10).

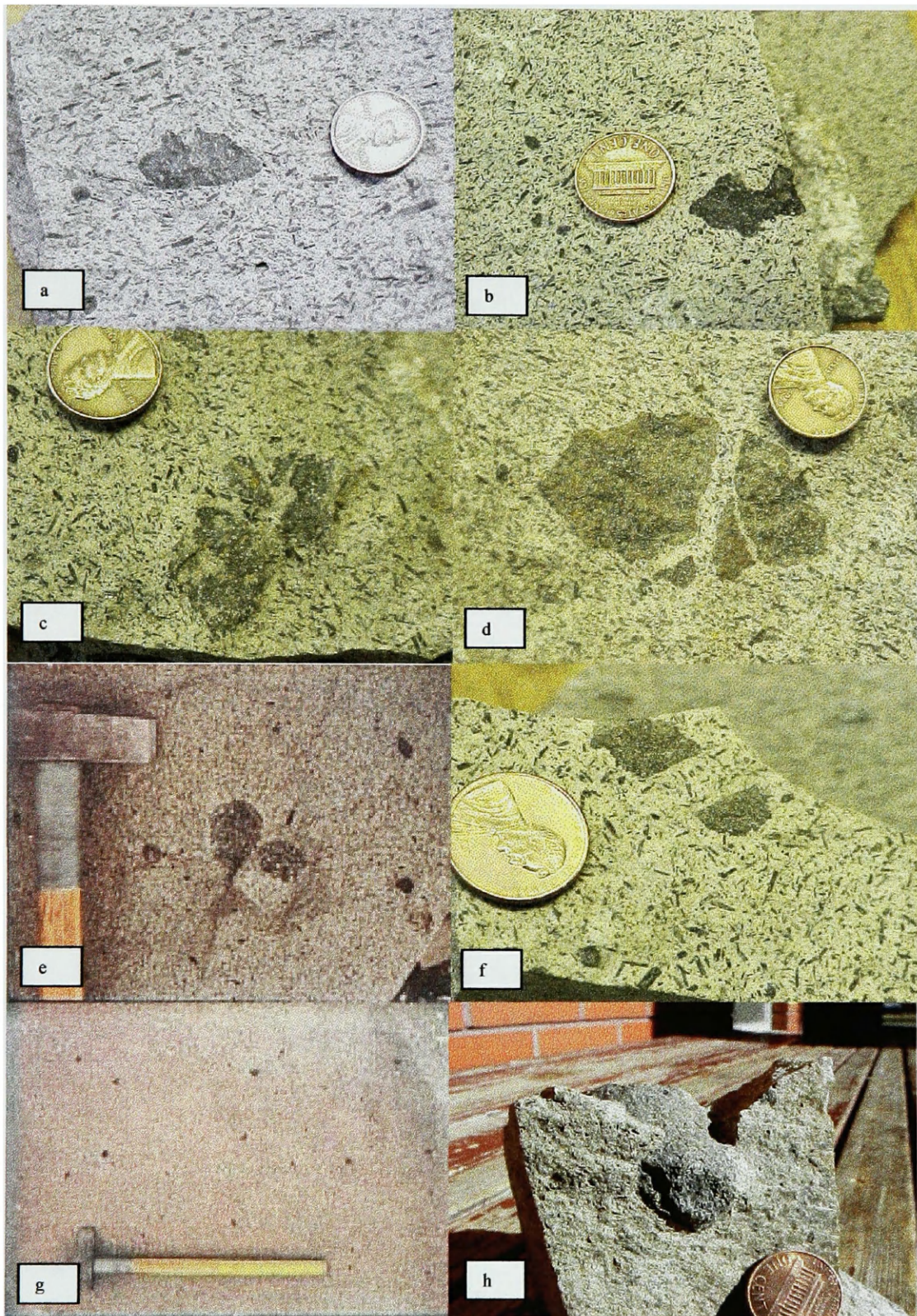


Figure 10: Four different stages of inclusion disaggregation: (a) stage 1; (b) stage 2; (c) stage 3; (d) stage 4; (e) single inclusion separating into two smaller, round inclusions; (f) small, fine-grained, brecciated shonkinite inclusion with an amphibole reaction rim; (g) distribution of small shonkinite inclusions at Suction Butte; (h) 3-dimensional view of ellipsoidal shonkinite inclusion. Penny (1.5cm in diameter) and hammer (handle ~4cm wide) provided for scale.

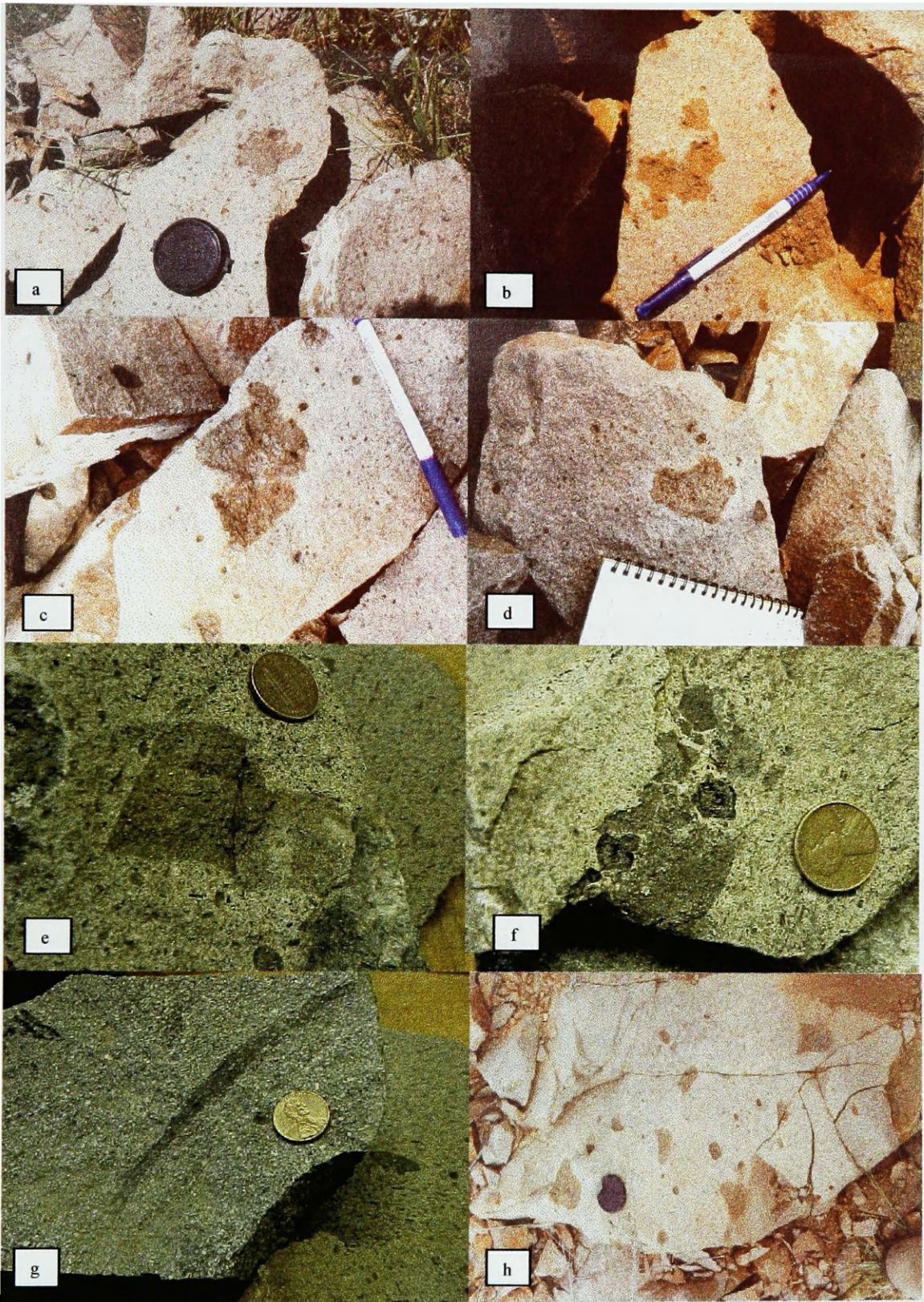


Figure 11: Shonkinite inclusion textures: (a-e) large shonkinite inclusions showing different stages of disaggregation from Deer Butte. Note the very thin felsic halo surrounding the large inclusion in (d); (f) shonkinite inclusion from McCann Butte showing significant breakup and formation of 2 anomalously large amphibole crystals in a reaction with presumably dry quartz latite melt; (g) shonkinite “schlieren” from Hansen Butte quartz latite; (h) distribution of inclusions at Deer Butte. Penny (1.5cm in diameter), pen (12cm in length), notebook (13cm along spiral), and lens cap (5.2cm in diameter) shown for scale.

Hastingsite amphibole forms directly adjacent to or rimming many of the inclusions (Figure 7d, 11f) at Deer Butte and McCann butte, quartz latite plutons that do not bear hastingsite as a major phenocryst phase. Assuming the plutons to be relatively dry due to the shallowness of their emplacement, the crystallization of hydrous phases such as hastingsite as a reaction mineral between co-existing quartz latite and shonkinite melts suggests that the shonkinite magma may have provided some water.

At the deepest exposure of the Deer Butte pluton, many of the largest inclusions (10-30cm in diameter) have a light-colored halo surrounding them, where felsic constituents migrated out of the inclusion in the beginning stages of chemical mixing or mingling, or quartz latite crystal mush began to locally melt (Figure 11). Inclusions with gradational contacts caused by very local (2-4mm halo) diffusional mixing are considered in equilibrium with their hosts (Didier, 1973; Didier & Barbarin, 1991). These larger inclusions could begin to hybridize with the surrounding magma because of the relatively longer time it took to cool within the host. Many felsic haloes around mafic inclusions in granites (Pabst, 1928, p. 341; Didier, 1973), may have formed by expulsion of residual melt.

If gas filter pressing operates in the plutonic environment, in situ differentiation of larger inclusions and expulsion of residual liquids could produce marked compositional effects, given the time scale of plutonic crystallization. If so, inclusions in plutons might be more mafic than their volcanic counterparts for a given host composition. This does not appear to be the case here, as the inclusions in the plutons are compositionally consistent with those seen in the pyroclastic deposits. Further studies of the texture, composition, and distribution of mafic inclusions in granite rocks may answer some of these questions (Bacon, 1986). Suction Butte inclusions are for the most part so small that this diffusion is not apparent. They may have released their heat and crystallized in the surrounding quartz latite before cations could be exchanged with the quartz latite in an attempt to hybridize.

Abundance and Distribution of Inclusions

I conducted point counts at fresh outcrops of Deer Butte to gain a sense of the distribution and proportion of the mafic inclusions. By point counting, I was able to evaluate the distribution of mafic inclusions throughout the pluton, and to estimate what minimum % volume of the mafic magma was dispersed through the plutonic bodies (Appendix IV). The point counts used a 36in x 36in (91.4cm x

91.4cm) sheet of transparent plastic upon which a grid with 1 inch (2.54cm) blocks was drawn with permanent marker. The number of grid intersections falling on mafic inclusions gauged the % shonkinite by volume of the rock.

At road level (SENE1/4, Section 34, T20N, R19E) in the deepest part of the pluton, the mean number of inclusions determined from 10 sites normalized to a 36in x 36in (91.4cm x 91.4cm) provided 55.3 inclusions and a mean estimated % volume of shonkinite of 2.32%.

At the summit of Deer Butte, some 200m higher in elevation, the mean density of inclusions from 7 sites provided 72.3 inclusions and a mean estimated % volume of shonkinite of 1.75%.

At the base of large outcrop on the NE flank of Suction Butte, the mean density of inclusions at 9 sites provided 44.8 inclusions and a 1.0% mean estimated volume of shonkinite. Nine sites 180m higher on the NW slope of the butte (9) contained 62.8 inclusions of smaller size, corresponding to an estimated 1.0% by volume of shonkinite magma.

Therefore, while the size and estimated volume of the mafic inclusions at Deer Butte and Suction Butte decreased at higher elevations within the plutons, the number of inclusions increased towards the top, suggesting greater breakup of the shonkinite magma in the upper part of the magma chamber. Disaggregation and brecciation of magmatic inclusions can be seen in Figure 10. I interpret this breakup to be the result of vigorous convection within the magma chamber.

Miarolitic Cavities

Big Timber and McCann Buttes both contain areas of abundant miarolitic cavities at shallow levels in the plutons. At the Big Timber Butte locality, large boulders of gas-vesicle laden quartz latite can be observed blanketing the flanks of nearly the entire intrusion, as well as outcropping and sitting on top of the southern platform (Figure 12a). Point counts were made using a 36in x 36in (91.4cm x 91.4cm) sheet of transparent plastic with a 1 inch (2.54cm) grid. The mean number of miarolitic cavities for 20 outcrops at Bit Timber Butte was 137.25 per 36 in² area. The estimated mean % by volume of these same 20 sites was 5.58%, with a significant standard deviation as values ranged from 1-25% (Appendix V).

Miarolitic cavities in samples found at the contact between overlying sands and the quartz latite showed significant preferred orientation. If the orientation of the overlying sediments were extended out

Big Timber Butte: Pooled gas at the top of a magma chamber flank

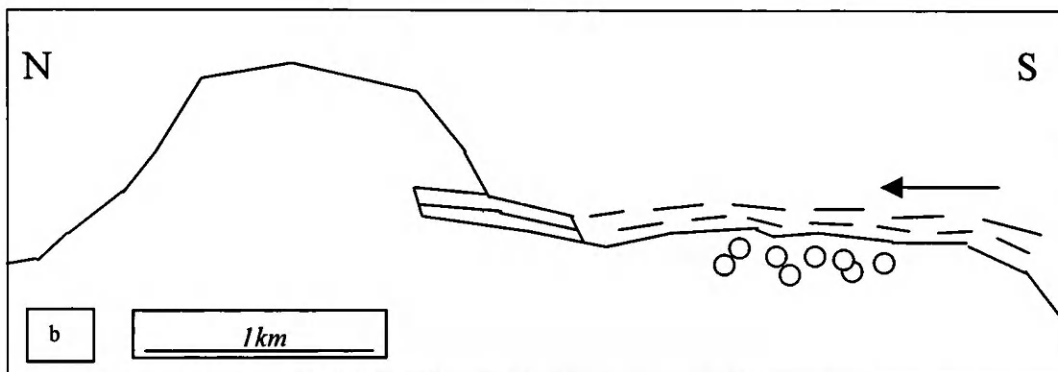
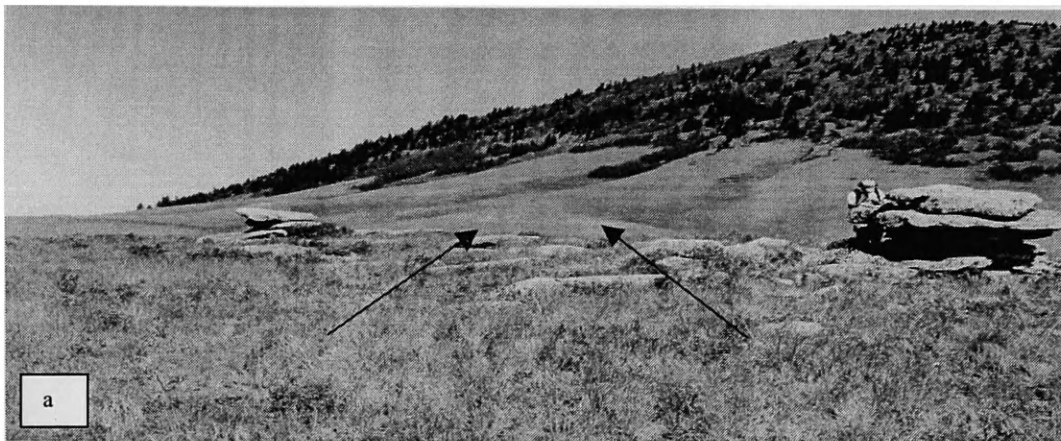
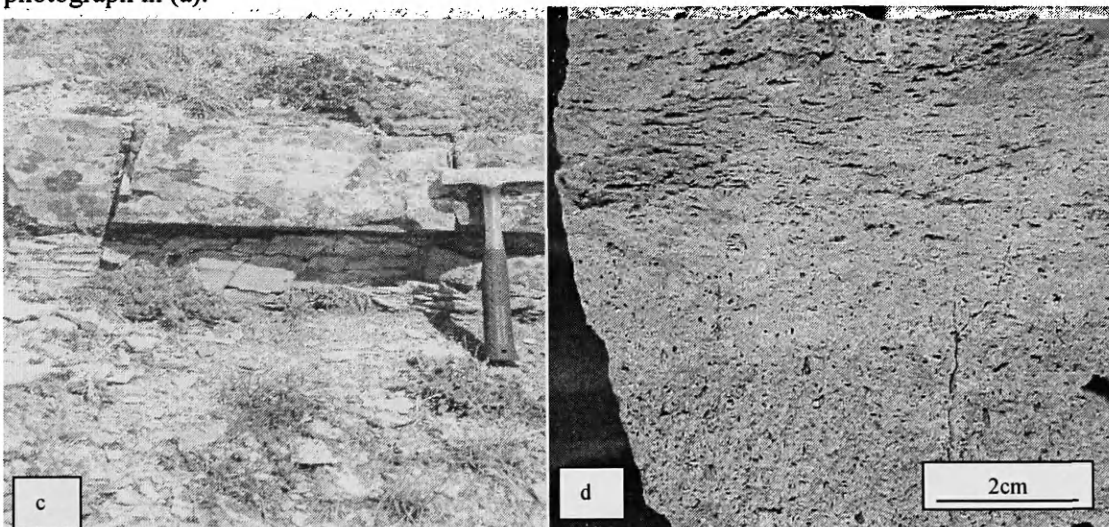


Figure 12: Pooled volatiles at Big Timber Butte: (a) large, vesicle-laden quartz latite blocks on southern flank of Big Timber butte. Arrows pointing to horizontal sedimentary strata 500 meters north of outcrops; (b) sketch of cross section (N-S) of Big Timber Butte. Dashed lines represent inferred orientation of sedimentary rocks over the pluton. Arrow shows the direction which the camera was pointed for the photograph in (a).



(c) contact between Big Timber Butte quartz latite and overlying sedimentary unit; (d) close-up look at quartz latite showing elongate gas vesicles parallel to the contact with sedimentary unit.

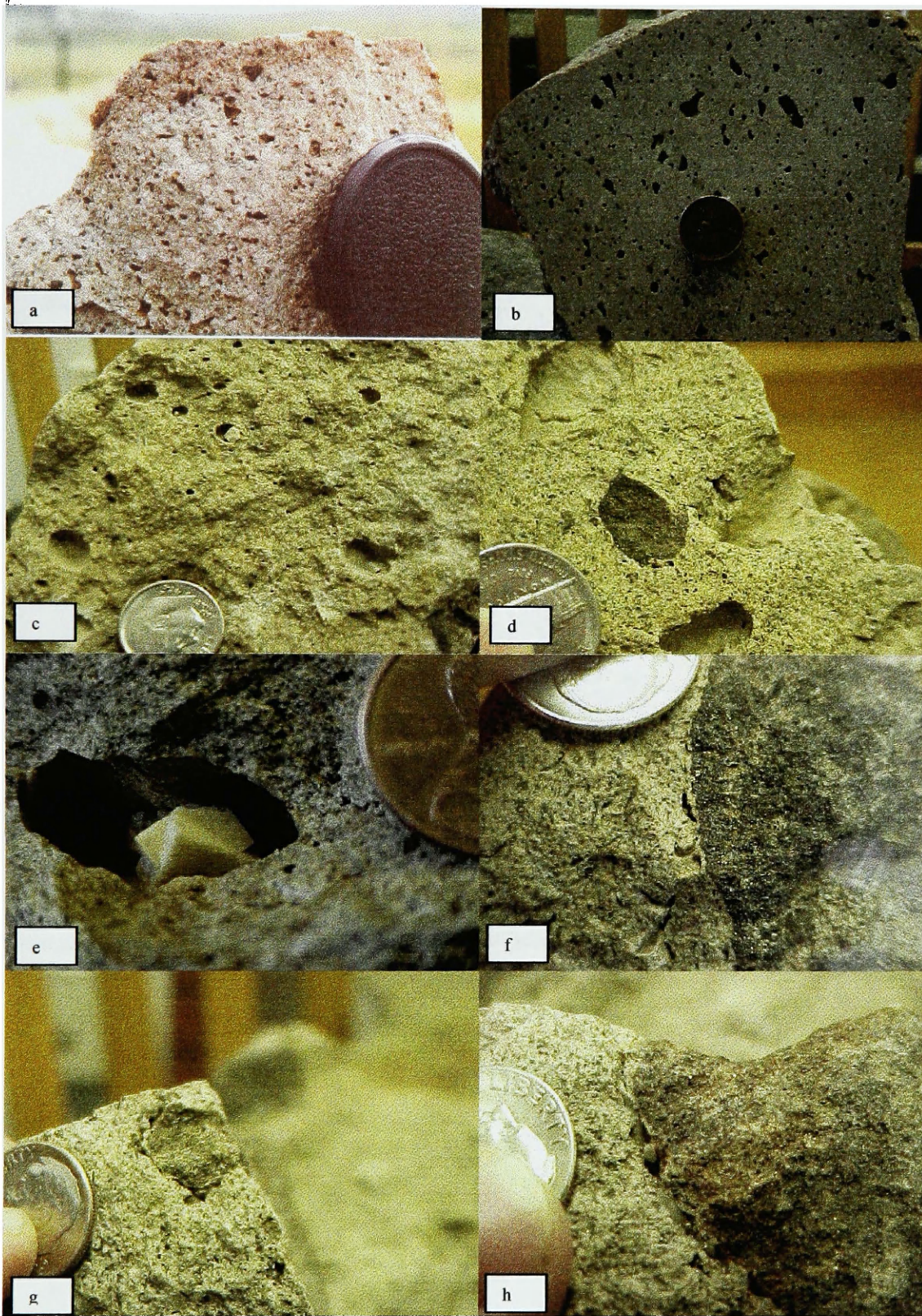


Figure 13: Mirolitic cavities: (a&b) photographs showing abundant, irregularly shaped gas vesicles up to 1cm in length (Big Timber Butte); (c) large sub-spherical gas vesicles at McCann Butte; (d) three large gas vesicles surrounding sub-spherical shonkinite inclusion; (e) beautifully twinned phillipsite crystals within large mirolitic cavity (2cm x 1.2cm); f,g,h.) mirolitic cavities on the margins of three shonkinite inclusions. Note the terminating quartz prisms in (h). Dime (1.25cm in diameter), nickel (1.5cm), penny (1.5cm), and lens cap (5.2cm) for scale.

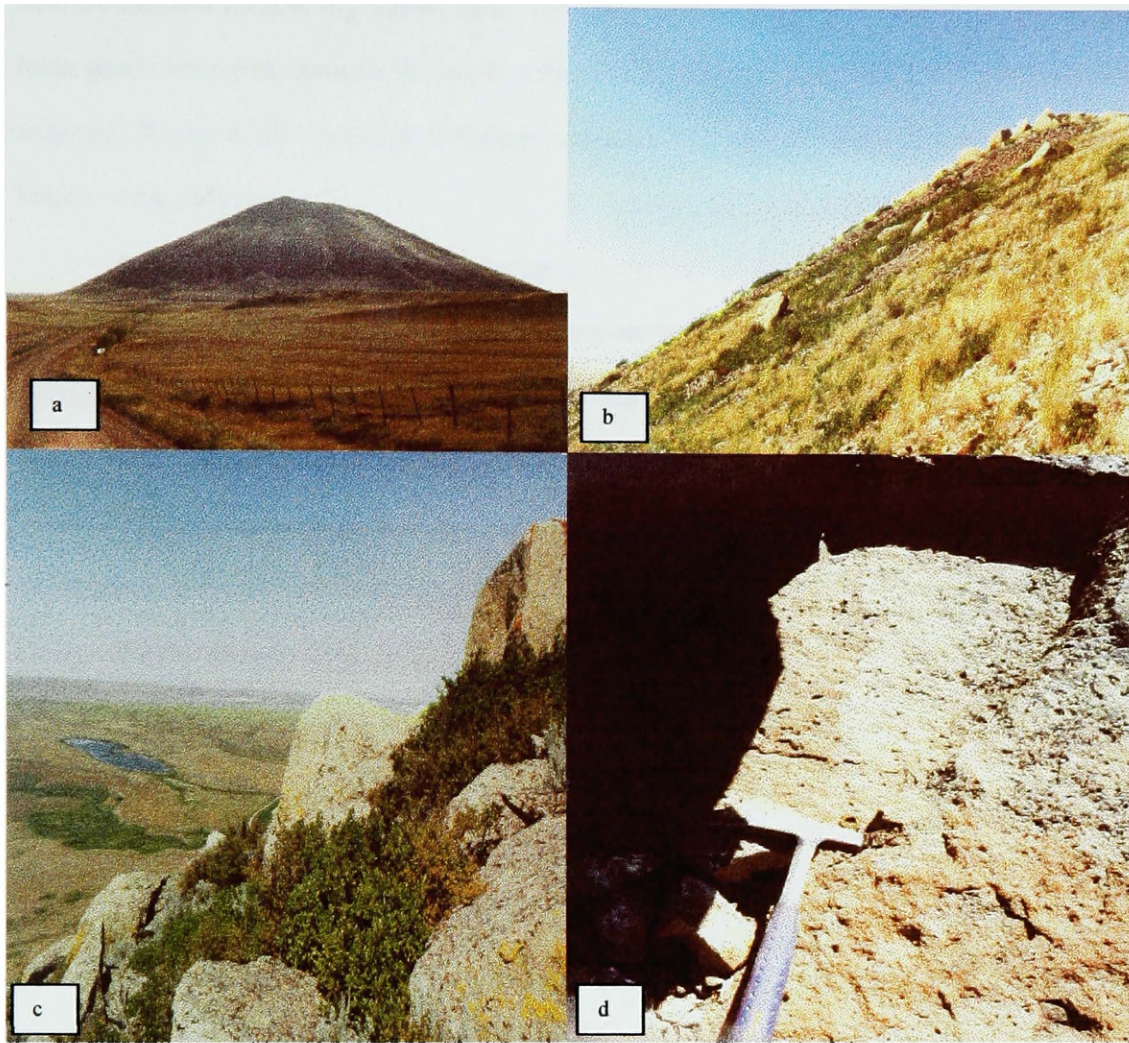


Figure 14: McCann Butte: (a) photograph of McCann Butte facing east along People's Creek Road; (b) top of McCann Butte. Large, vesicle-laden blocks can be seen concentrated at the peak and beginning to slide down the side of the butte; (c) view from the top of McCann Butte looking over large gas filled quartz latite blocks; (d) close-up view of vesicles in large quartz latite blocks. Hammer (handle 25cm in length) for scale.

onto the southern flank of Big Timber Butte, still 180m above contacts with other units, the outcrop of felsic quartz latite with abundant miarolitic cavities on the southern flank would be less than 20m below the sediments (Figure 12b). Therefore, the observed miarolitic cavities are likely pooled at the top margin of a branch of the intrusion.

Importantly, abundant small inclusions (2-6mm) can be seen in the miarolitic cavity-rich quartz latite. In some cases the mafic inclusions are strung out between gas vesicles, apparently connecting them. Dominantly spherical geometry would indicate cooling prior to complete gas exsolution (Sparks et al., 1994). Although locally the miarolitic cavities are spherical in shape, the majority of them have a convoluted and irregular geometry, suggesting that the host magma had completed gas exsolution, and was experiencing irregular, turbulent flow or flattening due to expansion as pressure was released within the magma chamber (Figure 12d).

At McCann Butte, the miarolitic cavities were seen in extremely large boulders that appeared to concentrate on top of the geometrically equidimensional butte (Figure 13). The mean number of miarolitic cavities seen at 20 outcrops at the summit of McCann Butte was 146.7. The mean estimated % by volume consisting of cavities was 9.85%, almost double that at Big Timber Butte.

Instead of fracturing in a sheet-like fashion as most of the dome quartz latite does, the boulders at the summit of McCann Butte appear blocky and irregular, and are extremely hard (likely a quartz matrix). The quartz latite itself appears much more felsic in chemistry than the rest of the plutonic rock. Most of the quartz latite blocks at the top of the butte do not appear to be in situ, but rather look like they settled on the top of the dome after a collapse of the magma chamber vent, or perhaps some kind of erosion event. The miarolitic cavities are locally flattened, but are mostly irregular and convoluted in shape. Although there are many vesicles as large as 2.5cm in length, there are thousands of tiny vesicles (<2mm) that are too numerous to count.

The cavities typically contain euhedral mineral grains that grew into the available space. Among the observed cavity minerals are quartz, orthoclase, and chlorite “flakes” or other secondary alteration minerals. In one spectacular sample, a larger miarolitic cavity contains twinned phillipsite crystals about 1cm in diameter (Figure 13). As at Big Timber Butte, abundant small mafic inclusions are present in the cavity-rich rock.

The presence of vesicles at the tops of plutons is interpreted to result from the pooling of exsolved volatiles at the top part of the Big Timber Butte and McCann Butte magma chambers. The volatiles either exsolved from the quartz latite melt as it ascended from depth, or exsolved from the shonkinite inclusions as they cooled in quartz latite. The shallow depth of emplacement of both plutons (<2.0 kbars) makes it unlikely that water remained dissolved in the quartz latite melt or as gas bubbles: it would be driven off as steam into the surrounding country rocks or fractures. It is indeterminable whether the shonkinite inclusions in the plutonic bodies ever vesiculated. However, the presence of vesicles enclosing plutonic inclusions and in the inclusions of equivalent pyroclastic quartz latite suggests that volatile phases were present. This does not guarantee they exsolved prior to eruption. The lack of vesicles in plutonic shonkinite inclusions could mean that vesicles were destroyed during final consolidation of the pluton. Of note is the presence of miarolitic cavities enveloping inclusions at McCann Butte and Big Timber Butte (Figure 13). The amount of gas exsolving from the quartz latite and/or shonkinite melts and nucleating on the inclusions might have been sufficient to buoyantly “float” the inclusions upward through the magma.

Convection

Whole-rock analyses

Whole-rock analyses were used to determine the extent of chemical mixing and convection that took place within the magma chamber. See Table 8 for representative analyses. X-ray fluorescence whole-rock analyses of 20 samples from dispersed localities on Deer Butte was conducted using the facilities at Washington State University in Pullman. The accuracy and precision of the data from the GeoAnalytical lab is good. Standard sample calibration curves which plot best fit lines through a graph of x-ray intensity vs. theoretical intensity provide a good estimate of accuracy (See Appendix II).

For most major elements the variation between the two standard sample beads is of the same order as their variation from the given value, with the inference that imprecision resulting from the preparation of the beads is equal to or greater than inaccuracies caused by inadequate matrix and interference corrections. Percentages are all well within the range of quartz latite. With the exception of Na, the total discrepancies from the “given” values are less than might reasonably be expected between two random samples collected

in the field from the same rock unit – lava flow, igneous intrusion, etc (Appendix II). Hence, this degree of inaccuracy may be regarded as insignificant for most purposes of geologic correlations or petrogenetic modelling. (Washington State University GeoAnalytical Labs)

The 20 quartz latite samples correlated well with previous work done by Tureck-Schwarz on similar rocks in the Bearpaw Mountains area. Mg and Ca showed the greatest variance, with standard deviation values that were 16% and 14%, respectively, of the calculated mean. However, there were no anomalous or extreme values which would lead one to believe the magma had significant chemical variation resulting from assimilation of country rock, hybridization, differentiation, differential settling, or local convection.

Although phenocryst type and size showed significant variation at hand-sample scale, this data shows overall homogenous chemistry for the entire pluton. The homogeneity breaks down at the cm scale, as seen in the variations in pyroxene and biotite content and the extent of resorption variation within a single thin section. Uniformity of composition of the bulk magma suggests that the pluton experienced convection which inhibited differentiation products from settling out and aided the distribution of dense shonkinite inclusions and salite xenocrysts from the shonkinite magma into the highest part of the pluton.

Hornblende Lineation

At Star Butte, the orientation of hornblende phenocrysts was measured to examine the uniformity of their lineation, to see if the pluton had undergone convection. Outcrops were exposed well enough to ascertain averages of hornblende crystal orientations for 11 locations. Twenty five trend and plunge measurements of individual grains were made at each of the 11 outcrops, from which a mean trend and plunge was calculated. Hornblende crystals were only measured where a three dimensional orientation could be seen. The dips varied from 25-52 degrees, but nearly all hornblende crystals pointed down and away from the center of exposure. Nine of the 11 means dip towards the NW quadrant, as there was significantly more outcrop on the W/NW side. The two means that were gathered from the eastern side of the butte plotted in the SE and NE quadrants, showing close to a 180 degree swing in the orientation of dip. Figure 15 shows the location and mean trend and plunges of the 11 outcrops.

Table 8: Representative whole rock analyses (latite)

From Deer Butte

Sample	MOS DB 1	MOS DB 5	MOS DB 10	MOS DB 14	MOS DB 17	MOS DB 19	MOS DB 22	MOS DB 25	MOS DB 29	MOS DB 33
	Normalized (weight.%)									
Date	13-Oct-96	13-Oct-96	13-Oct-96	13-Oct-96	13-Oct-96	13-Oct-96	13-Oct-96	13-Oct-96	14-Oct-96	14-Oct-96
Rock	Qtz. Latite	Qtz. Latite	Qtz. Latite	Qtz. Latite	Qtz. Latite	Qtz. Latite	Qtz. Latite	Qtz. Latite	Qtz. Latite	Qtz. Latite
SiO ₂	64.97	64.93	65.09	65.16	64.61	64.90	64.90	64.96	65.08	62.95
Al ₂ O ₃	15.08	15.10	15.25	15.33	15.17	15.17	15.25	15.29	15.29	14.81
TiO ₂	0.333	0.328	0.320	0.333	0.327	0.327	0.327	0.323	0.310	0.376
FeO*	3.56	3.56	3.38	3.71	3.75	3.64	3.65	3.65	3.59	4.62
MnO	0.074	0.065	0.078	0.070	0.076	0.076	0.078	0.075	0.066	0.079
CaO	3.28	3.21	3.23	2.69	3.49	3.14	3.16	2.93	2.94	4.19
MgO	2.70	2.79	2.64	2.65	2.65	2.72	2.55	2.70	2.64	3.24
K ₂ O	4.81	4.82	4.61	4.77	4.65	4.71	4.78	4.85	4.73	4.67
Na ₂ O	4.92	4.93	5.15	5.02	5.01	5.05	5.05	4.96	5.11	4.75
P ₂ O ₅	0.266	0.263	0.256	0.266	0.264	0.271	0.259	0.259	0.250	0.325
K+Na	9.737	9.752	9.760	9.786	9.655	9.761	9.826	9.818	9.836	9.414
Total	100.00	100.00	100.00	100.00	100.00	100.00	100.00	100.00	100.00	100.00
	Trace Elements (ppm):									
Ni	61	59	52	61	67	53	54	61	57	72
Cr	121	124	117	121	112	119	114	111	103	147
Sc	7	7	11	12	8	7	11	8	8	10
V	59	61	57	67	59	56	55	52	58	82
Ba	†2402	†2382	†2329	†2380	†2360	†2550	†2352	†2386	†2390	†2313
Rb	133	134	129	132	132	131	135	139	129	132
Sr	881	879	996	900	820	932	1033	1029	1001	980
Zr	141	136	141	141	141	144	146	143	142	142
Y	13	12	11	13	13	13	13	12	12	13
Nb	11.2	11.1	12.3	11.2	10.6	10.1	10.5	10.7	10.9	11.3
Ga	15	16	15	16	14	15	15	15	13	16
Cu	16	14	18	14	11	20	21	19	24	26
Zn	39	41	50	39	37	43	55	49	43	45
Pb	27	29	45	27	34	57	43	43	36	20
La	21	23	36	38	19	30	33	20	23	37
Ce	43	40	35	38	45	41	46	31	40	50
Th	8	6	8	7	8	9	6	7	8	9

*Major elements are normalized on a volatile-free basis, with total Fe expressed as FeO.

"R" denotes a duplicate bead made from the same rock powder.

"†" denotes values >120% of the highest standard for Ba.

Star Butte: Hornblende Orientations

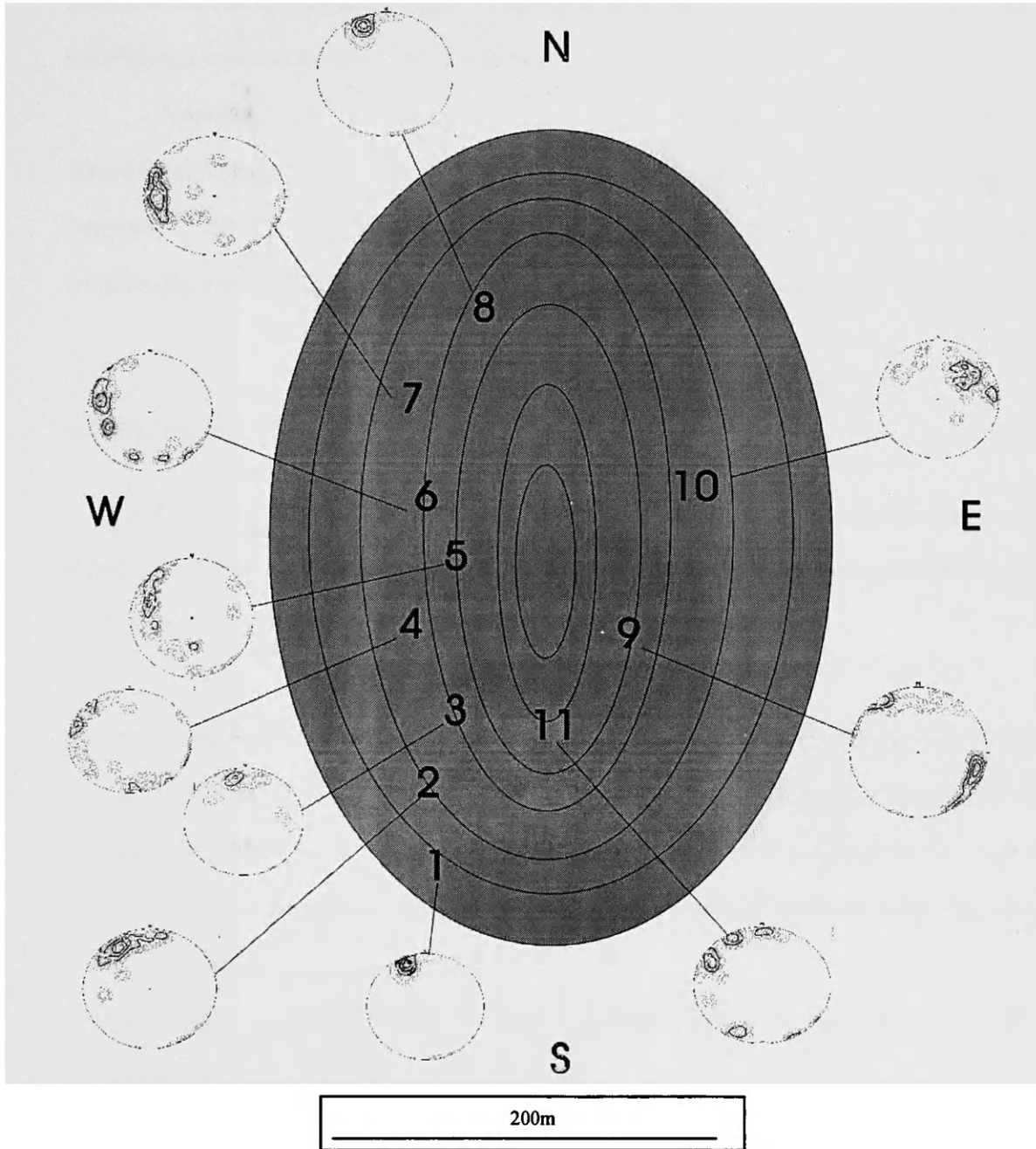


Figure 15: Star Butte hornblende orientations. Twenty five trend and plunge measurements of individual crystals were made at each of the 11 outcrops, from which mean trend and plunges were calculated. Nearly all of the individual crystals point down and away or up and towards the center of the exposed pluton, and parallel with the preferred orientation of fracture at the outcrops, suggestive of a convective flow pattern. Outcrops 5, 6, and 11 are good examples of how that individual grains lie in parallel planes that shallowly dip away from the center of the pluton.

Because of the significant topographic relief at Star Butte, and the proximity of sedimentary country-rock contacts, I interpret that most of the exposure is near the margins and also relatively near the top of the pluton. Based on this interpretation, the alignment of the hornblende crystals suggests a flow pattern which was moving magma down and away or up and towards the center of the butte, either option pointing to convective motion within the pluton.

A similar phenomenon was observed at Suction Butte, where the hornblende crystals commonly showed alignment that lay in a horizontal plane, and parallel with the preferred direction of fracture at the outcrops. There were also “flow corridors” at Suction Butte, observable on a smaller scale where hornblendes were aligned in a long, narrow region (3-5cm width extending for several meters).

Cooling rates within plutons

Estimates were calculated for the rate (in years) that it will take an igneous body of known size and initial temperature to thermally equilibrate (crystallize) with surrounding wet country rocks. Equations were obtained from Jaeger (1959), who made the following assumptions:

- a) The country rock is initially at a constant temperature, which will be taken as the zero of temperature, and at zero time, $t = 0$, magma is brought suddenly into contact with it. After intrusion, it is assumed that there is no motion of the magma. If there was movement in the magma (convection), it would move hotter magma against cooler country rocks, thereby cooling the pluton faster. Thus, the calculated time would be maximum.
- b) The magma has a definite melting point at temperature T_1 (relative to the country rock at zero temperature) and is intruded at this temperature.
- c) The country rock has thermal conductivity K_0 , density ρ_0 , specific heat c_0 , diffusivity $\delta_0 = K_0/\rho_0c_0$, and solidified magma has corresponding values K_1 , ρ_1 , c_1 , and δ_1 .
- d) The effects of transport of heat by volatiles from the magma and convection in the magma will be neglected.

Supposing a sheet of thickness D meters at its melting temperature T_1 is intruded into wet sediments which are assumed to extend indefinitely on either side. Crystallization will proceed inward from both contacts, the magma between the planes of crystallization remaining liquid (100% melt) at temperature T_1 . Assuming the initial temperature T_1 of the quartz latite magma to be 700°C , its thermal conductivity $K_1 = 0.0057$, and diffusivity $\delta_1 = 0.009$, the density (ρ_0) of country rocks = 2.8, and the specific heat (c_0) of wet country rocks = 0.25, this time of solidification (crystallization) t_s is given in years by:

$$t_s = (2D^2/8\delta_1^2\delta_1) \times 10^{-5}$$

where δ_1 is the root of $8(\Phi + \text{erf}\delta)e^{\delta^2} = c_1T_1/L_1B^{1/2}$

All of the plutonic bodies in the eastern Bearpaw Mountains are shallowly emplaced intrusions, whose sub-spherical shape will be treated as a sheet of a known thickness with parallel sides, assumption that the melt is static and is not subject to any kind of movement or convection. Using an estimated thickness (D) of 2000m for the plutonic bodies of the eastern Bearpaw mountains, a range of moderate porosities (0.05-0.2) as expected for shales, sandstones, and other fine-grained siliciclastic rocks, and a 300°C boiling point for water in rocks under at least 85.9 atm, the expected time of crystallization is anywhere from 30,000 - 35,000 years.

Felsic Pyroclastic Rocks

Rock types, texture

Felsic pyroclastic rocks can be seen in areas southwest and northwest from the cluster of plutonic quartz latite buttes. Three localities with abundant exposure and minimal weathering and alteration are the focus of the present study; Volcano Canyon, Extrusive Top, and Crooked Creek (see Figure 1).

At several localities in what is known as the Southern Volcanic Field, tuff and tuff-breccia deposits are interlayered; all contain abundant mafic inclusions in either quartz latite blocks or by themselves within the ash. At Volcano Canyon and Extrusive Top, these pyroclastic quartz latite deposits range from pink to pale green, are locally altered, and are ubiquitously porphyritic. The fine ash deposits are commonly flecked with tiny biotite crystals. The brecciated layers contain blocks of quartz latite as large

as 1.5m across, with plenty of inclusions visible, and locally chunks of wood and other organic debris. Locally, ash-fall deposits are evident, and sometimes show upward gradation from coarse to fine ash. The felsic chemistry and abundance of irregularly shaped gas vesicles make the blocks resemble the quartz latite found at the top of Big Timber Butte and McCann Butte. The felsic pyroclastic deposits are volumetrically smaller than the mafic pyroclastic deposits in both the southern and northern volcanic fields in the Bearpaw Mountains. Most of the volcanic rock deposited at distances greater than a 40km radius has been eroded away.

Shonkinite Inclusions

Shonkinite inclusions can be seen in quartz latite blocks, floating in quartz latite ash layers and matrix material, and in some cases are a part of both quartz latite blocks and ash in the pyroclastic deposits. The inclusions contain abundant gas vesicles that are usually spherical in shape (Figure 16), and much larger than any of the mineral grains (up to 6mm in diameter).

The shonkinite inclusions are spherical to elongated in shape, very fine-grained, cusped along margins, and appear to be widely distributed. Shonkinite inclusions in the pyroclastic rocks are texturally, mineralogically, and geometrically equivalent to those observed in plutonic rocks. Clinopyroxene, biotite, sanidine, plagioclase, and pseudomorphs of olivine are the dominant mineral phases, and locally grow euhedrally into vesicles in the inclusions.

Mineralogy of Pyroclastic Deposits

Mineral assemblages present in erupted melt allow for the determination of the thermodynamic conditions prevailing in the chamber prior to eruption. Clinopyroxene, biotite, K-feldspar, and plagioclase are the dominant mineral phases in quartz latite ash and blocks. Mineral phases are examined in all pyroclastic rock types and described as follows:

Clinopyroxene (+2V= 44°) grains in the ash and quartz latite blocks (25% of phenocrysts) are euhedral to subhedral, 1-4mm in length, and is locally pseudomorphically replaced by biotite, or a secondary alteration mineral. Clinopyroxene in the shonkinite inclusions within the pyroclastic quartz latite, however, is usually subhedral to anhedral, of smaller size (<2mm), and appears to have been slightly resorbed.

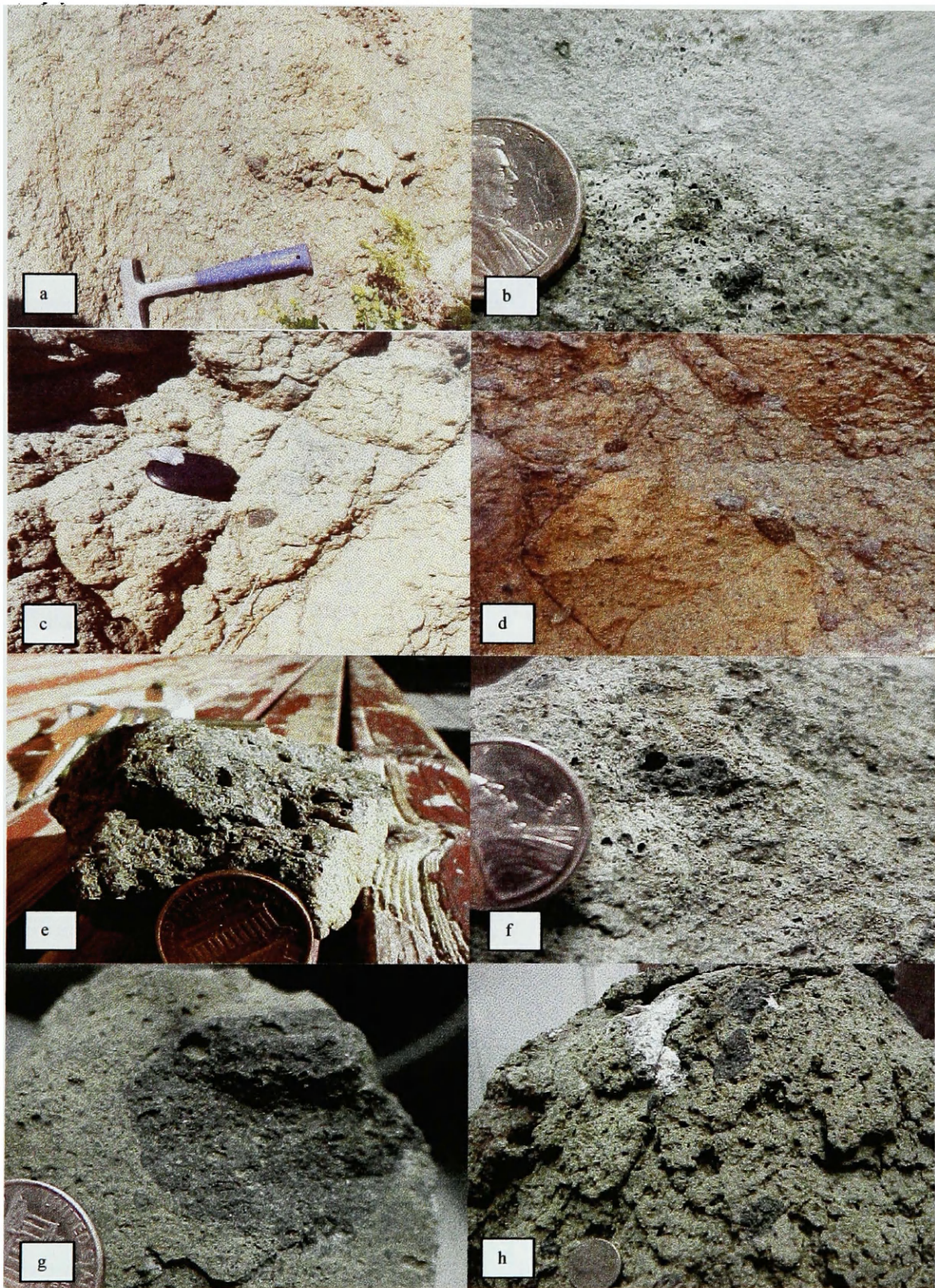


Figure 16: Inclusions in pyroclastic rocks: (a-c) subspherical shonkinite inclusions “floating” freely in quartz latite ash layers; (d) shonkinite inclusion in both quartz latite block and surrounding ash (field of view 1.5 meters wide); (e) large inclusion from pyroclastic quartz latite block with abundant spherical vesicles 2-4mm in diameter; (f) tiny shonkinite inclusion with abundant gas vesicles; (g) shonkinite inclusion with gas vesicles; (h) distribution of inclusions in large block of pyroclastic quartz latite. Penny (1.5cm in diameter), lens cap (5.2cm), and hammer (25cm long) for scale.

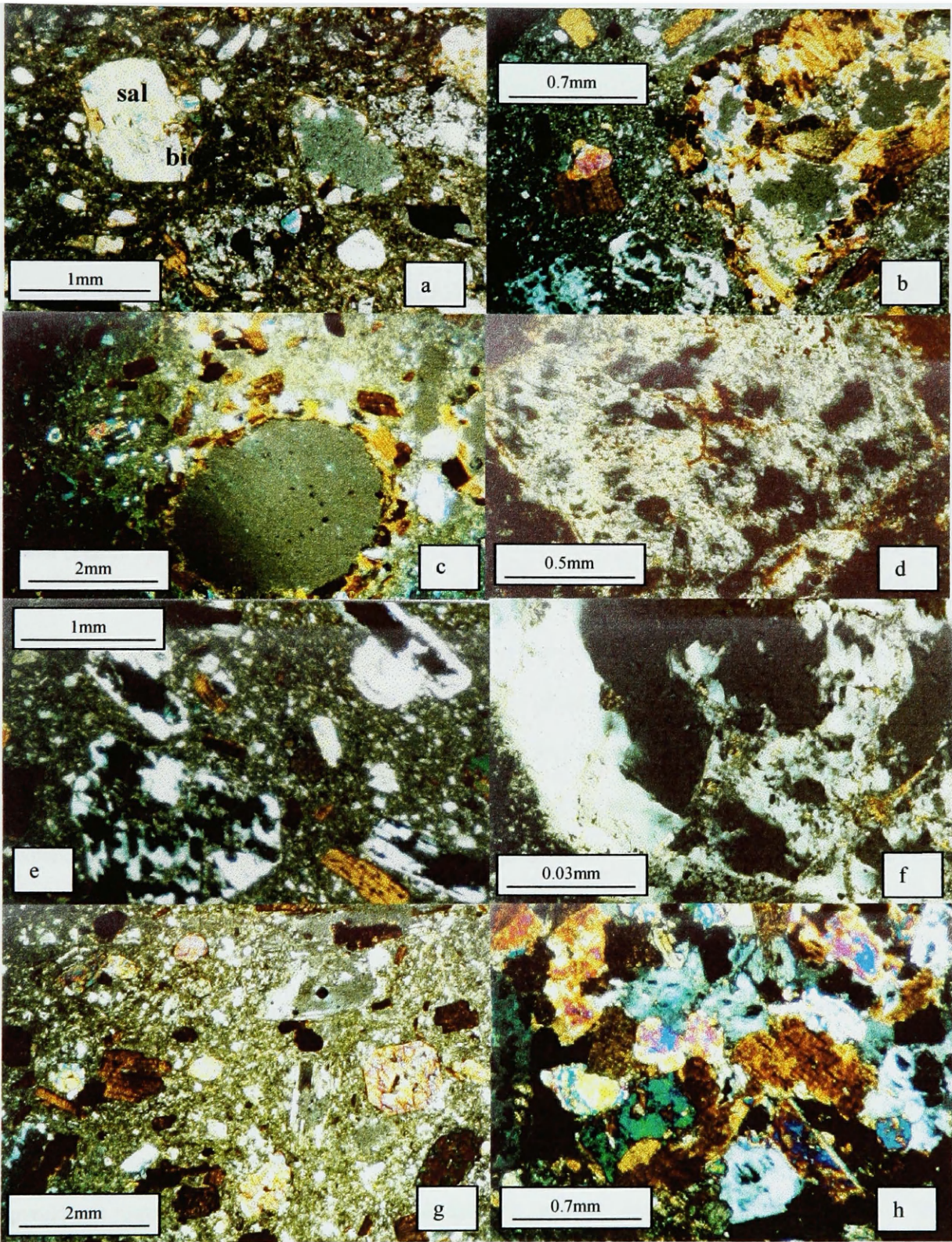


Figure 17: Textures from pyroclastic latite: (a) biotite (=bio) pseudomorphing salite (=sal); (b) shonkinite inclusion next to phillipsite pseudomorphing feldspar + melt inclusions; (c) large vesicle lined with biotite and cpx; (d) abundant melt inclusions in pseudomorphed feldspar phenocryst; (e) abundant skeletal feldspar grains; (f) zoom in on skeletal plagioclase; (g) pyroclastic latite tuff-breccia with euhedral biotite, clinopyroxene, and plagioclase-melt phenocrysts; (h) shonkinite inclusion with interstitial alkali feldspar containing melt pods in pyroclastic latite.

Biotite grains are euhedral laths and books from 1-3mm in length (20% of phenocrysts). Small clinopyroxene grains are commonly included within some of the larger books of biotite. Some grains show strain, and are bent around pods of glass, plagioclase, and/or clinopyroxene. Importantly, the biotite is *not* reacting to form an Fe-oxide mineral.

The textures, size, and occurrence of feldspar grains in the pyroclastic latite deposits vary significantly. In the blocks of quartz latite, most of the feldspar grains appear have grown around pods of melt that commonly make up 80% of the crystal volume. There are mixed assemblages of plagioclase and K-feldspar phenocrysts, many of which enclose large areas of clear glass (Figure 17). This contrasts with the usually dusty, smaller areas of glass in typical sieve textures. Although the edges of the grains are euhedral, the grain interior is a broken up mixture a zeolite mineral and trapped melt (Figure 17). This texture correlates with that seen in the cores of a small percentage of the feldspar phenocrysts from Deer Butte (Figure 5g, h).

There are two possible explanations for this texture. A model proposed by Halsor (1989) infers that fresh hydrous basaltic magma injected into an existing rhyolite magma was responsible for a similar texture; density instabilities were created as volatiles were released during crystallization. The ensuing mixing caused very rapid skeletal growth of plagioclase in the rhyolite, trapping pockets of magma. Plagioclase grains may have experienced a shattering effect, as trapped magma in the sieve texture cores expanded. The speed of eruption was so rapid that no quench textures formed, only glass, as Pearce (1987) discovered in the dacite erupted at Mt. St. Helens.

Another explanation is that the cores have been resorbed or re-melted due to eruption-induced pressure-release. Assuming the temperature of the grain remained constant, a decrease in pressure of the melt could have brought the grain back to a temperature above its solidus.

The feldspar grains (Ab-rich) “floating” independently in the quartz latite ash are both complete, euhedral crystals and grains which enclose melt. K-feldspar found in shonkinite inclusions (<5%) in the pyroclastic rocks is interstitial, relatively minor, shows no twinning, and contains abundant pods and lenses of glass, as well as some melt inclusions (Figure 17).

Vesicles can be seen in all of the different types of material in the pyroclastic deposits: in coarse pyroclastic breccia matrix, mixed ash deposits, in quartz latite blocks, within inclusions, at their margins,

and even surrounding inclusions (Figure 16). Most are sub-spherical to convoluted in shape, and are sometimes lined with biotite and clinopyroxene grains (Figure 17).

Much of the matrix material in the pyroclastic quartz latite is extremely fine-grained with a dusty brown color, indicative of a large percentage of glass. Elongated glass shards wrap around phenocrysts, and biotite and clinopyroxene phenocrysts are sometimes torn in half by a glass streak. Each thin section of pyroclastic rock shows several types of material with a variety of cooling histories. Some blebs of quartz latite have a groundmass that is ultra fine-grained (<0.1mm), whereas others have grains as large as 1mm.

Discussion

Examination of models

Two primary mechanisms are believed to be responsible for triggering and driving explosive volcanic eruptions. Crystallization of a hydrous magma can induce “second boiling” as sufficient vapor pressure is built up in a closed-system magma chamber. Secondly, replenishing a magma chamber with fresh magma from depth can trigger eruptions by adding heat and/or volatiles to the resident magma.

Replenishment from depth by a mafic magma is readily apparent in the quartz latite plutons of the eastern Bearpaw Mountains. Examination of the plutons reveals the co-existence of shonkinite with latite. Nearby volcanic rocks show a compositional and textural correlation to the latite plutons. These well-exposed plutons and associated volcanic rocks are windows into the cores of developing volcanoes, providing data that enables the testing of four models which seek to explain the role of interacting mafic and felsic magmas in triggering violent eruption.

The injection of hot, dense, mafic magma into the base of a silicic magma chamber has been proposed for many other calc-alkaline magma chambers as a means for triggering eruption (Feeley and Dungan, 1996; Clynne, 1996; Campbell and Turner, 1989; Bacon and Druitt, 1988; Sparks et al., 1977; Eichelberger, 1980). Their research has tested and refined variants of this mechanism, but most of the modeling has been based on the study of volcanic rocks alone. Four models presenting different scenarios regarding the injection or intrusion of mafic magma into cooler felsic magma are here tested with data from the plutons and volcanic rocks of the eastern Bearpaw Mountains field site.

Eichelberger's (1980) model

The model proposed by Eichelberger (1980) and built upon by Huppert et al. (1982) states that a volatile-bearing mafic magma injected into the base of a cooling felsic magma chamber will, upon partially crystallizing, have an initial density small enough to allow the mafic magma to be entrained as vesicular "foam". According to Eichelberger's model, unless the shonkinite magma was initially saturated with volatile phases, it would have to partially crystallize before its density could allow it to be entrained into and mingled with the latite magma. This crystallization would in turn exsolve gas and decrease density enough to buoyantly 'float' inclusions. Eichelberger's model suggests that if the shonkinite magma mostly crystallized prior to entrainment, then the transfer of heat from the shonkinite into the quartz latite would only be evident at or near the contact between the two.

Although salite xenocrysts (>2mm) from the shonkinite magma are ubiquitous in the quartz latite magma, there is no evidence of significant crystallization of the mafic magma prior to being mobilized throughout the magma chambers at the Bearpaws field site. Chilling of the mafic magma to a fine grain size is strong evidence pointing to mostly molten inclusions at the time of entrainment. The texture and extent of crystallization in mafic inclusions is largely dependent upon the initial temperature contrast (~1000°C and ~750°C) (Sparks and Marshall, 1986; Sparks et al., 1977). Concentric zonation from the core to rim of successively larger crystals, rounded rather than angular (broken) form, and the evidence of cusped margins indicate that the groundmass crystallization of the shonkinite occurred after the inclusions were dispersed and resident in the host magma (Bacon, 1986). Assuming an initially water-undersaturated shonkinite magma, this suggests post-entrainment groundmass crystallization and vapor exsolution in the shonkinite inclusions, contradicting the pre-entrainment crystallization required by Eichelberger's model.

Samples found throughout the Deer Butte pluton show local Ca and Mg enrichment, zonation within biotite and amphibole crystals, and resorbed quartz, evidence that supports a transfer of heat at all levels within the pluton. This does not support the local transfer of heat at the contact between pooled mafic magma and overlying felsic magma suggested by Eichelberger's model.

Conclusions of Sparks and Marshall (1986) regarding the increase in viscosity of mafic magma mingled with silicic magma also present a problem for any model requiring vesiculation prior to magma mingling. Vesiculation in the shonkinite magma brought on by crystallization would lead to an increase in

water content of the remaining shonkinite melt. Research by Sparks and Marshall (1986) showed that an increased water content would not only depress the liquidus and solidus temperatures of the mafic magma, but would increase the viscosity as well. Increased viscosity of the mafic magma relative to the felsic magma would therefore act as a strong inhibitor to the movement of pooled mafic magma within felsic magma, which does not support Eichelberger's model (Oldenburg et al, 1989; Frost & Mahood, 1987).

Feeley and Dungan's (1996) model

Feeley and Dungan's (1996) model suggests that prior to the development of density instabilities, an intruded mafic magma with enough heat and volume will chemically mix with the host felsic magma, generating a chemically hybrid boundary layer. Vigorous convection at the interface, and locally high mafic to felsic magma ratios allow for chemical mixing. Withdrawal of magma by eruption, or pluton-scale convection then entrains and distributes both hybrid and mafic inclusions throughout the felsic pluton.

As shown in the table of models above, a requisite for comparison with models by Sparks et al. (1977), Eichelberger (1980), and Murphy et al (2000) is that only a small volume of mafic magma (<4%) is present as inclusions within the host (Murphy et al, 2000; Sparks and Marshall, 1986; Eichelberger, 1980; Sparks et al., 1977). The chemical mixing (hybridization) process described in the model of Feeley and Dungan (1996), on the other hand, will only occur when the hotter magma has enough heat to allow the two magmas to reach thermal equilibrium very slowly, thereby averting any large scale chilling of the hotter mafic magma. This process can take place at great depth, or when the proportion of hot magma to cold magma is equal to sub-equal. The relative proportion of the two mingling magmas has been shown to have a direct correlation with the extent of hybridization and quenching of the hotter magma, as well as on the time between mixing and eruption (Sparks and Marshall, 1986; Bacon & Metz, 1984). It is well documented that a small percentage of hot mafic magma brought into contact with a relatively large proportion of felsic magma will cause the mafic magma to chill as fine-grained blebs and pillows (Blundy and Sparks, 1992; Bacon, 1986; Sparks and Marshall, 1986; Koyaguchi, 1986; Bacon and Metz, 1984; Vernon, 1983), crystallizing prior to reaching thermal equilibrium. A small volume ratio of mafic to felsic magma would therefore inhibit chemical mixing of the magmas.

The mean estimated volume % of shonkinite was 2.1% at Deer Butte, and 0.79% at Suction Butte. This small percentage of mafic magma relative to felsic magma does not support the model of Feeley and Dungan. Shonkinite inclusions at both Deer Butte and Suction Butte show fine grain size, cusped margins, and grain size that decreases outward from the center of the inclusion, all indicators that thermal equilibrium was reached fairly quickly. The fine-grain textures in the mafic inclusions must mean that crystallization began in the shonkinite magma immediately upon entering the cooler quartz latite magma. Therefore, textures in the mafic inclusions also do not support Feeley and Dungan (1996).

However, felsic halos on some of the largest inclusions near the base of exposure at Deer Butte suggest that hybridization might have occurred at depths greater than those exposed in the field, apparently supporting the model by Feeley and Dungan (1996). Larger inclusions will retain latent heat for a longer time than smaller inclusions. Inclusions retaining more heat will take longer to thermally equilibrate with surrounding magma, thereby crystallizing coarser grains, and averting a “chilling” effect. Complete hybridization can only occur when two different magmas both behave as liquids at the same temperature. The two magmas cannot easily mix if one of the magmas behaves as a solid when thermal equilibrium is reached. If the phases that form at lower temperatures in the shonkinite magma (such as alkali feldspar) are still liquid when the shonkinite and quartz latite magmas reach a common temperature, the two magmas could exchange components. This hybridization, however, would be present in higher parts of the pluton if convection mobilized the deeper parts of the magma chamber.

The apparent lack of hybrid inclusions among those distributed throughout the pluton suggests that this probably did not happen. There was also no evidence of a hybrid layer. Cusped margins and uniformly fine-grained inclusions point to the chilling of the shonkinite within the quartz latite, again minimizing the migration of cations from the shonkinite to the quartz latite. The coexistence of chemically distinct, homogeneous, and nearly pure end-member mafic inclusions and latite at Deer Butte argues against application of the model put forth by Feeley and Dungan (1997) to the Bearpaws field site.

Murphy et al.’s model (2000)

The scenario proposed by Murphy et al. (2000) for the magma chamber of the Soufriere Hills volcano involves the forcible intrusion of mafic magma as dikes or sills into a partially crystallized felsic

host. The intrusion of mafic magma transfers volatiles and heat, remobilizing the felsic crystal mush into a convective cycle, leading to eruption. Mafic inclusions form both as fragments of disrupted dikes and as quenched blobs of mafic magma emplaced by forceful intrusion and/or buoyant ascent of vesicular mafic magma. For this model to apply to the Bearpaws plutons, there must be evidence supporting the intrusion of relatively hot shonkinite magma into a mostly crystalline quartz latite with an extremely high viscosity. An injected mafic magma undercooled by contact with felsic magma will also act brittlely (Murphy et al., 2000; Foster and Hyndman, 1990; Vernon, 1984), so that fragmented and brecciated dike rock and xenoliths would be expected in a pluton having undergone this process. This model therefore requires variation and disequilibrium in the crystallizing histories of phenocrysts, locally heterogeneous bulk magma composition, and fine-grained inclusions with both rounded and angular geometry.

Amphibole grains at Suction Butte show normal and oscillatory zoning within the same thin section, and variable reaction-rim thicknesses, both of which suggest that the grains experienced locally different cooling histories. Resorption of amphibole exteriors has been interpreted as resulting from either the reheating of amphibole grains above their stability point at 880°C (Barclay et al., 1998), or that the grains experienced a pressure decrease (Rutherford and Hill, 1993; Murphy et al., 2000).

Salite grains at Deer Butte show normal, oscillatory and reverse zoning as well, but are strongly resorbed and altered. Given the earlier interpretation that intrusion of the shonkinite magma was responsible for the dispersal of salite xenocrysts at Deer Butte, any reverse zoning or heterogeneity from core to rim in the composition of salite grains is not necessarily the result of localized reheating in the quartz latite magma. Resorption of many but not all grain exteriors suggests that the grains were subject to pressure-relief melting or the contrast in composition of the salite was such that Ca and Mg tended to resorb back into the melt.

Biotite grains at Deer Butte also show resorption, reverse and normal zoning, and are altered to titanomagnetite. However, as grains that crystallized from the quartz latite melt, reverse zoning is an indication of reheating. Resorption of biotite could be the result of reheating, pressure-relief melting, or local contrast in melt composition. Embayed and resorbed quartz grains at Deer Butte also point to a reheating or pressure-releasing event.

At Deer Butte, three feldspar grain types vary in their relationships to each other. Sanidine enclosing plagioclase, plagioclase enclosing sanidine, and sanidine enclosing plagioclase and smaller anti-perthite xenocrysts are all evident. This shows the melt composition varied locally, crystallizing sanidine first in some areas, and plagioclase first in others.

The reverse and oscillatory zoning of biotite and amphibole phenocrysts, variation in phenocryst composition, and the resorption of salite, amphibole, biotite, and quartz all point to parts of Deer Butte having experienced one or more of the following:

- a) Localized reheating by the intrusion of shonkinite magma to a temperature above an original temperature at which biotite, alkali feldspar, and quartz formed.
- b) Pressure-relief melting as quartz latite magma ascended from depth.
- c) Pressure-relief melting as quartz latite magma chamber erupted.
- d) A change in melt composition as shonkinite magma was dispersed throughout the pluton.

Although it is indeterminable which of these was primarily responsible for the variation in texture and chemistry observed in the minerals of Deer Butte, some observations can be made noting the model proposed by Murphy et al. (2000). The model of Murphy et al. (2000) proposes a transfer of heat from an intruding/injected mafic magma into a felsic magma pluton, which sufficiently “thaws” and remobilizes the 60-65% crystalline pluton. Murphy et al. (2000) suggested that phenocrysts in the felsic magma experience different degrees of resorption and recrystallization under locally variable conditions, depending on their proximity to intruding bodies.

If a hot mafic inclusion (1000°C) that is spherical and 2cm in diameter is enclosed in a cooler felsic magma (750°C) that is 4cm in diameter, the volume ratio of mafic to felsic magma is 1 to 7 (14.3%). Assuming all else is equal, and given the initial temperature contrast (250°C), this volume ratio would cause the two magmas to reach a thermal equilibrium of 781°C, only 31°C higher than the original temperature of the felsic melt. Also, for a solid mineral crystal to go back into solution, the temperature of the surrounding melt must increase enough to overcome the minerals heat of fusion.

The estimated % by volume made up of shonkinite inclusions in the Deer Butte pluton is 2.4% and 0.75% in the Suction Butte pluton. The average size of the shonkinite inclusions was 2cm or less in

diameter. The small size and volume of the mafic inclusions at Suction Butte and Deer Butte, and the heat of fusion problem means any increase in temperature experienced by the surrounding quartz latite melt was local, on the cm scale. Larger inclusions, however, will have a greater local ratio of mafic to felsic magmas.

Therefore, heat transfer from dispersed, volumetrically-minor magmatic mafic inclusions to surrounding felsic magma will have a minimal effect on remobilizing and reheating an entire pluton. If the local ratio of mafic magma to felsic magma is sufficiently large, reheating could cause resorption, reverse zoning, reaction rims, and other disequilibrium textures. An example of this type of mafic magma to felsic magma ratio might be in areas adjacent to an injected dike or sill, or near the contact between a pooled body of dense mafic magma and overlying felsic magma. Variations in the local ratio of mafic to felsic magma could account for the variability in extent of resorption seen in the salite grains, and the heterogeneous thermal histories of biotite and amphibole grains.

However, as described earlier, the proportion of mafic magma to felsic magma has a direct effect on the extent of chemical mixing which takes place. Given pluton-scale convection, the absence of hybrid inclusions in either Deer Butte or Suction Butte suggests that there is no location within the pluton where local ratios of mafic to felsic magma allowed for significant reheating. Therefore, the absence of magma mixing and relatively small size and volume of shonkinite inclusions do not support the notion that the Deer Butte and Suction Butte plutons were 60-65% crystallized when reheated from an intruded shonkinite magma, and mobilized into pluton-scale convection. This does not support the model of Murphy et al. (2000).

Bulk magma composition at Deer Butte shows remarkable consistency at various levels and locations within the pluton. Ca and Mg showed very minor variations locally. This homogeneity is evident at a small enough scale to consider the mechanical and minor chemical mixing to have been more thorough here than that inferred at the Soufriere Hills volcano (Murphy et al., 1998; Devine et al., 1998), as salite xenocrysts are observed evenly distributed throughout most thin sections made from the Deer Butte pluton. The minimal variation in whole-rock chemistry suggests that there was thorough mixing of the latite magma by convection, eliminating any significant local chemistry changes brought on by the intrusion of

shonkinite magma. This extensive mixing is in support of Murphy et al.'s (2000) model, in that the chamber had enough gas and/or heat enough to begin convecting.

The presence of feldspar-rich felsic blobs with very small amounts of mafic minerals suggests that at least on the edges of the cooling pluton, partially crystallized quartz latite was remobilized and entrained by a quartz latite magma that had mingled with shonkinite inclusions (Figure 2-1.1). The high total mafic mineral content in the quartz latite surrounding the feldspar-rich blobs suggest there was some chemical mixing between the injected shonkinite and the reheated quartz latite. This feldspar-rich blob and surrounding contaminated latite is supporting evidence for the remobilization of a crystal mush by the intrusion of mafic magma as proposed by Murphy et al. (2000).

Shonkinite inclusions at both Deer Butte and Suction Butte show several stages of disaggregation. Inclusions show brecciation, but only at fractures through broken up inclusions (Figure 2d, f). Few angular shonkinite inclusions are observed in the quartz latite plutons. The exteriors or outer edges of most inclusions are rounded. The presence and disaggregation of only rounded inclusions is contradictory evidence to the model proposed by Murphy et al. (2000). Intrusion of mafic magma into a 50-60% crystalline pluton would instead form dikes and sills which in turn brecciate, forming fine-grained inclusions with broken or angular shapes.

Sparks' (1977) model

The model of Sparks et al. (1977) says that a mafic magma intruded/injected into a much cooler felsic magma will form initially magmatic inclusions, which begin to release heat and volatiles into the felsic magma as they quickly cool. Increased heat and gas content in the felsic magma then initiates rapid superheating and convection in the the felsic pluton, distributing mafic inclusions and associated volatiles to all parts of the pluton, pressurizing the magma chamber as gas exsolves, and triggering violent eruption.

Evidence summarized below supports Sparks et al.'s hypothesis: the mingling of two chemically distinct magmas, significant initial temperature and volatile-content contrast between the two magmas, correlation between plutonic and volcanic quartz latite, pluton-scale convection of magma, and consequent rapid pyroclastic eruption.

Coeval, mingling magmas

Bacon & Metz (1984), Bacon (1986), and Didier & Barbarin (1991) have proposed criteria for recognizing undercooled blobs of mafic magma that were injected into and crystallized in plutonic and volcanic rocks. Observations I have made indicate that indeed the inclusions found in the quartz latite plutons of the eastern Bearpaws Mountains represent mafic magma injected into and chilled within cooler, more silicic reservoirs. They include:

- 1.) The majority of inclusions are sub-spherical in shape; they differ from angular accidental xenoliths derived from solid wall rock or brecciated dikes and sills.
- 2.) Whole-rock chemical analyses of mafic inclusions show that they are shonkinitic in composition. (See Whole-rock analyses Appendix I). Tureck-Schwartz's study of the association of alkalic and sub-alkalic rocks in the Bearpaw Mountains revealed that shonkinite and quartz latite cannot be formed by differentiation of a single parent magma. Cumulates from quartz latite crystallization would not resemble the bulk composition of the inclusions. Their composition would be controlled by the crystallizing magma and physical properties of the precipitating phases.
- 3.) Inclusions have a fine-grained igneous texture characterized by abundant, elongated, strongly zoned euhedral crystals in an altered matrix, indicative of rapid cooling to just above the solidus. This texture differs from the glassy or microcrystalline groundmass characteristic of mafic magma quenched at the surface.
- 4.) Some large inclusions exhibit decrease in grain size towards their rims, increase in elongation of grains, and/or an outer hybrid rind containing reacted or resorbed amphibole phenocrysts from the host magma. These observations indicate that the inclusions were chilled against the host, and that both host and inclusions were molten at the same time.

Furthermore, mafic schlieren textures are absent from inclusions in the associated pyroclastic rocks. A rounded or sub-spherical appearance of the pyroclastic shonkinite inclusions suggest that they were likely molten at the time of distribution within the pluton. Alternatively, the mafic magma may have

partially crystallized upon entering the quartz latite, yielding a material with a high enough mechanical strength, and a low enough viscosity that they were not able to mechanically disaggregate during eruption.

Correlation between pyroclastic rocks and plutonic rocks

Similarities in texture, chemistry, and phenocryst phases suggest that pyroclastic quartz latite originated in plutonic quartz latite domes exposed in the southeast Bearpaw Mountains. The data include:

- 1.) The geometry, chemistry, distribution and size of shonkinite inclusions in pyroclastic quartz latite correlates well with the inclusions found in nearly all of the examined quartz latite plutons.
- 2.) Large pods of glass, and missing cores are evident in feldspar grains of both pyroclastic quartz latite and plutonic quartz latite. The glass inclusions are interpreted to be the result of pressure-relief melting as the magma chamber erupted.

Pluton-Scale Convection

Available data supports the contention that Suction Butte, Deer Butte, and Star Butte experienced vigorous pluton-scale convection. The data include:

- 1.) Numerically-even distribution of inclusions throughout the entire exposed pluton. Increase in the number of inclusions and decrease in the volume of shonkinite at higher levels within the pluton is interpreted to be the result of the breaking up of larger inclusions and pillows introduced at the base of the chamber. Subsequent vigorous convection likely disaggregated blobs and pillows, entraining the still molten magma as spherical to sub-spherical inclusions of shonkinite. These smaller inclusions were themselves subjected to disaggregation. The fine-grained nature of the small inclusions suggests that they were chilled once they were small enough that heat loss within them was rapid.
- 2.) Compositional homogeneity. Whole-rock chemistry data of the quartz latite shows a strong uniformity in samples taken from 20 different locations throughout the Deer Butte pluton.

- 3.) Hornblende crystal alignment. Amphibole grains in the quartz latite at Star Butte show a strong radial lineation trend away from the center of the buttes. Suction Butte amphiboles show a strong lineation in narrow flow corridors 5-10 cm wide, as well as a foliation in the exfoliating talus sheets.
- 4.) Heterogeneous reaction rim thicknesses on adjacent amphibole crystals at Suction Butte. Reaction rim thicknesses vary from 20 μ m to 75 μ m on amphibole grains from the same thin section, showing that grains present in the magma chamber at pressures < 1.6 kbars for different lengths of time have been thoroughly mixed together.
- 5.) Two distinct reaction rims on a small percentage of the amphiboles. Some amphibole grains show evidence of having been recycled from conditions of water saturation into water undersaturation, and back again, most likely due to magma chamber convection. This could also result, however, from the introduction of volatiles from a magma replenishment, secondary intrusion, or from surrounding country rocks.

Injection of hot, volatile-bearing mafic magma into relatively cool and dry magma

All available models demand the injection of mafic magma into the base of a relatively cooler silicic chamber. A significant initial temperature contrast is most likely responsible for the chilling and undercooling that is observed in many of the mafic inclusions. Rather distinct in temperature and volatile concentration, the two magmas would experience a rapid and local transfer of heat and volatiles. Magmatic shonkinite (~1000°C) that is volumetrically minor (1-3%) would rapidly transfer heat into cooler quartz latite (~750°C) magma. Quartz latite magma (~750°C) emplaced in plutons at low pressures (<2.0 kbars) is relatively dry, at most containing 5 wt% water (Holtz et al., 2001), while an intruded mafic magma could bear water and other volatiles. The following data support the injection of hot, volatile-bearing mafic magma (shonkinite) into relatively cool and dry felsic magma (quartz latite):

- 1.) Coeval shonkinite (~1000°C) and quartz latite (~750°C) magmas suggest an initial T contrast of ~250°C between the host magma and secondary intrusion.

- 2.) Exsolved gas bubbles found in the chilled inclusions of the pyroclastic rocks point to the saturation of a volatile phase within the shonkinite. Gas bubbles trapped in the shonkinite inclusions of erupted magma demonstrate that gases did not completely exsolve out of the inclusions into the host quartz latite. The inclusions in the gas-rich uppermost part of the magma chamber at McCann Butte are enclosed by gas bubbles. These bubbles were perhaps responsible for buoyantly floating the inclusions into higher parts of the magma chamber. Plutonic-hosted inclusions do not contain abundant gas vesicles. However, given compositional equivalency between pyroclastic and plutonic shonkinite inclusions, exsolved gas which had been present within the plutonic inclusions was released into the quartz latite. Exsolved gas that was not erupted was likely concentrated post-eruption at the top of the magma chamber as it ascended through the magma chamber during convection. This concentrated gas is represented by the large, vesicle-rich tumbled blocks at the top of McCann Butte.
- 3.) The cooling histories of feldspar grains at Deer Butte suggest an increase in temperature and/or a drastic decrease in pressure. Partial melting entrained xenocrysts of anti-perthite into quartz latite melt. Locally, plagioclase began to crystallize first, while in other areas of the magma chamber sanidine crystallized first. Eventually, local plagioclase crystallization gave way to sanidine. Continued rapid cooling eventually yielded an alkali feldspar rim. This alkali feldspar rim underwent a significant pressure decrease, developing a dusty sieve texture containing melt inclusions.
- 4.) Crystallization of thin amphibole rims around, and large amphibole phenocrysts adjacent to, shonkinite inclusions at Suction Butte suggest a temperature and/or water-content contrast between the two magmas. The shonkinite magma intruded into a presumably dry quartz latite magma, suggesting therefore that the initial shonkinite had a higher volatile content than the resident quartz latite.

Rapid supersaturation and eruption of quartz latite magma

Several observed features indicate a rapid rate of convection and volatile supersaturation which ultimately led to pyroclastic eruption. The data includes:

- 1.) Lack of reaction rims on erupted biotite and some plutonic amphibole grains. Experimental results by Rutherford and Hill (1993) indicate that amphibole grains which have been in undersaturated (water-depleted) conditions for longer than 4 days acquire an Fe-oxide reaction rim. The lack of reaction rims on some amphiboles collected from storage areas experiencing less than 1.6 kbars of overburden pressure suggests that amphibole ascent through the magma chamber was rapid, more than about 30 m/hr. Biotite in an undersaturated magma will form a magnetite reaction-rim in a similar fashion. Therefore the absence of reaction rims on biotites in erupted samples suggests a very brief time in a magma chamber at depths shallow enough for water vapor to exsolve. The absent and very thin (<5 μ m) reaction rims on some amphiboles at Suction Butte are evidence of a very rapid rise of at least some magma from amphibole-stable depths in the storage chamber.
- 2.) Blebs of shonkinite separating from inclusions in both tuff-breccia and plutonic samples suggest that at least some of the shonkinite magma was still partly molten when it was erupted. Small inclusions of the size seen at Deer Butte and Suction Butte (mostly 5mm-2cm) would be expected to chill rapidly if in contact with significantly cooler quartz latite. The presence of magmatic inclusions in tuff-breccia samples then points to a short time between the intrusion of shonkinite and the eruption of the quartz latite magma chambers.
- 3.) Skeletal feldspar grain growth in erupted samples. Most of the feldspar phenocrysts in pyroclastic samples have missing cores (sometimes replaced by zeolite minerals), or have a rounded or euhedral framework which surrounds large melt inclusions. This points to the rapid growth of feldspar around pods of melt. This texture is similar to that described by Halsor (1989) for a basaltic magma injected into the base of a felsic magma chamber, releasing volatiles which cause a density instability between the magmas. Subsequent eruption ended any approach to density stability and further equilibrium.

Conclusion

I interpret Deer Butte and Suction Butte to be quartz latite magma chambers that had partially crystallized before being intruded by a hot, dense shonkinite magma. The crystallization of the quartz latite plutons in the eastern Bearpaw Mountains was probably not as extensive as that described at the Soufriere

Hills volcano by Murphy et al., as salite xenocrysts from the shonkinite magma are intimately mixed and distributed throughout the plutons. Also, the shonkinite inclusions do not appear to have formed many angular or broken inclusions. If the shonkinite magma intruded a mostly crystalline pluton, dikes or sills would have formed, and subsequently brecciated as the dikes reheated the pluton and initiated convection.

Rather, the forcible injection of the shonkinite magma immediately dispersed inclusions and blobs of magmatic shonkinite within the quartz latite. Vigorous convection began as heat and volatiles transferred from the hot, relatively volatile-rich shonkinite magma into the cooler, drier quartz latite. Significant temperature contrast between the mingling magmas caused the smallest shonkinite blebs to completely crystallize as fine-grained inclusions, while larger blebs of shonkinite formed fine-grained rims around slower cooling interiors. As the shonkinite magma inclusions exchanged heat with the host quartz latite and crystallized, volatile phases exsolved, nucleated in and around the inclusions and lowered the density of the mafic blebs.

The lowering of the density of shonkinite inclusions as gas exsolution expanded their volume provided a second, independent force to distribute inclusions throughout the plutons. Continued exchange of heat, and the migration of volatiles from the inclusions into the quartz latite drove pluton-scale convection, effectively disaggregating and distributing the blebs of shonkinite magma to all levels within the pluton. The added volume and exsolved volatiles from the shonkinite magma sufficiently raised the vapor pressure within the convecting magma chamber to trigger explosive eruption. Pyroclastic quartz latite tuff and quartz latite tuff-breccia deposits from nearby volcanic fields contain abundant, vesicular shonkinite inclusions and pressure-relief melted feldspars, showing textural equivalence to the plutonic quartz latite. This result confirms the model proposed by Sparks et al. (1977), and also incorporates some of the findings of Murphy et al. (2000).

References

- Bacon, Charles R., 1986. Magmatic inclusions in silicic and intermediate volcanic rocks. *Journal of Geophysical Research*, v. 91, p. 6091-6112.
- Bacon, Charles R., and Metz, 1984. Magmatic Inclusions in rhyolite, continental basalts, and compositional zonation beneath the Coso volcanic field, California. *Contributions to Mineralogy and Petrology*, v. 85, p. 362-365.
- Bacon, Charles R., and Druitt, T.H., 1988. Compositional evolution of the zoned calc-alkaline chamber of Mount Mazama, Crater Lake, Oregon. *Contributions to Mineralogy and Petrology*, v. 98, p. 224-256.
- Barclay, J., Rutherford, M.J., Carroll, M.R., Murphy, M.D., Devine, J.D., Gardner, J., and Sparks, R.S.J., 1998. Experimental phase equilibria constraints on pre-eruptive storage conditions of the Soufriere Hills magma. *Geophysical Research Letters*, v. 25, p. 3437.
- Blake, S., 1984. Volatile saturation during the evolution of silicic magma chambers as an eruption trigger. *Journal of Geophysical Research*, v. 89, B10, p. 8237-8244.
- Blundy, J.D. and Sparks, R.S.J., 1992. Petrogenesis of mafic inclusions in granitoids of the Adamello Massif. *Journal of Petrology*, v. 33, p. 1039-1104.
- Burnham, C.W., and Jahns, R.H., 1962. A method for determining the solubility of water in silicate melts. *American Journal of Science*, v. 260, p. 721-745.
- Campbell, I.H., and Turner, J.S., 1985. Turbulent mixing between fluids with different viscosities. *Nature*, v. 313, p. 39-42.
- Campbell, I.H. and Turner, J.S., 1989. The influence of viscosity on fountains in magma chambers. *Journal of Petrology*, v. 30, p. 885-923.
- Carroll, M.R., Holloway, eds., 1994. *Volatiles in Magmas*, *Reviews in Mineralogy*, v.30, p. 281-323.
- Clynne, Michael A., 1999. A complex magma mixing origin for rocks erupted in 1915, Lassen Peak, California. *Journal of Petrology*, v. 40, p. 105-132.
- Didier, J., 1973. *Granites and their enclaves*. Elsevier, New York, 393 pp.
- Didier, J., and Barbarin, B., 1991. *Enclaves and granite petrology*. Elsevier, New York, 625 pp.
- Devine, J.D., Murphy, M.D., Rutherford, M.J., Barclay, J., Sparks, R.S.J., Carroll, M.R., Young, S.R., and Gardner, J.E., 1998. Petrologic evidence for pre-eruptive pressure-temperature conditions, and recent reheating, of andesitic magma erupting at the Soufriere Hills Volcano, Montserrat, W.I. *Geophysical Research Letters*, v. 25, p. 3669-3672.
- Devine, J.D., Rutherford, M.J., and Gardner, J.E., 1998a. Petrologic determination of ascent rates for the 1995-1997 Soufriere Hills Volcano andesitic magma. *Geophysical Research Letters*, v. 25, p. 3673-3676.
- Dingwell, D.B. 1998. Recent experimental progress in the physical description of silicic magma relevant to explosive volcanism. *In: Gilbert, J.S. and Sparks, R.S.J. (eds) The Physics of Explosive Volcanic Eruptions*. Geological Society, London, Special Publications, v. 145, p. 9-26.
- Eichelberger, J.C., 1980. Vesiculation of Mafic magma during replenishment of silicic magma reservoirs. *Nature*, v. 288, p. 446-450.

- Eichelberger, J.C., 1995. Silicic Volcanism: Ascent of viscous magmas from crustal reservoirs. *Annual Reviews of Earth and Planetary Science*, v. 23, p. 41-63.
- Feeley, T.C., and Dungan, M.A., 1996. Compositional and dynamic controls on mafic-silicic magma interactions at continental volcanoes: evidence from Cordon El Guadal, Tatar-San Pedro Complex, Chile: *Journal of Petrology*, v. 37, p. 1547-1577.
- Fisher, B., 1946, *Igneous rocks of the northeastern Bearpaw Mountains, MT.*: PhD thesis, Harvard University; 127 pp.
- Foster, D.A., and Hyndman, D.W. (1990). Magma mixing and mingling between synplutonic mafic dikes & granite in the Idaho-Bitterroot batholith. *GSA Memoir 174*, p. 137-143.
- Frost, T.P., and Mahood, G.A., 1987. Field, chemical, and physical constraints of mafic-felsic interactions in the Lamarck Granodiorite, Sierra Nevada, California: *Geological Society of America Bulletin*, v. 49, p. 272-291.
- Furman, T., and Spera, F.J., 1985. Co-mingling of acid and basic magmas with implications for the origin of mafic I-type xenoliths; field and petrochemical relations of the unusual dike complex at Eagle Lake, Sequoia National Park, California, USA: *Journal of Volcanology and Geothermal Resources*, v. 24, p. 151-178.
- Garcia, M.O., and Jacobsen, S.S., 1979. Crystal clots, amphibole fraction and the evolution of calc-alkaline magmas, *Contributions to Mineralogy and Petrology*, v. 69, p. 319-327.
- Hamilton, D.L., Burnham, C.W., and Osborn, E.F., 1964. The solubility of water and effects of oxygen fugacity and water content on crystallization in mafic magmas. *Journal of Petrology*, v. 5, p. 21-39.
- Hearn, C.B., 1976. *Geologic and tectonic map of the Bearpaw Mountains Area, North Central Montana*: U.S.G.S. Miscellaneous Investigations Series. Map I-191.
- Hearn, Carter, et al., 1989. *Montana High Potassium Igneous Province Field Trip Guidebook T346*, 28th International Geological Congress, American Geophysical Union, Washington D.C., p. 51-61.
- Holtz, F., Johannes, W., Tamic, N., and Behrens, H., 2001. Maximum and minimum water contents of granite melts generated in the crust; a re-evaluation and implications. *Lithos*, v. 56, p. 1-14.
- Huppert, Herbert E., Sparks, R.S.J., and Turner, Stewart, 1982. Effects of volatiles on mixing in calc-alkaline magma systems. *Nature*, v. 297.
- Huppert, Herbert E., and Turner, J. Stewart, 1991. Comments on 'On Convective Style and Vigor in Sheet like Magma Chambers' by Bruce D. Marsh. *Journal of Petrology*, v. 32, Part 4, p. 851-854.
- Hyndman, D.W., 1985. *Petrology of Igneous and Metamorphic Rocks*, 2nd Edition; McGraw-Hill Book Co., New York, p. 149-152.
- Jaeger, J.C., 1959, Temperatures outside a cooling intrusive sheet. *American Journal of Science*, v. 257, p. 44-54.
- Jakes, P., and White, A.J.H., 1972. Hornblendes from calc-alkaline volcanic rocks of island arcs and continental margins, *American Mineralogist*, v. 57, p. 887-902.

- Johannesmeyer, T.C., 1999. Magma Mingling and Mixing in the late Cretaceous Ringing Rocks Pluton, Jefferson County, Montana and Implications for the generation of the Boulder Batholith, Masters Thesis, University of Montana, Missoula; 208 pp.
- Kuochi, A, and Sunagawa, Ichiro, 1985. A model for mixing basaltic and dacitic magmas as deduced from experimental data. *Contributions to Mineralogy and Petrology*, v. 89, p.17-23.
- Larsen, E.S., 1940. Petrographic province of central Montana: *Geological Society of America Bulletin*, v. 51, p. 887-948.
- MacGregor, A.G., 1938. The volcanic history and petrology of Montserrat, with observations on Mt. Pelee in Martinique, Royal Society expedition: to Montserrat, B.W.I., *Philoso. Trans. R. Soc., Ser. B*, v. 229, 1-90.
- Marvin, R.F., Hearn, B.C., Mehnert, H.H., Naeser, C.W., Zartman, R.E., and Lindsay, D.A., 1980. Late Cretaceous – Paleocene – Eocene igneous activity in north-central Montana: *Isochron west*, v. 29, p. 5-25.
- Murphy, M.D., et al., 1998. The role of magma mixing in triggering the current eruption at the Soufriere Hills volcano, Montserrat, West Indies. *Geophysical Research Letters*, v. 25, p. 3433-3436.
- Murphy, M.D., et al., 2000. Remobilization of andesite magma by intrusion of mafic magma at the Soufriere Hills Volcano, Montserrat, West Indies. *Journal of Petrology*, v. 41, p. 21-42.
- Navon, O., and Lyakhovsky, V. 1998. Vesiculation processes in silicic magmas. *In: Gilbert, J.S. and Sparks, R.S.J. (eds.) The Physics of Explosive Volcanic Eruptions*. Geological Society, London, Special Publications, v. 145, p.27-50.
- Nicholls, J., and Russell, J.K., eds., 1990. *Modern Methods of Igneous Petrology: Understanding Magmatic Processes*, *Reviews in Mineralogy*, v. 24, 314 pp.
- Oldenburg et al., 1989. Dynamic Mixing in Magma Bodies. *Journal of Geophysical Research*, v. 94, p. 9232-9236.
- Pabst, A., 1928. Observations on the inclusions in granitic rocks of the Sierra Nevada, Univ. of California Publications Bulletin, Dept. of Geological Sciences, v. 17, p. 325-387.
- Pearce, T.H., Russell, J.K., and Wolfson, I., 1987. Laser-interference and Normanski interference imaging of zoning profiles in plagioclase phenocrysts from the May 18, 1980 eruption of Mt. St. Helens, Washington. *American Mineralogist*, v. 72, p. 1131-1143.
- Rutherford, M.J., and Hill, Peter M., Magma ascent rates from amphibole breakdown: An experimental study applied to the 1980-1986 Mount St. Helens eruptions. *Journal of Geophysical Research*, v. 98, p. 19667-19685.
- Schmidt, R.G., Pecora, W.T., Bryant, B., and Ernst, W.G., 1961, Geology of the Lloyd Quadrangle Bearpaw Mountains, Blaine County, MT., U.S.G.S. Bulletin 1081-E, p. 159-188.
- Schmidt, R.G., Hearn, B.C., and Pecora, W.T., 1964, Geology of the Cleveland Quadrangle, Bearpaw Mountains, Blaine County, MT: U.S.G.S. Bulletin 1041-p, p. 1-26.
- Shelly, D., 1997. *Igneous and metamorphic rocks under the microscope*, Chapman and Hall, New York, - 527 pp.
- Sparks, R.S.J., and Gilbert, J.S., eds., 1998. *The Physics of Explosive Volcanic Eruptions*, The Geological Society Special Publication No.145, 186 pp.

- Sparks, R.S.J., 1997. Causes and consequences of pressurization in lava dome eruptions, *Earth and Planetary Sciences Letters*, v. 150, p. 177-189.
- Sparks, R.S.J., and Marshall, L.A., 1986. Thermal and mechanical constraints on mixing between mafic and silicic magmas. *Journal of Volcanology and Geothermal Research*, v. 29, p. 99-124
- Sparks, R.S.J., Sigurdssen, H., and Wilson, L., 1977. Magma Mixing: a mechanism for triggering acid explosive eruptions, *Nature*, v. 267, p. 315-318.
- Tureck-Schwartz, Kathy, 1992. The association of alkalic and sub-alkalic rocks in the Bearpaw Mountains, Montana, Masters Thesis, University of Montana, Missoula; 160 pp.
- Tureck-Schwartz, K., and Hyndman, D.W., 1991. High-potassium igneous rocks of the Bearpaw Mountains, north-central Montana, Central Montana alkalic province guidebook; Special Publication 100, Montana Bureau of Mines and Geology, p. 111-120.
- Tureck-Schwarz, K., and Zieg, G.A., 1989. North Moccasin project final report: unpublished Cominco American Resources report, Spokane, WA.
- Tureck-Schwarz, K., and Zieg, G.A., 1989. South Moccasin project final report: unpublished Cominco American Resources report, Spokane, WA.
- Turner, J.S. and Campbell, I.H., 1986. Convection and mixing in magma chambers. *Earth Science reviews*, v. 23, p. 255-352.
- Tuttle, O.F., and Bowen, N.L., 1958. *Origin of granite in light of experimental studies*, Geological Society of America, Memoir 74, 152 pp.
- Van der Laan, S.R., and Wyllie, P.J., 1993, Experimental interactions of granitic and basaltic magmas and implications for mafic enclaves: *Journal of Petrology*, v. 34, p. 491-517.
- Vernon, R.H., 1983. Microgranitoid enclaves in granites-globules of hybrid magma quenched in a plutonic environment. *Nature*, v. 309, p. 438-439.
- Voight, B., et al., 1999. Magma flow instability and cyclic activity at Soufriere Hills Volcano, Montserrat, British West Indies, *Science*, v. 283, p. 1138.
- Weed, W.H., and Pirsson, L.V., 1896, The Bearpaw Mountains, MT., *American Journal of Science*, 4th series, v. 1, p. 283-301, 351-362; v. 2, p. 136-148, 188-199.
- Wilson, L., Sparks, R.S.J., Huang, T.C., and Watkins, N.D., 1978. The control of volcanic column heights by eruption energetics and dynamics, *Journal of Geophysical Research*, v. 83, p. 1829-1836

X-Ray Fluorescence Whole Rock Analyses Data

See Appendix IV for expected error range for each element

Sample	Latite									
	MOS DB 1	MOS DB 4	MOS DB 5	MOS DB 10	MOS DB 14	MOS DB 15	MOS DB 16	MOS DB 17	MOS DB 18	MOS DB 19
Date	13-Oct-96	13-Oct-96	13-Oct-96	13-Oct-96	13-Oct-96	13-Oct-96	13-Oct-96	13-Oct-96	13-Oct-96	13-Oct-96
Unnormalized Results (Weight %):										
SiO ₂	63.59	63.74	63.52	64.43	63.86	62.90	64.22	63.11	63.29	64.16
Al ₂ O ₃	14.76	14.83	14.77	15.09	15.02	14.84	15.18	14.82	14.85	15.00
TiO ₂	0.326	0.325	0.321	0.317	0.326	0.329	0.321	0.319	0.317	0.323
FeO	3.49	3.42	3.48	3.34	3.64	3.63	3.54	3.66	3.57	3.60
MnO	0.072	0.067	0.064	0.077	0.069	0.067	0.065	0.074	0.071	0.075
CaO	3.21	3.32	3.14	3.20	2.64	3.88	2.73	3.41	3.16	3.10
MgO	2.64	2.63	2.73	2.61	2.60	2.20	2.65	2.59	2.58	2.69
K ₂ O	4.71	4.68	4.72	4.56	4.67	4.62	4.59	4.54	4.57	4.66
Na ₂ O	4.82	4.87	4.82	5.10	4.92	4.66	5.20	4.89	4.85	4.99
P ₂ O ₅	0.260	0.262	0.257	0.253	0.261	0.260	0.271	0.258	0.258	0.268
K+Na	9.530	9.550	9.540	9.660	9.590	9.280	9.790	9.430	9.420	9.650
Total	97.87	98.14	97.83	98.98	98.00	97.39	98.77	97.67	97.52	98.87
Normalized Results (Weight %):										
SiO ₂	64.97	64.95	64.93	65.09	65.16	64.59	65.02	64.61	64.90	64.90
Al ₂ O ₃	15.08	15.11	15.10	15.25	15.33	15.24	15.37	15.17	15.23	15.17
TiO ₂	0.333	0.331	0.328	0.320	0.333	0.338	0.325	0.327	0.325	0.327
FeO*	3.56	3.48	3.56	3.38	3.71	3.73	3.58	3.75	3.66	3.64
MnO	0.074	0.068	0.065	0.078	0.070	0.069	0.066	0.076	0.073	0.076
CaO	3.28	3.38	3.21	3.23	2.69	3.98	2.76	3.49	3.24	3.14
MgO	2.70	2.68	2.79	2.64	2.65	2.26	2.68	2.65	2.65	2.72
K ₂ O	4.81	4.77	4.82	4.61	4.77	4.74	4.65	4.65	4.69	4.71
Na ₂ O	4.92	4.96	4.93	5.15	5.02	4.78	5.26	5.01	4.97	5.05
P ₂ O ₅	0.266	0.267	0.263	0.256	0.266	0.267	0.274	0.264	0.265	0.271
K+Na	9.74	9.73	9.75	9.76	9.79	9.53	9.91	9.65	9.66	9.70
Trace Elements (ppm):										
Ni	61	57	59	52	61	57	58	67	64	53
Cr	121	116	124	117	121	116	114	112	115	119
Sc	7	14	7	11	12	8	16	8	9	7
V	59	65	61	57	67	66	58	59	66	56
Ba	†2402	†2415	†2382	†2329	†2380	†2302	†2312	†2360	†2360	†2550
Rb	133	135	134	129	132	128	131	132	125	131
Sr	881	871	879	996	900	1057	823	820	882	932
Zr	141	140	136	141	141	142	140	141	140	144
Y	13	13	12	11	13	13	13	13	14	13
Nb	11.2	12.2	11.1	12.3	11.2	10.9	11.1	10.6	10.7	10.1
Ga	15	15	16	15	16	14	14	14	12	15
Cu	16	20	14	18	14	15	15	11	11	20
Zn	39	38	41	50	39	35	34	37	35	43
Pb	27	26	29	45	27	31	31	34	26	57
La	21	35	23	36	38	33	27	19	44	30
Ce	43	53	40	35	38	33	40	45	49	41
Th	8	9	6	8	7	10	8	8	9	9

Major elements are normalized on a volatile-free basis, with total Fe expressed as FeO.

"R" denotes a duplicate bead made from the same rock powder.

"†" denotes values >120% of our highest standard.

Sample	Latite				Deer Butte				
	MOS DB 20	MOS DB 22	MOS DB 23	MOS DB 25	MOS DB 26	MOS DB 27	MOS DB 29	MOS DB 32	MOS DB 33
Date	13-Oct-96	13-Oct-96	13-Oct-96	13-Oct-96	13-Oct-96	14-Oct-96	14-Oct-96	14-Oct-96	14-Oct-96

Unnormalized Results (Weight %):

SiO2	63.91	64.13	64.46	64.12	64.64	64.18	64.18	59.71	61.25
Al2O3	14.98	15.07	15.14	15.09	15.25	15.12	15.08	14.29	14.41
TiO2	0.318	0.323	0.313	0.319	0.318	0.321	0.306	0.437	0.366
FeO	3.54	3.61	3.49	3.60	3.57	3.55	3.54	5.07	4.50
MnO	0.074	0.077	0.079	0.074	0.072	0.073	0.065	0.102	0.077
CaO	3.36	3.12	3.10	2.89	2.48	2.95	2.90	4.55	4.08
MgO	2.61	2.52	2.53	2.66	2.30	2.48	2.60	4.35	3.15
K2O	4.62	4.72	4.77	4.79	4.63	4.83	4.66	4.80	4.54
Na2O	5.02	4.99	5.02	4.90	5.16	4.91	5.04	4.43	4.62
P2O5	0.262	0.256	0.259	0.256	0.255	0.261	0.247	0.380	0.316
K+Na	9.640	9.710	9.790	9.690	9.790	9.740	9.700	9.230	9.160
Total	98.69	98.82	99.16	98.70	98.67	98.68	98.62	98.12	97.30

Normalized Results (Weight %):

SiO2	64.76	64.90	65.01	64.96	65.51	65.04	65.08	60.85	62.95
Al2O3	15.18	15.25	15.27	15.29	15.46	15.32	15.29	14.56	14.81
TiO2	0.322	0.327	0.316	0.323	0.322	0.325	0.310	0.445	0.376
FeO*	3.58	3.65	3.51	3.65	3.61	3.60	3.59	5.17	4.62
MnO	0.075	0.078	0.080	0.075	0.073	0.074	0.066	0.104	0.079
CaO	3.40	3.16	3.13	2.93	2.51	2.99	2.94	4.64	4.19
MgO	2.64	2.55	2.55	2.70	2.33	2.51	2.64	4.43	3.24
K2O	4.68	4.78	4.81	4.85	4.69	4.89	4.73	4.89	4.67
Na2O	5.09	5.05	5.06	4.96	5.23	4.98	5.11	4.51	4.75
P2O5	0.265	0.259	0.261	0.259	0.258	0.264	0.250	0.387	0.325
K+Na	9.77	9.83	9.87	9.82	9.92	9.87	9.84	9.41	9.41

Trace Elements (ppm):

Ni	59	54	57	61	53	55	57	106	72
Cr	117	114	114	111	107	114	103	196	147
Sc	16	11	11	8	10	12	8	11	10
V	67	55	58	52	53	58	58	83	82
Ba	†2386	†2352	†2389	†2386	†2410	†2338	†2390	†2651	†2313
Rb	131	135	140	139	125	147	129	137	132
Sr	1023	1033	1038	1029	1025	1025	1001	886	980
Zr	142	146	145	143	153	143	142	144	142
Y	12	13	12	12	13	12	12	15	13
Nb	10.7	10.5	10.1	10.7	10.9	10.7	10.9	10.4	11.3
Ga	14	15	14	15	17	15	13	15	16
Cu	17	21	17	19	14	19	24	36	26
Zn	49	55	58	49	55	44	43	60	45
Pb	39	43	37	43	54	36	36	29	20
La	32	33	19	20	18	19	23	27	37
Ce	51	46	42	31	58	36	40	42	50
Th	7	6	8	7	8	7	8	10	9

Major elements are normalized on a volatile-free basis, with total Fe expressed as FeO.

"R" denotes a duplicate bead made from the same rock powder.

"†" denotes values >120% of our highest standard.

Deer Butte Latite						
Sample	MOS DB	MOS DB	Mean	St.dev.	Max	Min
Date	4	4R				
	13-Oct-96	14-Oct-96				
Un-normalized Results (Weight %)						
SiO ₂	63.74	63.54	63.47	1.18	64.64	59.71
Al ₂ O ₃	14.83	14.87	14.90	0.25	15.25	14.29
TiO ₂	0.325	0.323	0.330	0.028	0.437	0.306
FeO	3.42	3.68	3.70	0.42	5.07	3.34
MnO	0.067	0.067	0.073	0.008	0.102	0.065
CaO	3.32	3.31	3.25	0.47	4.55	2.48
MgO	2.63	2.69	2.72	0.44	4.35	2.20
K ₂ O	4.68	4.68	4.65	0.10	4.83	4.36
Na ₂ O	4.87	4.93	4.91	0.17	5.20	4.43
P ₂ O ₅	0.262	0.264	0.270	0.029	0.380	0.247
K+Na	9.550	9.610	9.560	0.189	9.790	9.160
Total	98.14	98.35	98.27	0.55	99.16	97.30
Normalized Results (Weight %)						
SiO ₂	64.95	64.60	64.58	1.02	65.51	60.85
Al ₂ O ₃	15.11	15.12	15.16	0.20	15.46	14.56
TiO ₂	0.331	0.328	0.336	0.029	0.445	0.310
FeO*	3.48	3.74	3.77	0.44	5.17	3.38
MnO	0.068	0.068	0.074	0.008	0.104	0.066
CaO	3.38	3.37	3.31	0.49	4.64	2.51
MgO	2.68	2.74	2.77	0.45	4.43	2.26
K ₂ O	4.77	4.76	4.74	0.10	4.89	4.46
Na ₂ O	4.96	5.01	4.99	0.16	5.26	4.51
P ₂ O ₅	0.267	0.268	0.275	0.031	0.387	0.250
K+Na	9.73	9.77	9.73	0.15	9.92	9.41
Trace Elements (ppm)						
Ni	57	55	61	12	106	52
Cr	116	120	122	20	196	103
Sc	14	8	10	3	16	7
V	65	61	63	8	83	52
Ba	†2415	†2405	†2309	†79	†35	†59
Rb	135	135	132	6	147	117
Sr	871	880	938	82	1010	809
Zr	140	140	142	3	153	140
Y	13	14	13	1	15	11
Nb	12.2	10.2	11.0	0.6	12.3	10.1
Ga	15	15	15	1	17	12
Cu	20	14	19	6	36	11
Zn	38	40	44	8	60	34
Pb	26	27	36	13	75	20
La	35	23	28	8	44	18
Ce	53	36	43	7	58	31
Th	9	9	8	1	10	6

Major elements are normalized on a volatile-free basis, with total Fe expressed as FeO.
 "R" denotes a duplicate bead made from the same rock powder.

#Taken from Tureck-Schwarz, 1992, p.127-128.

Deer Butte

~Taken from Nash & Wilkinson, Contr.Min.Pet., v.25 (1970), p.244-245.

Sample	Mafic Inclusions					Mean	St.dev.	Max	Min
	MOS DB R	MOS DB 2	MOS DB 6	MOS DB 11	MOS DB I				
Date	14-Oct-96	14-Oct-96	14-Oct-96	14-Oct-96	14-Oct-96				
Unnormalized Results (Weight %):									
SiO2	48.20	46.49	47.70	48.99	50.78	48.43	1.60	50.78	46.49
Al2O3	8.82	11.94	7.93	11.35	12.27	10.46	1.96	12.27	7.93
TiO2	0.647	2.048	0.656	0.812	0.717	0.98	0.60	2.05	0.65
FeO	10.38	13.59	11.00	9.32	9.12	10.68	1.80	13.59	9.12
MnO	0.144	0.200	0.145	0.160	0.159	0.16	0.02	0.20	0.14
CaO	6.57	7.79	6.56	8.81	6.87	7.32	0.97	8.81	6.56
MgO	15.28	9.53	16.62	9.15	8.96	11.91	3.73	16.62	8.96
K2O	2.87	3.51	2.49	4.66	4.71	3.65	1.01	4.71	2.49
Na2O	1.27	1.81	0.96	2.17	2.55	1.75	0.65	2.55	0.96
P2O5	0.733	1.244	0.774	1.031	0.734	0.90	0.23	1.24	0.73
K+Na	4.140	5.320	3.450	6.830	7.260	5.40	1.65	7.26	3.45
Total	94.92	98.15	94.84	96.46	96.87	96.25	1.40	98.15	94.84
Normalized Results (Weight %):									
SiO2	50.78	47.36	50.30	50.79	52.42	50.33	1.84	52.42	47.36
Al2O3	9.29	12.16	8.36	11.77	12.67	10.85	1.90	12.67	8.36
TiO2	0.682	2.087	0.692	0.842	0.740	1.01	0.61	2.09	0.68
FeO*	10.94	13.85	11.60	9.67	9.42	11.09	1.78	13.85	9.42
MnO	0.152	0.204	0.153	0.166	0.164	0.17	0.02	0.20	0.15
CaO	6.92	7.94	6.92	9.13	7.09	7.60	0.96	9.13	6.92
MgO	16.10	9.71	17.52	9.49	9.25	12.41	4.05	17.52	9.25
K2O	3.02	3.58	2.63	4.83	4.86	3.78	1.03	4.86	2.63
Na2O	1.34	1.84	1.01	2.25	2.63	1.82	0.66	2.63	1.01
P2O5	†0.77	†1.27	†0.82	†1.07	†0.76	0.94	0.22	1.27	0.76
K+Na	†2.11	†3.11	†1.83	†3.32	†3.39	2.75	0.73	3.39	1.83
Trace Elements (ppm):									
Ni	602	245	699	126	162	366.80	264.78	699.00	126.00
Cr	912	576	959	407	751	721.00	231.11	959.00	407.00
Sc	19	32	17	24	25	23.40	5.86	32.00	17.00
V	157	236	136	173	156	171.60	38.32	236.00	136.00
Ba	1720	1464	1537	†2952	†3712				
Rb	121	129	111	165	162	137.60	24.51	165.00	111.00
Sr	441	321	373	752	973	572.00	279.72	973.00	321.00
Zr	112	379	103	149	129	174.40	115.71	379.00	103.00
Y	16	54	16	29	23	27.60	15.73	54.00	16.00
Nb	13.6	19.7	15.3	11.5	10.1	14.04	3.73	19.70	10.10
Ga	17	20	18	20	17	18.40	1.52	20.00	17.00
Cu	6	5	6	73	53	28.60	32.19	73.00	5.00
Zn	141	183	149	121	120	142.80	25.75	183.00	120.00
Pb	26	33	29	30	48	33.20	8.64	48.00	26.00
La	50	54	52	51	38	49.00	6.32	54.00	38.00
Ce	70	112	71	101	74	85.60	19.53	112.00	70.00
Th	10	4	8	2	0	4.80	4.15	10.00	0.00

Major elements are normalized on a volatile-free basis, with total Fe expressed as FeO.

"R" denotes a duplicate bead made from the same rock powder.

"†" denotes values >120% of our highest standard.

Sample	#Tur.-Sch. BP-S42	#Tur.-Sch. BP-S27	~Nash Shonk.sag
Date			
SiO2	53.39	51.61	47.00
Al2O3	12.16	9.95	12.91
TiO2	0.508	0.662	0.800
FeO	7.42	8.22	8.37
MnO	0.141	0.161	0.150
CaO	6.47	7.30	9.70
MgO	12.38	14.88	7.75
K2O	4.31	4.46	6.45
Na2O	2.80	2.19	1.85
P2O5	0.417	0.577	0.910
K+Na	7.110	6.650	8.300
Total	100.00	100.01	95.89

Appendix II

Chemical Analyses – Methods, Precision, and Accuracy

(taken from http://www.wsu.edu/~geology/Pages/Services/DJ_Paper/DJPaper.html)

At the Washington State University Laboratory in Pullman, WA., about 24 cc of the sample is milled in a Tema swigmill with tungsten carbide surfaces for 2 minutes. Three and one half grams of this rock powder is then mixed with 7.0 grams of spec. pure lithium tetraborate for 10 minutes. This mixture is then fused for 5 minutes at 1000 degrees C in 24 crucibles. The resulting beads are then reground in the Tema swigmill for 35 seconds and then refused for 5 minutes. After the second fusion the lower flat surfaces of the glass beads are ground on a lap with 240 grit SiC for 10 seconds, with 600 grit SiC for 10 seconds, and finished on a glass plate, briefly with 600 grit. The beads are then ultrasonically washed, dried, and loaded into the X-Ray fluorescence spectrometer (XRF).

XRF Analysis:

Analyses are made by comparing the x-ray intensities for each element of the unknown samples with those of eight international standards. The standards are recalibrated every three weeks or after a run of between one and two hundred unknown samples.

Precision:

Two fused tetraborate bead samples are used as internal standards. They are run every 28 samples to provide a check on instrumental performance and a measure of instrument precision.

Accuracy:

Absolute accuracy is impossible to quantify as no absolute standards are available. The best estimate of accuracy is derived from standard sample calibration curves shown as best straight line computer fit through plots of x-ray intensity versus “theoretical intensity”. The scatter of points about this line is a measure of accuracy of the method for each element. For most major elements the variation between the two standard sample beads (see below) is of the same order as their variation from the given value, with the inference that imprecision resulting from preparation of the beads (see Instrumental Precision, next page) is equal to or greater than inaccuracies caused by inadequate matrix and interference corrections. With the exception of Na, the total discrepancies from the “given” values are less than might reasonably be expected between two random samples collected in the field from the same rock unit – lava flow, igneous intrusion, etc. Hence, this degree of inaccuracy may be regarded as insignificant for most purposes of geologic correlations or petrogenetic modelling. For trace elements the precision for Ni, Cr, Sc, V, and Ba is significantly less than for Rb, Sr, Zr, Nb, Y, Ga, and Zn. Each of the elements Ni, Cr, Sc, V, and Ba can be regarded only as semi-quantitative below 30ppm. Rb, Sr, Zr, Nb, and Y have satisfactory precisions and accuracies down to 10ppm.

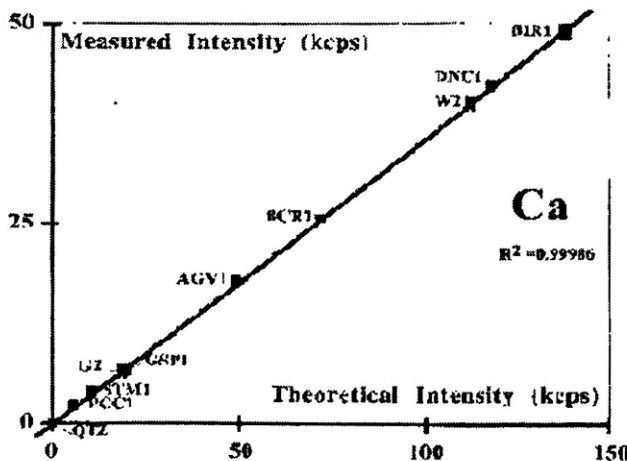
Appendix II cont.

Table 1: Overall Instrumental precision

Table 4 (a) Instrumental precision measured over an 8 month period on a single bead of GSP-1 (b) Precision measured on ten separate beads made from the same basalt powder analyzed during a single XRF run

Date	(a) GSP-1		(b) MAT		
	Avg N=75	StDev	Avg N=10 different beads	StDev	Range
Unnormalized Results (Weight %)					
SiO2	64.46	0.18	64.57	0.10	0.01
Al2O3	15.36	0.11	15.48	0.00	0.12
TiO2	0.667	0.004	2.707	0.007	0.010
FeO	1.88	0.01	1.54	0.11	0.38
MnO	0.030	0.001	0.038	0.001	0.002
CaO	2.02	0.01	5.09	0.02	0.08
MgO	1.10	0.10	1.87	0.02	0.06
K2O	6.58	0.06	2.80	0.01	0.02
Na2O	2.91	0.15	3.29	0.02	0.06
P2O5	0.287	0.003	0.885	0.002	0.000
Total	100.24	0.36	88.58	0.19	0.80
Normalized Results (Weight %)					
SiO2	69.29	0.09	64.36	0.06	0.21
Al2O3	16.31	0.07	13.67	0.04	0.11
TiO2	1.666	0.004	7.627	0.007	0.024
FeO*	3.25	0.11	12.72	0.09	0.31
MnO	0.027	0.001	0.211	0.001	0.004
CaO	2.01	0.01	6.46	0.00	0.09
MgO	1.06	0.10	2.81	0.02	0.08
K2O	6.55	0.07	2.84	0.01	0.03
Na2O	2.90	0.05	2.49	0.00	0.06
P2O5	0.286	0.002	0.887	0.003	0.000
Trace Elements (ppm)					
Ni	10	1	0	0	0
Cr	18	2	1	1	3
Co	4	2	2	0	11
V	54	6	194	4	18
Ba	1294	4	1.91	16	51
Rb	403	1	46	1	2
Sr	293	1	275	1	6
Zr	527	1	424	1	3
Y	30	1	47	1	3
Nb	27.4	0.6	26.2	0.8	4.2
Ce	24	1	11	2	6
Cu	31	2	2	2	6
Zn	103	2	123	2	4
Pb	53	-	10	1	3
Li	104	10	35	11	40
Fe	399	10	74	5	17
Th	106	2	0	0	5

Figure 2: Example calibration plot for Ca. Note: "theoretical intensity" is computed from wt. % of element using a fundamental parameters program for matrix corrections, and is equivalent to given concentration.



Appendix III

Petrography of Chemically Analyzed Samples

NOTE: In most samples, accessory minerals such as apatite, iddingsite, and sphene were ignored because they were not central to the research.

DB-R Deer Butte Quartz latite (Tlfb)

30% Phenocryst/nongroundmass minerals

Salite: 7%; Strongly resorbed; locally zoned; altering to carbonate on the rims;

Plagioclase: 5%; Large phenocrysts (glomeroporphyritic), locally zoned; albite and pericline twinning, usually rimmed by K-spar or other lower relief feldspar; dusty sieve texture very common, altering to carbonate.

Biotite: 5-7%; Strongly resorbed; rimmed by/reacting to magnetite/titano-magnetite/carbonate grains

Sanidine: 10%; Found rimming plagioclase grains; in groundmass

Magnetite: 2%; Altering biotite, also in groundmass.

Quartz: 5%; Mostly in late stage patches and groundmass

Carbonate: 5-7%

*Phenocrysts of 0.5-3mm, commonly glomeroporphyritic plagioclase, resorbed salite (pyroxene) and biotite floating in a sericitized and carbonate-altered sanidine, quartz, and plagioclase groundmass. One large mafic inclusion that appears to have completely sericitized (remnant biotite and Fe-oxides).

DB-13: Porphyritic Quartz latite

*30% Phenocryst/nongroundmass minerals

Plagioclase: 10%; resorbed, rounded cores of large feldspar phenocrysts (glomeroporphyritic), locally zoned; albite and pericline twinning, usually thickly rimmed by alkali feldspar or other lower relief feldspar.

Biotite: 5% Strongly resorbed; rimmed by/reacting to magnetite/titano-magnetite/carbonate grains

Sanidine: 15% Found rimming plagioclase grains; marked by dusty sieve texture of glass streaks; locally normal zoned;

Magnetite: 2% Altering biotite, also in groundmass.

Quartz: 5% Mostly in late stage patches and groundmass;

Carbonate: 5-7%

*Phenocrysts of ½-3mm, commonly glomeroporphyritic sanidine, and resorbed biotite floating in a sericitized and carbonate altered sanidine, quartz, and plagioclase groundmass. (Photo) One zoned sanidine near the edge of the slide has quartz at its end that has a strange texture in it (almost graphic).

DB-R#: Porphyritic Quartz latite

*40% Phenocryst/nongroundmass minerals

Salite: 6-8%; colorless/lt.green, strongly resorbed; usually altered by carbonate; occurs exclusively as sub-phenocrysts; normally zoned;

Plagioclase: 10%; as resorbed, rounded *cores* of large feldspar phenocrysts (glomeroporphyritic), locally zoned; albite and pericline twinning, usually thickly rimmed by alkali feldspar or other lower relief feldspar.

Sanidine: 15%; thickly mantling plagioclase; occurs as primary groundmass constituent; dusty sieve texture on nearly every grain in TS.

Biotite: 5%; Strongly resorbed, breaking down into magnetite/titanomagnetite; locally included in

plagioclase grains.

Carbonate: 10%; Altering salite, plagioclase, biotite, filling in veinlets, etc. Appears to have replaced some of the mafic inclusions entirely (remnant biotite, Fe-oxide).

Quartz: 5%; late stage interstitial grains; contains a strange glassy inclusion.

*Sanidine, salite and biotite phenocrysts in a K-spar, sanidine and quartz matrix. Biotite phenocrysts breaking down into Fe-oxide (one great example), salite resorbed, carbonate flooding in most of the sample. Sanidine has dusty sieve texture, inclusions.

DB-5: Porphyritic Quartz latite

*35% Phenocryst/nongroundmass minerals

Salite: 2-3%; colorless/lt.green, strongly resorbed; usually altered by carbonate; occurs exclusively as sub-phenocrysts; normally zoned;

Plagioclase: 15%; as resorbed, rounded *cores* of large feldspar phenocrysts (glomeroporphyritic), occasionally zoned; albite and pericline twinning, usually thickly rimmed by alkali feldspar or other lower relief feldspar.

Sanidine: 15%; thickly mantling plagioclase; occurs as primary groundmass constituent; dusty sieve texture on nearly every grain in TS.

Biotite: 2-3%; Strongly resorbed, breaking down into magnetite/titanomagnetite; locally included in plagioclase grains.

Carbonate: 10%; Altering salite, plagioclase, biotite, filling in veinlets, etc. Appears to have replaced some of the mafic inclusions entirely (remnant biotite, Fe-oxide).

Quartz: 5%; late stage interstitial grains; contains a strange glassy inclusion.

*Sanidine, salite and biotite phenocrysts in a K-spar, sanidine and quartz matrix. Biotite phenocrysts breaking down into Fe-oxide (one great example), salite resorbed, carbonate flooding in most of the sample. Sanidine has dusty sieve texture, inclusions.

DB-3: Porphyritic Quartz latite (Tlfb) + (Inclusion)

*30% Phenocryst/nongroundmass minerals

Salite: 8-10% Oscillatory, normal zoning; some resorption, some euhedral xstals; altering to sericite/clay
Plagioclase: 5-7% Resorbed, lg subhedral xstals (up to 7mm); commonly mantled by k-spar, poikilitically includes biotite, salite; abundant dusty sieve texture;

Sanidine: 15% Occasional large euhedral phenocryst, seen most as a thick mantle on plagioclase cores (but in one case it's the opposite)

Biotite: 5% Widespread as smaller phenocryst, contains/rimmed by magnetite/titano-magnetite; locally resorbed

Great examples of sieve textures, poikilitic overgrowths in plag. phenocryst grains.

Mafic Inclusion

Hb: 35% interlocking; generally fine grained; associated with magnetite

Biotite: 30% ; occurs as books; associated with magnetite

Sanidine: 20% interlocking; simple twinning

Magnetite: 5% minor accessory; associated with Hb and biotite.

Inclusion has a sharp margin, cusped edge, but there are small inclusions that look like they have "flaked" off of the edges. Could be a xenolith of some kind. There are two smaller inclusions that contain clinopyroxene; probably different from the large inclusion.

DB-4: Porphyritic Quartz latite (Tlfb)

*30% Phenocryst/nongroundmass minerals

Salite: 6-8% Colorless/lt.green, strongly resorbed; usually altered by carbonate; occurs exclusively as

Sub-phenocrysts; normally zoned (1 large crystal with oscillatory zoning); glomeroporphyritic.
Plagioclase: 5% Occurs as phenocrysts (glomeroporphyritic), and in groundmass; mantled by alkali feldspar; heavily altered by carbonate; dusty sieve texture evident (but filled in with carbonate); albite and pericline twinning, subtle zoning.
Sanidine: 10% Mantling plagioclase; occurs as primary groundmass constituent.
Biotite: 5% Strongly resorbed, breaking down into magnetite/titanomagnetite; occ included in plagioclase grains
Carbonate: 10% Altering salite, plagioclase, biotite, filling in veinlets, etc. Appears to have replaced some kind of mafic inclusion entirely (remnant biotite, Fe-oxide).

Plagioclase, salite and biotite phenocrysts in a plagioclase and K-spar matrix. Biotite phenocrysts breaking down into Fe-oxide (one great example), salite resorbed, carbonate flooding in most of the sample. Plagioclase has dusty sieve texture, inclusions.

DB-9: Porphyritic Quartz latite

*30% Phenocryst/nongroundmass minerals

Salite: 7%; colorless/lt.green, strongly resorbed; usually altered by carbonate; occurs exclusively as sub-phenocrysts; normally zoned;
Plagioclase: 5%; as resorbed, rounded *cores* of large feldspar phenocrysts (glomeroporphyritic), occasionally zoned; albite and pericline twinning; usually thickly rimmed by alkali feldspar or other lower relief feldspar.
Alkali feldspar (2V=25-40): 15%; thickly mantling plagioclase as large phenocrysts (1-6mm); occurs as primary groundmass constituent; dusty sieve texture on nearly every grain in TS. Sometimes includes Hb crystals that are not present in groundmass of quartz latite.
Biotite: 5-10%; Strongly resorbed, breaking down into magnetite/titanomagnetite; locally included in plagioclase grains.
Carbonate: 5%; Altering salite, plagioclase, biotite, filling in veinlets, etc. Appears to have replaced some of the mafic inclusions entirely (remnant biotite, Fe-oxide).
Quartz: 5%; late stage interstitial grains; contains a strange glassy inclusion.

*Sanidine, salite and biotite phenocrysts in a K-spar, sanidine and quartz matrix. Biotite phenocrysts breaking down into Fe-oxide (one great example), salite resorbed, carbonate flooding in most of the sample. Sanidine has dusty sieve texture, inclusions. There are 4 small shonkinite inclusions (4mm in diameter) throughout the TS.

SB-6: Porphyritic Quartz latite

*Phenocrysts of Hb and Plagioclase comprise 20% of the rock.

Hornblende: 15%; euhedral phenocrysts (1-5mm); (magnetite/titanomagnetite) in the core; rimmed by Fe-oxide due to breakdown; poikilitically includes sanidine (may be late stage as Hb breaks down with drop in pressure); oscillatory/normal/reverse zoning;
Sanidine: 5% Locally a microphenocryst, but mostly as very fine grained groundmass; resorbed; carlsbad twinning; dusty sieve texture; sometimes includes Fe-oxide.
Plagioclase: 2-3% groundmass mineral; a few times mantles plagioclase.
Quartz: up to 8% Occurs interstitially and in veinlets.
Fe-oxide: 5-7% mostly altering biotite, locally as a groundmass mineral

SB-11: Porphyritic Quartz latite

*Phenocrysts of Hb and Plagioclase comprise 25% of the rock. Groundmass consists of fine grained sanidine, plagioclase, and quartz.

Hornblende: 15%; euhedral phenocrysts (1-5mm); (magnetite/titanomagnetite) in the core; rimmed by Fe-oxide due to breakdown; poikilitically includes sanidine (may be late stage as Hb breaks down with drop in pressure); oscillatory/normal/reverse zoning; twinned.
Sanidine: 5% Occasional microphenocryst, but mostly as very fine grained groundmass; resorbed;

simple twinning; dusty sieve texture; sometimes includes Fe-oxide.
Plagioclase: 2-3%; occasional microphenocryst with albite twinning; includes Hb.
Quartz: 5% Occurs interstitially and in veinlets.
Fe-oxide: 5-7% mostly altering biotite, locally as a groundmass mineral.

SB-10: Porphyritic Quartz latite

*Phenocrysts of Hb and Plagioclase comprise 20% of the rock. Groundmass consists of fine grained sanidine, plagioclase, and quartz.

Hornblende: 15%; euhedral phenocrysts (1-5mm); (magnetite/titanomagnetite) in the core; rimmed by Fe-oxide due to breakdown; poikilitically includes sanidine; oscillatory/normal/reverse zoning; twinned; glomeroporphyritic.

Plagioclase: 5%; occasional resorbed phenocryst w/albite twinning; includes Hb.

Quartz: 5% Occurs interstitially and in veinlets.

Fe-oxide: 5-7%; mostly altering Hb, locally as a groundmass mineral.

SB-2: Porphyritic Quartz latite (Tlhf) + (Inclusion)

*Phenocrysts of Hb and Plagioclase/Alkali feldspar comprise 20% of the rock.

Hornblende: 10% Strongly resorbed, in some cases almost entirely altered to Fe-oxide (magnetite/titanomagnetite) in the core; rimmed by Fe-oxide due to breakdown; poikilitically includes plagioclase (may be late stage as Hb breaks down with drop in pressure).

Plagioclase: 5% Occasional microphenocryst, but mostly as very fine grained groundmass; resorbed; carlsbad twinning; dusty sieve texture; a few times mantled by K-spar; sometimes includes Fe-oxide.

Alkali feldspar: 5% groundmass mineral; a few times mantles plagioclase.

Quartz: up to 8% Occurs interstitially and in veinlets.

Fe-oxide: 5-7% mostly altering biotite, locally as a groundmass mineral

Mafic Inclusion

Biotite: 60% of inclusion; dominant mineral; occurs as laths/books

Fe-oxide(Magnetite/titano-magnetite): Up to 10% of inclusion; ubiquitous.

Sanidine: 15% of inclusion; show simple twinning in microcryst laths.

*Very fine grained inclusion, rounded at edges. Appears to have been magmatic, as the margins seem cusped and curvaceous, and parts of it are pulling away. There is a veinlet of coarser plagioclase cutting the inclusion up.

SB-R: Porphyritic Quartz latite (Tlhf) + Inclusion

*Phenocrysts compose 10% of quartz latite

Hornblende: 8% Phenocrysts (0.5-2mm) rimmed by Fe-oxide, breaking down to Fe-oxide in their core;

Plagioclase: 2-3% Mostly as subhedral interlocking groundmass grains.

Sanidine: 5% groundmass mineral

Quartz: up to 8% Occurs interstitially and in veinlets.

Fe-oxide: 6-8% Rimming and decomposing Hb crystals.

Mafic Inclusion (shonkinite):

Biotite: 30-35% of inclusion; occasionally breaks down to/includes Fe-oxide; mostly in inclusion interior

Hornblende: 20% of inclusion; dominant mineral rimming the inclusion (+lots of Fe-oxide and carbonate)

Salite: 30-35% of inclusion

Sanidine: 5-10% of inclusion; occurs as laths, interstitial microcrysts, and poikilitic crystals within Hb.

Fe-oxide: 10% of inclusion; larger crystals located interstitially along with plag.; smaller crystals seen rimming Hb and Biotite.

SB-8: Porphyritic Quartz latite (Tlhf) + Inclusion

*Phenocrysts comprise 15-20% of quartz latite

Hornblende: 10% Phenocrysts (0.5-2mm) rimmed by Fe-oxide, breaking down to Fe-oxide in their core;
Alkali feldspar (2V=25-40): 5% Mostly as subhedral interlocking groundmass grains; locally enclosed by Hb.

Plagioclase: 2-3% groundmass mineral

Fe-oxide: 6-8% Rimming and decomposing Hb crystals.

Carbonate: 5-7% altering in halo around inclusion.

Quartz: up to 8% Occurs interstitially and in veinlets.

*Fantastic example of Hb decomposing to Fe-oxide, water, etc. toward edge of slide

Mafic Inclusion:

Biotite: 35% of inclusion; rimming small carbonate pods; altering to sericite/carbonate

Salite: 20% of inclusion; twinned; resorbed slightly; altering to sericite/carbonate

Sanidine: 20% of inclusion

Carbonate: 20% as alteration of biotite/salite pyx.

*Inclusion contains pods of carbonate-altered biotite

SB-10: Porphyritic Quartz latite + Inclusion

*Phenocrysts comprise 15% of quartz latite

Hornblende: 10%; phenocrysts (0.5-3mm) rimmed by Fe-oxide, breaking down to Fe-oxide in their core; normalzoned; twinned; glomeroporphyritic.

Sanidine: 3%; mostly as subhedral interlocking groundmass grains; locally enclosed by Hb; also as groundmass mineral.

Plagioclase: groundmass mineral

Fe-oxide: 2-3%; rimming and decomposing Hb crystals.

Quartz: up to 8% of TS; occurs interstitially and in veinlets.

Carbonate: 2-3% altering cores of Hb crystals.

*One small Hb crystal is breaking down into plag., biotite, and Fe-oxide.

Mafic Inclusion:

Hornblende: 15%; the only complete grains are at the margin of the inclusion; breaking down into microcryst titanomagnetite/magnetite;

Fe-oxide: 15%; altering Hb grains (small crystals); occurs as interstitial phenocrysts.

Sanidine: 30%; occurs as altered phenocrysts, interstitially.

Carbonate: 35%; altering most of the inclusion.

*Inclusion appears to have reacted to the surrounding magma (Fe-oxide rim)

SB-6: Porphyritic Quartz latite (Tlfpb)

*Phenocrysts comprise 25% of quartz latite

Hornblende: 10%; Phenocrysts (0.5-3mm) rimmed by Fe-oxide, breaking down to Fe-oxide in their core; normal, oscillatory, reverse zoning; twinned; glomeroporphyritic; includes salite locally; included by/includes plag.; interior replaced by sanidine; in one case it has grown over a resorbing biotite, preserving an otherwise unstable mineral.

Plagioclase: 5%; many medium (0.5-2mm) phenocrysts with albite + pericline twins; pseudomorphs into Hb locally (*great example); slightly resorbed.

Sanidine: 5%; oscillatory zoned laths; glomeroporphyritic; commonly includes biotite, salite; dusty sieve texture; abundant in groundmass.

Salite: 5%; bright green phenocrysts (1/4-2mm); rounded/resorbed; glomeroporphyritic; reverse, normal, and oscillatory zoning.

Mafic Inclusions:

*Several tiny inclusions that are breaking up within the host quartz latite. A single biotite grain has broken off of one and is resorbed; also mantled by Hb. Inclusions composed of Salite, Hb, and sanidine, in order of decreasing abundance.

SB-11: Porphyritic Quartz latite + Inclusion

*Phenocrysts comprise 15-20% of quartz latite

Hornblende: 10% Phenocrysts (0.5-3mm) rimmed by Fe-oxide, breaking down to Fe-oxide/Biotite in their core; normal zoned; twinned; glomeroporphyritic.

Sanidine: 2% Mostly as subhedral interlocking groundmass grains; locally enclosed by Hb; one dusty sieve textured phenocryst.

Plagioclase: groundmass mineral

Fe-oxide: 5%; rimming and decomposing Hb crystals.

Quartz: up to 10%; occurs interstitially and in veinlets.

Mafic Inclusion

Salite: 45% of inclusion; altered to carbonate in core of inclusion; associated with Fe-oxide;

Biotite: 10%; in the middle of decomposing Hb grains

Titano-magnetite/magnetite: 15% of inclusion; seen rimming Hb, as interstitial microcrysts

Plagioclase: 15%; as laths and small crystals filling spaces between Hb and Biotite;

Carbonate: 15%; altering Hb and biotite in the core of inclusion;

*Inclusion is ripping apart on one side, Fe-oxide and Hb crystals are floating off into the quartz latite.

HB-2 Porphyritic Quartz latite (Tlhf)

*Phenocrysts and shonkinite take up 50% of the slide

Hornblende: 10%; forms reaction rim (1mm-6mm) around inclusion; euhedral laths; locally resorbed, twinned.

Plagioclase: 30%; strong oscillatory/reverse/normal zoning, euhedral phenocrysts of 1/2-6mm, pericline + albite twinning; abundant as groundmass; growing poikilitically over Hb.

Sphene: trace mineral.

Sanidine: 10% of quartz latite as groundmass material.

Quartz: 5%; veinlets, stringers, and in groundmass.

Phenocrysts of reverse/normal/oscillatory zoned plagioclase, Hb in a plag./K-spar groundmass.

Mafic Inclusion

Hb: Found rimming the inclusion; growing poikilitically around biotite

Orthopyroxene: 10% of inclusion

Clinopyroxene: 60-70% of inclusion, needles of clinopyroxene in the core, greenish augite between Hb and needles.

Biotite: 5% as microcrysts in groundmass

Sanidine: <5% as round grains

Magnetite/Titanomagnetite: 20% of inclusion, only mixed in with pyroxenes; no association with Hb.

Quartz: a few veins

HB-3: Porphyritic Quartz latite + Inclusion

*Phenocrysts and inclusion comprise 70% of TS

Plagioclase: 30%; occurs as large phenocrysts (1-6mm), groundmass grains; show strong reverse, oscillatory, normal zoning; albite and carlsbad twinning; glomeroporphyritic; some dusty sieve texture.

Hornblende: 10%; euhedral phenocrysts, commonly enclosed by and/or enclosing plag. grains; poikilitically overgrowing or mantling salite; twinned; normal, oscillatory zoning;

Salite (pyx.): 10%; strongly resorbed; *one great example mantled/enclosed by Hb;

Quartz: 10%; Occurs interstitially and in veinlets.
Titano-magnetite/magnetite: 5%; small (0.5-1mm) phenocrysts
Sphene: trace mineral

Mafic Inclusion:

Clinopyroxene: 70% of inclusion; uniformly fine grained (0.5-3mm); commonly twinned.
Sanidine: 20% of inclusion; interstitial fine grained groundmass
Titano-magnetite/magnetite: 5% of inclusion; very fine grained (smaller than in quartz latite)
*Inclusion appears to be strung out

HB-4: Porphyritic Quartz latite

*Phenocrysts and inclusion comprise 70% of TS

Plagioclase: 35%; occurs as large phenocrysts (1-6mm), groundmass grains; show strong reverse, oscillatory, normal zoning; albite and carlsbad twinning; glomero-porphyritic; some dusty sieve texture.
Hornblende: 15%; euhedral phenocrysts, commonly enclosed and/or enclosing plag. grains; poikilitically overgrowing or mantling salite; twinned; normal, oscillatory zoning;
Salite (pyx.): 10%; strongly resorbed; *one great example mantled/enclosed by Hb;
Quartz: 5%; Occurs interstitially and in veinlets.
K-spar: 5%; one phenocryst, minor in groundmass.
Titano-magnetite/magnetite: 5%; small (0.5-1mm) phenocrysts

Mafic Inclusion (Shonkinite):

Hornblende: 15%; mantling/pseudomorphing clinopyroxene on one side of the inclusion, as a reaction mineral between inclusion and magma
Clinopyroxene (Salite): 25%; ½-3mm light green crystals enclose analcime/K-spar grains; and occasional orthopyroxene grain.
Orthopyroxene (Hypersthene): 10%; small transparent crystals
Sanidine: 10%; commonly enclosing small Analcime/K-spar microcrysts; growing around clinopyroxene, Hb, and Biotite; simple twinning.
Analcime/K-spar: 5%; very fine grained euhedral hexagons found within plag. and sanidine.
Plagioclase: 5%; encloses Hb, Salite, Biotite, as an interstitial mineral
Biotite/Iddingsite: 20%; interlocking ½-2mm crystals
*Great example of a shonkinite inclusion.

HB-8: Porphyritic Quartz latite + Inclusion

*Phenocrysts and inclusion comprise 70% of TS.

Plagioclase: 35%; occurs as large phenocrysts (1-6mm), groundmass grains; show strong reverse, oscillatory, normal zoning; albite and pericline twinning; glomeroporphyritic; some dusty sieve texture; locally includes small sanidine crystals
Hornblende: 15%; euhedral phenocrysts, commonly enclosed and/or enclosing plag. grains; poikilitically overgrowing or mantling salite; twinned; normal, oscillatory zoning;
Salite (pyx.): 10%; strongly resorbed
Sanidine: 5%; as groundmass and as occasional inclusion within plag. phenocrysts.
Quartz: 5%; Occurs interstitially and in veinlets.
Titano-magnetite/magnetite: 5%; small (0.5-1mm) phenocrysts
Iddingsite: 2%; altering Hb.
Apatite: tr. Accessory mineral.

Mafic Inclusion:

Hornblende: 15%; mantling/pseudomorphing clinopyroxene on one side of the inclusion, as a reaction

mineral between inclusion and magma

Clinopyroxene (Salite): 45%; ½-3mm light green crystals enclose analcime/K-spar grains; and occasional orthopyroxene grain.

Plagioclase: 5%; commonly enclosing small Analcime/K-spar microcrysts; growing around clinopyroxene, Hb, and Biotite; albite and pericline twinning;

Sanidine: 5%; encloses Hb, Salite, Biotite, as an interstitial mineral

Biotite/Iddingsite: 20%; interlocking ½-2mm crystals

Titano-magnetite/magnetite: 5%; mostly associated with Hb that is rimming the inclusion.

*Inclusion rimmed by Hb on one side, having reacted with the host magma. Inclusion is very fine grained, with biotite-rich pods inside it. Good example of quench texturing. One smaller inclusion filled with Fe-oxide can be seen, as well as the edge of a larger inclusion on the side of the slide.

HB-10: Porphyritic Quartz latite + Inclusions

*Phenocrysts and inclusion comprise 60% of TS.

Plagioclase: 20%; occurs as large phenocrysts (1-6mm), groundmass grains; show strong reverse, oscillatory, normal zoning; albite and pericline twinning; glomeroporphyritic; some dusty sieve texture; locally includes small sanidine crystals, as well as Hb.

Hornblende: 10%; euhedral phenocrysts, commonly enclosed and/or enclosing plag. grains; poikilitically overgrowing or mantling salite; twinned; normal, oscillatory zoning;

Salite (pyx.): 10%; strongly resorbed

Sanidine: 5%; in groundmass and as small inclusions within plag. phenocrysts.

Quartz: 5%; Occurs interstitially and in veinlets.

Titano-magnetite/magnetite: 5%; small (0.5-1mm) phenocrysts

Iddingsite: 2%; altering Hb.

Apatite: tr. Accessory mineral.

Mafic Inclusions:

Hornblende: 15%; rims the entire inclusion; commonly serves as a reaction mineral between inclusion and magma

Clinopyroxene (Salite): 45%; 1/4-3mm light green crystals enclose analcime/K-spar grains; and occasional orthopyroxene grain; twinned; resorbed. Usually fine-medium grained.

Sanidine: 10%; commonly enclosing small hexagonal Analcime/K-spar microcrysts; growing around clinopyroxene, Hb, and Biotite.

Biotite: 20%; interlocking ½-2mm crystals

Titano-magnetite/magnetite: 5%; mostly associated with Hb that is rimming the inclusion.

*In addition to the lone large inclusion, there are numerous small inclusion consisting of biotite, very fine salite, and magnetite grains that are rimmed by Hornblende. Great examples of shonkinite in disequilibrium with surrounding magma.

ST-2: Porphyritic Quartz latite (Tlfpb)

*Phenocrysts make up 35% of TS

Salite ($Z^{\wedge}C=40-44$ degrees): 10%; bright green phenocrysts (1/4-2mm); rounded/resorbed; glomeroporphyritic; reverse, normal, and oscillatory zoning.

Plagioclase: 5%; one large phenocryst near slide edge mantled by K-spar.

Sanidine: 15%; oscillatory zoned; glomeroporphyritic; commonly includes biotite, salite; dusty sieve texture.

Biotite: 5%; resorbed; decomposing into Fe-oxide; rimmed and replaced by Fe-oxide.

Mafic Inclusion:

*45% non groundmass material.

Clinopyroxene (Salite): 45%; 1/4-3mm light green crystals enclose analcime/K-spar grains; and occasional

orthopyroxene grain; twinned; zoned; slightly resorbed. Usually fine-medium grained.
Sanidine: 10%; commonly enclosing small hexagonal Analcime/K-spar microcrysts; growing around clinopyroxene, Hb, and Biotite.
Biotite: 30%; interlocking ½-2mm crystals, breaking down into Fe-oxide; resorbed
Titano-magnetite/magnetite: 10%; mostly associated with Biotite.

*Inclusion is very fine grained, suggesting a quench texture. One small bleb appears to have broken off of one corner.

BT-1: Porphyritic Quartz latite (T1)

*Abundant sub-spherical to convoluted gas vesicles riddle the TS. Great example of shonkinite clot next to gas vesicle. Gas vesicles and phenocrysts make up 55% of TS.

Plagioclase: 20%; resorbed laths include biotite, sanidine; ubiquitous dusty sieve texture; albite + pericline twinning;

Sanidine: 10%; mostly in groundmas; but sometimes included by plagioclase phenocrysts.

Salite: 10%; slightly resorbed; commonly includes biotite; mantled by thin rim of brownish sericite;

Biotite/Sericite: 15%; breaking down into Fe-oxide, rimmed by Fe-oxide; commonly included in plag. grains; biotite alters to sericite in one round inclusion; as well as along margins of miarolitic cavities.

Quartz: 10%; late stage interstitial mineral; commonly grows into miarolitic gas vesicles, or completely fills them.

Mafic Inclusion:

Salite: 65% of inclusion; resorbed; altering to biotite; includes sanidine;

Biotite: 25% of inclusion; altering locally to sericite;

Sanidine: 8% of inclusion; euhedral laths included by biotite, growing interstitially.

*Inclusion surrounded by plenty of gas vesicles lined with quartz crystals.

BT-9: Porphyritic Quartz latite

*Abundant sub-spherical to convoluted gas vesicles riddle the TS. Great example of shonkinite clot next to gas vesicle. Gas vesicles and phenocrysts make up 50% of TS.

Plagioclase: 15%; resorbed laths include biotite, sanidine; ubiquitous dusty sieve texture; albite + pericline twinning;

Sanidine: 10%; mostly in groundmas; but sometimes included by plagioclase phenocrysts.

Salite: 10%; slightly resorbed; commonly includes biotite; mantled by thin rim of brownish sericite;

Biotite/Sericite: 15%; breaking down into Fe-oxide, rimmed by Fe-oxide; commonly included in plag. grains; biotite alters to sericite in one round inclusion; as well as along margins of miarolitic cavities; resorbed.

Quartz: 10%; late stage interstitial mineral; commonly grows into miarolitic gas vesicles, or completely fills them.

*Abundant small inclusions trailing off of larger inclusion. The largest inclusion appears to have gas vesicles surrounding it (they have been filled in with quartz). The inclusions all have very fine grained biotite, with larger salite phenocrysts.

BT-12: Porphyritic Quartz latite

*Abundant sub-spherical to convoluted gas vesicles riddle the TS. Great example of shonkinite clot next to gas vesicle. Gas vesicles and phenocrysts make up 55% of TS.

Plagioclase: 15%; resorbed laths include biotite, sanidine; ubiquitous dusty sieve texture; albite + pericline twinning;

Sanidine: 10%; mostly in groundmas; but sometimes included by plagioclase phenocrysts.

Salite: 10%; slightly resorbed; commonly includes biotite; mantled by thin rim of brownish sericite;
Biotite/Sericite: 15%; breaking down into Fe-oxide, rimmed by Fe-oxide; commonly included in plag.
grains; biotite alters to sericite in one round inclusion; as well as along margins of miarolitic
cavities; resorbed.

Quartz: 10%; late stage interstitial mineral; commonly grows into miarolitic gas vesicles, or completely
fills them;

*There are several small inclusions (4-6mm long) primarily composed of very fine grained salite, biotite,
and sanidine. The largest inclusion appears to have gas vesicles surrounding it (they have been filled in
with quartz). The inclusions all have very fine grained biotite, with an locally larger salite phenocryst.

BT-13: Vesicular Porphyritic Quartz latite

*Abundant sub-spherical to convoluted gas vesicles riddle the TS. Great example of shonkinite clot next to
gas vesicle. Gas and phenocrysts comprise 60% of TS.

Plagioclase: 30%; resorbed laths include biotite, sanidine; ubiquitous dusty sieve texture; albite + pericline
twinning;

Sanidine: 15%; mostly in groundmass as larger euhedral laths; but sometimes included by plagioclase
phenocrysts.

Salite: 5%; slightly resorbed; commonly includes biotite; mantled by thin rim of brownish sericite;

Biotite/Sericite: 10%; breaking down into Fe-oxide, rimmed by Fe-oxide; commonly included in plag.
grains; biotite alters to sericite in one round inclusion; as well as along margins of miarolitic
cavities; resorbed.

Quartz: 10%; late stage interstitial mineral; commonly grows into miarolitic gas vesicles, or completely
fills them (amygdules);

Mafic Inclusion (shonkinite):

Salite: 30%; resorbing phenocrysts; one large phenocryst (6-7mm) on the outside of the inclusion shows
oscillatory zoning.

Biotite: 30%; large phenocrysts (1-4mm) resorbing and altering locally to sericite;

Aegerine: 5%; occurs in large (1-4mm) clots of needles; mostly on outside of inclusion.

Sanidine: 25%; mostly as interstitial groundmass mineral;

Plagioclase: 5%; occasional microcryst with albite twinning.

Magnetite: tr. Accessory mineral

*There is a very fine grained clot trailing off the large inclusion that looks like the state of Florida (photo).
Large salite phenocryst may have been incorporated from quartz latite.

MC-1: Porphyritic Quartz latite + Inclusion

*Phenocrysts and Inclusions comprise 65% of the TS.

Hornblende: 7-10%; ½-5mm grains are mantled/replaced by Fe-oxide, in one case at several zones
throughout the grain; twinning; zoning; resorbing;

Biotite: 5%; grains almost totally resorbed; remnants are left with patches of Fe-oxide grains.

Salite: 25%; 1/4-3mm grains; slightly resorbed; shows strong normal/oscillatory/reverse zoning.

Sanidine: 5%; small euhedral grains (up to 1mm) and laths enclosed in salite, and floating in groundmass.

Fe-oxide: 10%; ubiquitous in groundmass, replacing and altering biotite and Hb.

Mafic Inclusion:

Salite: 35% of inclusion; strongly zoned (oscillatory, reverse, normal); ½-2mm grains.

Hornblende: 25% of inclusion; encloses plag., salite, and sanidine; breaking down to Fe-oxide on rims and
in core areas.

Biotite: 25% of inclusion; breaking down to Fe-oxide; resorbing slightly.

Sanidine: 10%; small euhedral grains (up to 2mm) and laths enclosed in salite, biotite, Hb.

Nepheline: up to 5%; small, cloudy euhedral laths (length fast).

Plagioclase: 5%; interstitial material that appears to have grown last or next to last.

Fe-oxide: 5%; large grains dispersed throughout inclusion.

*Fantastic example of disaggregating shonkinite inclusion. There is quartz veining in one corner of the slide. There are several smaller inclusions throughout the TS.

MC-5: Porphyritic Quartz latite

*Phenocrysts and Inclusions comprise 65% of the TS.

Hornblende: 5%; 1mm grains are mantled/replaced by Fe-oxide; twinning; subtle zoning on two grains.
Biotite: 5%; grains almost totally resorbed; remnants are left with patches of Fe-oxide grains.
Salite: 20%; 1/4-3mm grains; slightly resorbed; shows strong normal/oscillatory/reverse zoning.
Sanidine: 5%; small euhedral grains (up to 1mm) and laths enclosed in salite, and floating in groundmass.
Fe-oxide: 10%; ubiquitous in groundmass, replacing and altering biotite and Hb.

Mafic Inclusion:

Salite: 35% of inclusion; strongly zoned (oscillatory, reverse, normal); 1/2-2mm grains.
Hornblende: 25% of inclusion; encloses plag., salite, and sanidine; breaking down to Fe-oxide on rims and in core areas.
Biotite: 25% of inclusion; breaking down to Fe-oxide; resorbing slightly.
Sanidine: 10%; small euhedral grains (up to 2mm) and laths enclosed in salite, biotite, Hb.
Nepheline: up to 5%; small, cloudy euhedral laths (length fast).
Plagioclase: 5%; interstitial material that appears to have grown last or next to last.

SC-2: Porphyritic Quartz latite

Phenocrysts, inclusions, and disaggregating clots comprise 55% of TS

Plagioclase: 20%; large (up to 8mm) phenocrysts; mantled by K-spar of some kind; ubiquitous dusty sieve texture; includes salite, sanidine, apatite; glomeroporphyritic.
Biotite: 5%; usually breaking down into Fe-oxide; slightly resorbed; one small biotite clot that appears to be replacing what might have been an olivine grain.
Salite: 15%; strong normal zoning; rounded/resorbed 1-2mm grains;
Quartz: 5%; Occurs interstitially and in veinlets.

*There are several clots of fine grained salite+biotite inclusions, as well as some disaggregating blocks of Fe-oxide-rich, coarser grained groundmass. (Photo)

JB-3: Porphyritic Quartz latite (Tlfbhp)

*Phenocrysts and inclusion comprise 60% of TS

Plagioclase: 20%; dusy sieve texture prominent; resorbed; glomeroporphyritic; locally includes biotite and Hb; albite and pericline twinning.
Sanidine: 5%; twinned laths with little or no sieving; included in plagioclase grains, found in groundmass.
Biotite: 5%; very fine microphenocrysts (1/4-0.5mm) in groundmass.
Hornblende: 10%; large (1-5mm) phenocrysts; altering to Fe-oxide on rims; twinned; slight normal zoning.
Salite: 10%; twinned; normal/oscillatory/reverse zoning; subhedral grains up to 6mm in length; slightly resorbed
Magnetite/Titano-magnetite: 10%; ubiquitous Fe-oxide grains in groundmass, and rimming biotite and Hb grains.

Mafic Inclusion:

Hornblende: 35%; medium (1-5mm) interlocking crystals.
Salite: 30%
Biotite: 15%;
Plagioclase: 10%; mostly as a late stage interstitial mineral; enclosed by an occasional Hb
Sanidine: 5%; occasional lath included by Salite.
Analcime: 5% small rounded or hexagonal groundmass minerals.

CC-1: Pyroclastic quartz latite porphyritic tuff

*35% phenocrysts in an ash/glassy groundmass. Heavily altered/oxidized phenocrysts. Appears to be horizons of ash and coarser grained matrix material.

Sanidine: 5%; slightly resorbed euhedral laths; simple twinning;

Plagioclase: 15%; albite and pericline twinning; glass inclusions in a sieve texture on outside of grains; carbonate alteration; includes biotite;

Salite: 10%; mostly altered to sericite/carbonate; dark oxidation rims euhedrally surrounding remnant salite; resorbed; sometimes mantled by biotite.

Biotite: 5%; some grains are entirely unaltered, others have been entirely altered to something black;

Glass: 8%; swirls around phenocrysts, otherwise found in patches and streaks throughout the slide.

ET-A: Pyroclastic quartz latite porphyritic tuff

*Inclusions of quartz latite and shonkinite in a phenocryst rich, 25% glass matrix. Abundant gas vesicles.

Sanidine: 25%; occurs as microphenocryst laths (1/4-0.5mm); *note the very strange texture-appears to have dusty sieve texture/secondary alteration, but is commonly missing the inner parts of the phenocryst, or it has strangely crystallized as glass in the interior; simple twinning; resorbed to some degree.

Salite: 25%; occurs as resorbed phenocrysts (1-3mm) in glass, subhedral phenocrysts in quartz latite inclusions and shonkinite; commonly includes biotite; some grains have fuzzy black mantling from alteration; twinned; very fine grained within shonkinite inclusions.

Biotite: 15%; occurs as isolated unaltered, unreacted books in quartz latite inclusions; as very fine grained clots and twisted, bent up slivers in glass matrix; interlocking crystals in shonkinite; locally mantles salite.

Plagioclase: 5%; occasional microphenocryst (1/4-0.5mm) in quartz latite inclusions.

Glass: 25%; commonly surrounding inclusions; in streaks, blebs, and clots;

Vesicles: 5-10%

ET-3a: Volcanic Quartz latite

*Abundant gas stringers (very small), phenocrysts comprise 65% of TS.

Plagioclase: 15%; commonly mantles salite; larger phenocrysts (0.5-4mm) that have been slightly resorbed
Sanidine: 10%; resorbed, melted homogenous phenocrysts (0.5-2mm); *note the very strange texture-appears to have dusty sieve texture/secondary alteration, but is commonly missing the inner parts of the phenocryst, or it has strangely crystallized as glass in the interior; microphenocrysts in groundmass form cubic crystals.

Salite: 20%; 1/2-4mm euhedral/subhedral phenocrysts; poikilitically encloses biotite.

Biotite: 15%; importantly, it is unaltered, (rare for biotite or Hb); brown books.

Glass: 5%; occurs as stringers and blebs; found in the interior of plagioclase grains.

Gas vesicles: several spherical holes can be seen in the thin section, lined by mafic minerals (salite, biotite, analcime).

Mafic Inclusions:

Biotite: 40%; occurs as 2mm long interlocking books, or as very fine grained clots; poikilitically overgrown by salite grains; encloses analcime.

Salite: 30%; grains 1/4mm-3mm; includes sanidine; mantled by coarser grained biotite.

Analcime/Sanidine: 5-10%; very fine grained; low 2V; occurs as small euhedral crystal poikilitically enclosed by biotite/salite.

*Smaller inclusions can be seen throughout the TS, in which biotite grains are bent and stressed, surrounding very fine grained salite. Cores of inclusions are usually missing.

ET-7: Pyroclastic quartz latite porphyritic tuff

*Inclusions of quartz latite and shonkinite in a phenocryst rich, 25% glass matrix. Occasional gas vesicles. One large mafic inclusion takes up a third of the slide.

Sanidine: 15%; occurs as microphenocryst laths (1/4-0.5mm); *note the very strange texture-appears to have dusty sieve texture/secondary alteration, but is commonly missing the inner parts of the phenocryst, or it has strangely crystallized as glass in the interior; simple twinning; resorbed to some degree; ubiquitous in shonkinite inclusions.

Salite: 25%; occurs as resorbed phenocrysts (1-3mm) in glass, euhedral phenocrysts in quartz latite inclusions and shonkinite; commonly includes biotite; some grains have fuzzy black mantling from alteration; twinned; very fine grained within shonkinite inclusions.

Biotite: 15%; occurs as isolated unaltered, unreacted books in quartz latite inclusions; as very fine grained clots and twisted, bent up slivers in glass matrix; interlocking crystals/fine grained clots in shonkinite; locally mantles salite.

Plagioclase: 10%; common microphenocrysts (1/4-3mm) in mafic quartz latite inclusion; commonly altered to sericite.

Analcime: 5%; euhedral hexagons and subhedral circular grains in mafic quartz latite inclusion;

Glass: 25%; commonly surrounding inclusions; in streaks, blebs, and clots; makes background dark.

Vesicles: 5%

ET-8: Pyroclastic quartz latite porphyritic tuff

*Inclusions of quartz latite and shonkinite in a phenocryst rich, 25% glass matrix. Occasional gas vesicles.

Sanidine: 20%; occurs as microphenocryst laths (1/4-0.5mm); *note the very strange texture-appears to have dusty sieve texture/secondary alteration, but is commonly missing the inner parts of the phenocryst, or it has strangely crystallized as glass in the interior; simple twinning; resorbed to some degree; ubiquitous in shonkinite inclusions.

Salite: 25%; occurs as resorbed phenocrysts (1-3mm) in glass, euhedral phenocrysts in quartz latite inclusions and shonkinite; commonly includes biotite; some grains have fuzzy black mantling from alteration; twinned; very fine grained within shonkinite inclusions;

Biotite: 15%; occurs as isolated unaltered, unreacted books; interlocking crystals/fine grained clots altering to chlorite (in core) in shonkinite; locally mantles salite;

Analcime: 5%; euhedral hexagons and subhedral circular grains in mafic quartz latite inclusion;

Glass: 25%; commonly surrounding inclusions; in streaks, blebs, and clots; makes background dark.

Vesicles: 5%

*(Photo) There is a strange ring of mafic minerals that appears to have enclosed a portion of the quartz latite groundmass. There are at least 6 shonkinite inclusions 5mm in diameter throughout the TS.

ET-11: Volcanic quartz latite

*Abundant gas stringers (very small), phenocrysts comprise 65% of TS.

Plagioclase: 15%; commonly mantles salite; *note the very strange texture-appears to have dusty sieve texture/secondary alteration, but is commonly missing the inner parts of the phenocryst, or it has strangely crystallized as glass in the interior.

Salite: 30%; locally slightly resorbed; replaced and mantled by biotite; poikilitically encloses biotite.

Biotite: 20%; importantly, it is unaltered, (rare for biotite or Hb)

Glass: 5%; occurs as stringers and blebs that apparently all line up in similar directions; found in the interior of plagioclase grains.

Mafic Inclusions:

Biotite: 40%; occurs as 2mm long interlocking books, or as very fine grained clots; poikilitically overgrown by salite grains; encloses analcime.

Salite: 30%; grains 0.5mm-4mm; includes sanidine; mantled by biotite.

Analcime/Sanidine: 5-10%; very fine grained; low 2V; occurs as small euhedral crystal poikilitically enclosed by biotite/salite.

*Several smaller inclusions can be seen throughout the TS, in which biotite grains are bent and stressed. They are very fine grained, dominated by biotite and salite.

ET-6a: Pyroclastic quartz latite porphyritic tuff

*Streaks and clots of quartz latite in a phenocryst rich, 25% glass matrix. Abundant convoluted gas cavities.

Sanidine: 15%; occurs as microphenocryst laths (1/4-0.5mm); *note the very strange texture-appears to have dusty sieve texture/secondary alteration, but is commonly missing the inner parts of the phenocryst, or it has strangely crystallized as glass in the interior; simple twinning; resorbed to some degree;

Salite: 35%; occurs as resorbed phenocrysts (1-3mm) in glass, subhedral phenocrysts in quartz latite streaks; commonly includes biotite; twinned.

Biotite: 15%; occurs as isolated, unreacted books in quartz latite inclusions (some secondary alteration); as very fine grained clots and twisted, bent up slivers in glass matrix (altering to chlorite); locally mantles salite.

Plagioclase: 5%; occasional microphenocryst (1/4-0.5mm) in quartz latite streaks.

Glass: 25%; commonly surrounding inclusions; in streaks, blebs, and clots.

Appendix IV

Distribution and Abundance of Mafic Inclusions at Deer Butte and Suction Butte

Point counts conducted using a sheet of 36in x 36in transparent plastic upon which a grid with 1inch squares had been drawn with permanent marker

All data was subsequently converted to metric units (91.4cm x 91.4cm)

* # of Inclusions and Intersections normalized to a 36in x 36in area (or 91.4cm x 91.4cm)

Deer Butte (DB)

Sample	Locality	Description of location	#Incl.	#Inter.	Incl.A (cm) ²	Tot. A (cm) ²	#Incl. *norm.	#Inter. *norm.	%vol. est.	Size diameter
DB-a	DB; SWNE 34 T28N R19E	outcrop on W side of road, 3m in from road	51	31	173.4	8354	51	31	2.08	1/2-30cm
DB-b	DB; SWNE 34 T28N R19E	1.5m to the N, 1m below DB-a	40	19	82.7	3721	114.8	42.75	2.22	1/2-10cm
DB-c	DB; SWNE 34 T28N R19E	fresh exposure 1/2 way up the outcrop	27	12	64.0	3721	90	27	1.72	1/2-10cm
DB-d	DB; SWNE 34 T28N R19E	block down at talus slope to the east of Suction Cr.Rd.	45	20	128.0	3721	60.75	45	3.44	1/2-10cm
DB-e	DB; NENE 34 T28N R19E	most western outcrop at Deer Butte summit	26	8	64.0	3721	101.3	18	1.72	1/2-10cm
DB-f	DB; NENE 34 T28N R19E	2nd outcrop from the west at the top of Deer Butte	25	5	48.0	3721	58.5	11.25	1.29	1/2-10cm
DB-g	DB; NENE 34 T28N R19E	2nd outcrop from the west at the top of Deer Butte	49	16	101.3	8354	49	16	1.21	1/2-10cm
DB-h	DB; NENE 34 T28N R19E	2nd outcrop from the west at the top of Deer Butte	39	11	53.3	3721	87.75	24.75	1.43	1/2-10cm
DB-i	DB; NENE 34 T28N R19E	3rd outcrop from the west at the top of Deer Butte	25	7	64.0	3721	56.25	15.75	1.72	1/2-10cm
DB-j	DB; NENE 34 T28N R19E	3rd outcrop from the west at the top of Deer Butte	30	8	80.0	3721	67.5	18	2.15	1/2-10cm
DB-k	DB; SWNW 35 T28N R19E	2nd canyon S of butte in creekbed 30m from turn	38	9	48.0	3721	85.5	20.25	1.29	1/2-15cm
DB-l	DB; SWNW 35 T28N R19E	2nd canyon in creekbed 20m from N60W turn	16	13	80.0	3721	36	29.25	2.15	1/2-15cm
DB-m	DB; SWNW 35 T28N R19E	bend of 30yd section trending N80E, 3m up N slope	48	40	234.7	8354	48	40	2.81	1/2-15cm
DB-n	DB; SWNW 35 T28N R19E	bend of 30yd section trending N80E, 3m up N slope	39	26	314.7	8354	39	26	3.77	1/2-15cm
DB-o	DB; SWNW 35 T28N R19E	bend of 30yd section trending N80E, 3m up N slope	33	16	136.0	3721	74.25	36	3.66	1/2-15cm
DB-p	DB; SENE 34 T28N R19E	2nd canyon, S slope, across N gully, vertical face	36	26	106.7	8354	36	26	1.28	1/2-15cm
DB-q	DB; SENE 34 T28N R19E	up 2nd canyon, N slope, 40m from road in bedrock	29	16	74.7	8354	29	16	0.89	1/2-15cm
DB-r	DB; SENE 34 T28N R19E	up 2nd canyon, N slope, 40m from road in bedrock	27	13	53.3	3721	60.75	29.25	1.43	1/2-6cm
DB-s	DB; SENE 34 T28N R19E	2nd canyon, 8m up N slope, 40m from rd	23	36	128.0	3721	51.75	81	3.44	1/2-10cm
DB-t	DB; SENE 34 T28N R19E	2nd canyon, 5m up N slope, 35m from rd	27	10	48.0	3721	60.75	22.5	1.29	1/2-15cm
DB-u	DB; SWNE 34 T28N R19E	southern end of Suction Cr.Rd.outcrop, 7m from rd	31	13	74.7	3721	69.75	29.25	2.01	1/2-10cm
DB-v	DB; SWNE 34 T28N R19E	southern end of Suction Cr.Rd.outcrop, 10m from rd	24	9	48.0	3721	54	20.25	1.29	1/2-15cm
DB-w	DB; SWNE 34 T28N R19E	southern end of Suction Cr.Rd.outcrop, 12m from rd	25	18	80.0	3721	56.25	40.5	2.15	1/2-15cm
DB-x	DB; SWNE 34 T28N R19E	southern end of Suction Cr.Rd.outcrop, 15m from rd	27	26	128.0	3721	60.75	58.5	3.44	1/2-15cm
DB-y	DB; SWNE 34 T28N R19E	southern end of Suction Cr.Rd.outcrop, 15m from rd	33	16	72.0	3721	74.25	36	1.94	1/2-15cm

Mean	32.5	16.96	99.4	4833	62.91	30.41	2.06 %
Standard Deviation					20.82	15.32	0.87 %
Highest outcrop of butte (7 sites)					70.04	17.29	1.75 %
Lowest outcrop of butte (10 sites)					55.33	35.93	2.32 %

Suction Butte (SB)

Sample	Locality	Description of location	#Incl.	#Inter.	Incl. A (cm) ²	Tot. A (cm) ²	#Incl. *norm.	#Inter. *norm.	%vol. est.	Size diameter
SB-a	SB; SWSW 12 T28N R19E	middle of talus bulge (high point in talus pile), E wall	22	6	30.9	2540	49.5	13.5	1.22	1/2-2cm
SB-b	SB; SWSW 12 T28N R19E	middle of talus bulge (high point in talus pile), E wall	39	12	48.5	5715	39	12	0.85	1/2-3cm
SB-c	SB; SWSW 12 T28N R19E	southern end of talus bulge	28	9	39.7	2540	63	20.25	1.56	1/2-3cm
SB-d	SB; SWSW 12 T28N R19E	middle of talus bulge (high point in talus pile), E wall	27	10	44.1	2540	60.75	22.5	1.74	1/2-5cm
SB-e	SB; SWSW 12 T28N R19E	north end of talus bulge	24	7	35.3	5715	24	7	0.62	1/2-3cm
SB-f	SB; SWSW 12 T28N R19E	north end of talus bulge	28	12	30.9	2540	63	27	1.22	1/2-5cm
SB-g	SB; SWSW 12 T28N R19E	north end of talus bulge	29	8	35.3	5715	29	8	0.62	1/2-2cm
SB-h	SB; NESE 11 T28N R19E	north end of talus bulge	37	9	35.3	5715	37	9	0.62	1/2-2cm
SB-i	SB; NESE 11 T28N R19E	north end of talus bulge	38	8	35.3	5715	38	8	0.62	1/2-2cm
SB-j	SB; NESE 11 T28N R19E	30m from N end of eastern wall outcrop, 15m fr.trees	30	12	30.9	5715	30	12	0.54	1/2-2cm
SB-k	SB; NESE 11 T28N R19E	50m from N end of eastern wall outcrop	27	10	44.1	5715	27	10	0.77	1/2-3cm
SB-l	SB; NESE 11 T28N R19E	5m up on outcrop above fresh talus, S of talus bulge	24	9	35.3	5715	24	9	0.62	1/2-2cm
SB-m	SB; SWSW 12 T28N R19E	outcrop right at talus level, 25m south of talus bulge	39	7	35.3	5715	39	7	0.62	1/2-2cm
SB-n	SB; SWSW 12 T28N R19E	southern end of talus bulge, 15m below SB-n	36	10	41.9	5715	36	10	0.73	1/2-2cm
SB-o	SB; SWSW 12 T28N R19E	outcrop cliff, behind pine tree, 200m to N of contact	37	10	30.9	2540	83.25	22.5	1.22	1/2-2cm
SB-p	SB; SWSW 12 T28N R19E	large talus piece, 15m below outcrop on NW face	53	13	46.3	5715	53	13	0.81	1/2-2cm
SB-q	SB; NWSE 11 T28N R19E	large talus piece, 15m below outcrop on NW slope	59	9	39.7	5715	59	9	0.69	1/2-2cm
SB-r	SB; NWSE 11 T28N R19E	outcrop on N side, on fairly fresh eastern face	23	4	26.5	2540	51.75	9	1.04	1/2-2cm
SB-s	SB; NESE 11 T28N R19E	large talus chunk on N slope, 1/2 between treelines	23	8	61.7	2540	51.75	18	2.43	1/2-2cm
SB-t	SB; NESE 11 T28N R19E	E-SE face of boulder 200m down from outcrop	32	8	28.7	2540	72	18	1.13	1/2-2cm
SB-u	SB; NESE 11 T28N R19E	E-SE face of boulder 200m down from outcrop	57	5	22.1	5715	57	5	0.39	1/2-2cm
SB-v	SB; NESE 11 T28N R19E	W face of same boulder as SB-t	35	7	22.1	2540	78.75	15.75	0.87	1/2-2cm
SB-w	SB; NESE 11 T28N R19E	boulder, 35m down from outcrop, between treelines	26	5	13.2	2540	58.5	11.25	0.52	1/2-2cm
SB-x	SB; SWSW 12 T28N R19E	outcrop N of talus bulge, above SB-u, v, and w	28	6	13.2	2540	63	13.5	0.52	1/2-2cm
SB-y	SB; SWSW 12 T28N R19E	outcrop N of talus bulge, 30m S along cliff from SB-x	44	7	26.5	5715	44	7	0.46	1/2-2cm

Mean	33.8	8.44	34.1	4318	49.25	12.69	0.79 %
Standard Deviation					16.77	5.751	0.47 %
Highest outcrops of Suction Butte (9 sites)					62.78	13.5	1.01 %
Lowest outcrops of Suction Butte (9 sites)					44.81	14.14	1.01 %

Appendix V

Distribution and abundance of miarolitic cavities in Big Timber Butte and McCann Butte

All counted gas cavities were a minimum of 1/2cm in diameter

(*)Denotes the presence of innumerable vesicles smaller than 1/2cm in diameter or length

All values for # of Cavities and # of Intersections were normalized to a 24in x 24in area (or 61cm x 61cm)

Big Timber Butte (BTB)

Sample	Location	Description of locality	Area	# Cavities	# Inters.	Est.vol.%
BT-a	BTB; NWNE 26 T29N R18E	most N'ern valley, N ridge in large boulder	61 x 61cm	99	13	2.83
BT-b	BTB; NWNE 26 T29N R18E	most N'ern valley, N ridge in large boulder	61 x 61cm	76	14	3.05
BT-c	BTB; NWNE 26 T29N R18E	50m NE of BT-a,b	30.5 x 30.5cm	260	32	6.97
BT-d	BTB; NWNE 26 T29N R18E	70m E of BT-c, underside of large boulder	30.5 x 30.5cm	228	20	4.36
BT-e	BTB; NWNE 26 T29N R18E	underside of boulder 10m S of BT-d	30.5 x 30.5cm	188	24	5.23
BT-f*	BTB; SWNE 26 T29N R18E	E face of boulder, close to E nose of ridge	61 x 61cm	125	16	3.49
BT-g*	BTB; SWNE 26 T29N R18E	5m NE of BT-f, E face of boulder	30.5 x 30.5cm	72	16	3.49
BT-h	BTB; SWNE 26 T29N R18E	15m S of ridgetop, S face of boulder	30.5 x 30.5cm	196	40	8.71
BT-I	BTB; SWNE 26 T29N R18E	SE side of boulder 7m south of ridgetop on W end	91 x 91cm	115	17	3.70
BT-j	BTB; SWNE 26 T29N R18E	3m down N slope, 200m from W edge of tree line	61 x 61cm	212	40	8.71
BT-k	BTB; NWNE 26 T29N R18E	boulder, 50m from treeline, 375m from canyon	30.5 x 30.5cm	224	116	25.27
BT-L	BTB; SWNE 26 T29N R18E	40m from treeline, 425m W of canyon end	30.5 x 30.5cm	132	24	5.23
BT-m	BTB; SWNE 26 T29N R18E	15m from top on S slope	30.5 x 30.5cm	104	20	4.36
BT-n*	BTB; SWNE 26 T29N R18E	3m below gap in tree line, near E end of ridge	61 x 61cm	47	8	1.74
BT-o	BTB; SWNE 26 T29N R18E	Below split in tree line, 7m E-NE of BT-n	30.5 x 30.5cm	112	20	4.36
BT-p	BTB; SWNE 26 T29N R18E	boulder, 3m below tree line, 10m E/NE from BT-o	30.5 x 30.5cm	184	28	6.10
BT-q	BTB; SENE 26 T29N R18E	N side of rd in canyon, 350m from fence	30.5 x 30.5cm	148	32	6.97
BT-r*	BTB; SENE 26 T29N R18E	N side of rd in canyon, 300m from fence	61 x 61cm	51	7	1.53
BT-s	BTB; SENE 26 T29N R18E	S side of rd, under talus slope, 275m from fence	30.5 x 30.5cm	96	20	4.36
BT-t	BTB; SENE 26 T29N R18E	S side of rd in canyon, 80m from fence	91 x 91cm	76	5	1.09

Mean	137.25	25.6	5.58 %
Standard			
Deviation	63.94	23.44	5.11 %

McCann Butte (MC)

Sample	Location	Description of locality	Area	# Cavities	# Inters.	Est.vol.%
MC-a	MC; NESW 6 T29N R21E	5m from the top on the W slope	61 x 61cm	178	89	19.39
MC-b	MC; NESW 6 T29N R21E	5m from the top on the W slope	61 x 61cm	83	52	11.33
MC-c	MC; NESW 6 T29N R21E	12m from the top on the NW-W face	61 x 61cm	137	73	15.90
MC-d	MC; NESW 6 T29N R21E	15m from the top, NW face	61 x 61cm	213	126	27.45
MC-e	MC; NESW 6 T29N R21E	Isolated boulder, 30m from the top on W slope	61 x 61cm	104	62	13.51
MC-f	MC; NESW 6 T29N R21E	Small exposure on boulders, due south of top 25m	30.5 x 30.5cm	132	48	10.46
MC-g	MC; NESW 6 T29N R21E	Small exposure on boulders, due south of top 25m	30.5 x 30.5cm	172	24	5.23
MC-h	MC; NESW 6 T29N R21E	5m SW of top, one of largest boulders	30.5 x 30.5cm	128	44	9.59
MC-i	MC; NESW 6 T29N R21E	8m S of top, among big boulders	30.5 x 30.5cm	156	48	10.46
MC-j	MC; NESW 6 T29N R21E	S face of one of largest boulders, 3m from peak	30.5 x 30.5cm	176	32	6.97
MC-k	MC; NESW 6 T29N R21E	S face of one of largest boulders, 3m from peak	30.5 x 30.5cm	268	24	5.23
MC-L	MC; NESW 6 T29N R21E	Facing E on large boulder, 5m from top	30.5 x 30.5cm	148	32	6.97
MC-m	MC; NESW 6 T29N R21E	New flat surface, just below MC-L	30.5 x 30.5cm	88	20	4.36
MC-n	MC; NESW 6 T29N R21E	S side of Indian rock pile, 13m south of peak	30.5 x 30.5cm	132	48	10.46
MC-o	MC; NESW 6 T29N R21E	Boulder, 100m down from top on SE slope	61 x 61cm	130	27	5.88
MC-p	MC; NESW 6 T29N R21E	1m away from MC-o on underside of next boulder	30.5 x 30.5cm	168	52	11.33
MC-q	MC; NESW 6 T29N R21E	underside of boulder, 5m east of MC-p	61 x 61cm	139	27	5.88
MC-r	MC; NESW 6 T29N R21E	boulder towards E edge of pile, 3m E of MC-q	30.5 x 30.5cm	196	36	7.84
MC-s	MC; NESW 6 T29N R21E	S face of boulder, 5m S/SE of MC-o	30.5 x 30.5cm	136	28	6.10
MC-t*	MC; NESW 6 T29N R21E	E face of boulder, farthest point in pile from peak	61 x 61cm	50	12	2.61

Mean 146.7 45.2 9.85 %
Standard

Appendix VI

Pyroxenes

	oxide weight percent										
	SiO ₂	TiO ₂	Al ₂ O ₃	FeO	MnO	MgO	CaO	Na ₂ O	K ₂ O	Oxide Totals	Fe/Mg
DB-#32/33 1a	54.27	0.18	0.77	3.60	0.13	17.39	23.28	0.24	0.00	99.85	0.21
DB-#32/33 1b	54.12	0.19	0.83	5.29	0.18	16.23	23.20	0.26	0.00	100.31	0.33
DB-#32/33 1c	54.00	0.19	1.07	6.43	0.26	15.12	23.47	0.48	0.00	101.00	0.43
DB-#32/33 1d	53.88	0.06	1.37	6.51	0.34	13.93	23.13	1.02	0.00	100.24	0.47
DB-#32/33 1e	53.81	0.06	1.31	6.60	0.30	14.05	22.94	1.06	0.00	100.14	0.47
DB-#32/33 1f	52.38	0.11	1.49	11.38	0.48	10.98	21.02	1.71	0.00	99.55	1.04
DB-#32/33 2a	53.87	0.16	0.80	3.41	0.14	17.01	23.57	0.32	0.00	99.28	0.20
DB-#32/33 2b	52.82	0.06	1.58	7.41	0.42	13.85	22.95	0.92	0.00	100.00	0.53
DB-#32/33 2c	54.01	0.04	1.10	6.88	0.29	13.74	22.50	1.37	0.00	99.93	0.50
DB-#32/33 2d	53.50	0.03	1.36	7.84	0.29	13.34	22.36	1.20	0.00	99.91	0.59
DB-#32/33 3a	52.16	0.10	1.52	11.53	0.50	10.75	20.27	2.07	0.00	98.90	1.07
DB-#32/33 3b	53.18	0.12	1.62	11.58	0.44	11.07	21.02	1.97	0.00	101.00	1.05
DB-#32/33 3c	53.04	0.12	1.66	11.46	0.39	10.97	20.94	1.96	0.00	100.54	1.04
DB-#32/33 3d	52.30	0.13	1.64	11.55	0.60	11.06	21.55	1.30	0.00	100.15	1.04
DB-#32/33 3e	51.74	0.13	1.80	11.63	0.55	10.76	21.67	1.42	0.00	99.70	1.08
DB-R #6 Pyx 1a	53.73	0.06	1.06	6.76	0.26	14.34	21.76	1.08	0.03	99.07	0.47
DB-R #6 Pyx 1b	55.04	0.03	0.69	6.63	0.24	14.76	22.62	1.12	0.00	101.14	0.45
DB-R #6 Pyx 1c	56.15	0.04	0.47	5.77	0.33	15.81	22.39	0.83	0.00	101.78	0.37
DB-R #6 Pyx 1d	52.92	0.18	1.87	9.41	0.35	12.87	22.94	0.64	0.00	101.18	0.73
DB-R #6 Pyx 1e	52.61	0.16	1.98	10.53	0.31	12.07	22.48	1.01	0.00	101.15	0.87
DB-R #7 Pyx. 1a	54.77	0.21	0.80	3.67	0.14	17.23	23.85	0.21	0.00	100.89	0.21
DB-R #7 Pyx. 1b	54.59	0.22	1.11	3.69	0.09	16.86	23.68	0.25	0.00	100.48	0.22
DB-R #7 Pyx. 1c	46.85	0.31	1.43	5.25	0.15	12.61	22.47	0.35	0.01	89.43	0.42
DB-R #7 Pyx. 1C	54.20	0.07	0.88	9.37	0.52	12.48	21.81	1.70	0.00	101.04	0.75
DB-R #7 Pyx. 1d	53.45	0.10	1.53	10.41	0.44	11.79	21.10	1.89	0.00	100.71	0.88
DB-R #7 Pyx. 1e	52.26	0.19	1.88	11.46	0.49	10.87	21.82	1.37	0.00	100.36	1.05
DB-R #2 Pyx. 1a	52.94	0.38	1.72	6.37	0.21	14.99	23.14	0.37	0.01	100.14	0.42
DB-R #2 Pyx. 1b	52.89	0.42	1.96	7.39	0.22	14.33	23.15	0.47	0.00	100.82	0.52
DB-R #2 Pyx. 1c	53.09	0.29	1.66	7.33	0.21	14.39	22.90	0.52	0.00	100.39	0.51
DB-R #2 Pyx. 1d	54.03	0.21	0.98	4.96	0.17	16.29	23.57	0.26	0.00	100.47	0.30
DB-R #2 Pyx. 1e	54.43	0.05	1.10	4.62	0.17	15.12	23.60	1.09	0.00	100.18	0.31
DB-1 Pyx 1	53.65	0.12	1.24	7.97	0.33	14.93	21.24	0.71	0.00	100.18	0.53
DB-1 Pyx 2	52.90	0.13	2.11	9.11	0.34	12.62	22.23	1.04	0.00	100.49	0.72
DB-1 Pyx 4	54.14	0.06	1.41	7.02	0.30	13.98	22.22	1.15	0.01	100.28	0.50
DB-1 Pyx 5a	54.62	0.06	0.75	5.81	0.20	15.53	22.79	0.77	0.00	100.53	0.37
DB-1 Pyx 5b	54.35	0.20	0.76	5.92	0.23	16.60	22.30	0.29	0.02	100.67	0.36
DB-1 Pyx 5c	52.50	0.09	1.69	11.20	0.52	11.44	21.74	1.27	0.00	100.47	0.98
DB-1 Pyx 5d	54.62	0.04	1.16	7.74	0.29	13.73	21.74	1.56	0.00	100.90	0.56

Appendix VI cont.

Biotite

	oxide weight percent										
	SiO2	TiO2	Al2O3	FeO	MnO	MgO	CaO	Na2O	K2O	Total	Fe/Mg
DB-5 #28/29 1a	39.23	0.79	11.79	7.41	0.00	21.36	0.00	0.53	9.43	90.53	0.35
DB-5 #28/29 1b	39.71	0.66	12.32	7.06	0.05	21.96	0.00	0.60	9.59	91.96	0.32
DB-#28/29 1c	40.60	0.61	12.30	5.17	0.02	23.71	0.01	0.67	9.64	92.74	0.22
DB-#28/29 2a	40.37	0.66	12.49	5.80	0.01	22.78	0.01	0.70	9.51	92.33	0.25
DB-#28/29 2b	39.99	0.57	12.75	5.13	0.05	23.14	0.00	0.71	9.56	91.89	0.22
DB-#28/29 2c	39.61	0.63	12.64	8.38	0.02	21.34	0.00	0.66	9.53	92.81	0.39
DB-#26/27 1a	37.85	1.06	13.10	8.49	0.04	19.89	0.01	0.64	9.38	90.46	0.43
DB-#26/27 1b	39.63	1.45	12.26	8.51	0.06	20.72	0.55	0.68	8.72	92.57	0.41
DB-#26/27 1c	39.32	0.80	13.04	6.08	0.00	22.44	0.01	0.72	9.64	92.06	0.27

+ F, Cl standards

	SiO2	TiO2	Al2O3	FeO	MnO	MgO	CaO	Na2O	K2O	F	Cl	Total
DB-1 Bio1	39.08	1.00	13.57	9.28	0.09	20.23	0.00	0.62	9.41	3.64	0.06	96.98
DB-1 Bio2	39.27	0.81	12.81	8.68	0.05	21.42	0.00	0.70	9.42	4.07	0.08	97.31
DB-1 Bio3	39.88	0.64	13.12	5.11	0.03	23.30	0.00	0.58	9.76	3.65	0.01	96.09
DB-1 Bio4	39.16	0.89	13.95	5.34	0.03	22.85	0.00	0.68	9.52	3.95	0.01	96.38

Appendix VI cont.

Feldspars

		oxide weight percent										Ternary Plot			
		SiO2	TiO2	Al2O3	FeO	MnO	MgO	CaO	Na2O	K2O	Oxide Totals	Sum	Ca %	Na %	K %
DB-5 #30/31 a	albite	68.43	0.00	19.78	0.01	0.00	0.00	0.22	11.37	0.15	99.95	11.73	1.852	96.88	1.268
DB-5 #30/31 b	orthoclase	63.38	0.00	19.19	0.00	0.00	0.01	0.02	0.60	15.09	98.29	15.71	0.101	3.802	96.1
DB-5 #30/31 c	albite	68.50	0.02	19.49	0.03	0.00	0.00	0.36	11.15	0.46	100.01	11.97	2.977	93.15	3.87
DB-5 #30/31 e	orthoclase	64.60	0.00	19.52	0.01	0.01	0.00	0.03	0.63	15.22	100.03	15.88	0.203	3.99	95.81
DB-5 #30/31 d	alkali feld	67.66	0.00	18.86	0.07	0.00	0.01	0.10	10.12	2.18	99.00	12.40	0.835	81.61	17.56
DB-5 #30/31 A	albite	68.41	0.00	19.51	0.04	0.03	0.01	0.28	11.52	0.14	99.93	11.94	2.357	96.5	1.144
DB-5 #30/31 B	plag	67.60	0.00	19.59	0.08	0.00	0.00	0.47	9.58	2.78	100.11	12.83	3.675	74.69	21.63
DB-5 #30/31 C	albite	66.60	0.00	20.75	0.16	0.02	0.04	0.30	10.49	0.93	99.29	11.72	2.575	89.46	7.962
DB-5 #30/31 D	orthoclase	64.42	0.00	19.70	0.09	0.00	0.03	0.04	0.84	14.91	100.04	15.80	0.275	5.316	94.41
DB-5 #30/31 E	alkali feld	65.89	0.00	18.48	0.11	0.02	0.00	0.13	8.16	5.37	98.17	13.66	0.932	59.76	39.31
DB-13 #19 1a	plag	64.74	0.00	21.96	0.10	0.00	0.00	3.02	9.06	1.43	100.31	13.51	22.37	67.08	10.55
DB-13 #19 1b	plag	64.79	0.01	21.79	0.12	0.02	0.01	3.04	8.84	1.43	100.05	13.31	22.83	66.43	10.74
DB-13 #19 1c	plag	65.97	0.00	22.08	0.11	0.00	0.01	2.93	9.00	1.41	101.51	13.35	21.97	67.46	10.56
DB-13 #19 1d	plag	65.39	0.00	21.74	0.07	0.00	0.01	3.05	8.97	1.44	100.66	13.46	22.67	66.63	10.7
DB-13 #19 1e	plag	65.64	0.00	21.76	0.13	0.01	0.00	2.93	9.09	1.39	100.96	13.42	21.86	67.75	10.39
DB-13 #15 1a	sanidine	66.07	0.00	19.30	0.14	0.00	0.00	0.40	5.73	7.74	99.38	13.87	2.895	41.32	55.78
DB-13 #15 1b	sanidine	67.53	0.00	19.26	0.20	0.00	0.00	0.33	5.82	7.85	100.98	14.00	2.391	41.56	56.05
DB-13 #15 1c	sanidine	65.98	0.00	19.42	0.14	0.00	0.00	0.43	5.64	7.50	99.11	13.58	3.187	41.57	55.24
DB-13 #15 1d	sanidine	65.46	0.00	19.90	0.13	0.02	0.01	0.71	6.91	5.97	99.11	13.59	5.218	50.83	43.95
DB-13 #20 1a	plag	63.49	0.00	21.91	0.19	0.00	0.00	3.24	8.64	1.48	98.96	13.37	24.22	64.67	11.11
DB-13 #20 1b	plag	63.64	0.02	21.82	0.16	0.00	0.01	3.34	8.68	1.51	99.17	13.52	24.68	64.18	11.14
DB-13 #20 1c	sanidine	63.31	0.00	19.49	0.23	0.00	0.00	0.57	5.19	7.20	95.99	12.95	4.372	40.06	55.56
DB-13 #20 1d	alkali feld	65.07	0.00	19.57	0.03	0.02	0.00	0.77	6.07	5.06	96.59	11.90	6.476	50.99	42.53
DB-13 #18 1a	plag	63.45	0.00	21.62	0.17	0.01	0.00	3.33	8.88	1.15	98.60	13.36	24.95	66.48	8.571
DB-13 #18 1b	plag	64.07	0.01	21.49	0.19	0.00	0.01	3.10	8.86	1.43	99.16	13.39	23.17	66.19	10.64
DB-13 #18 1c	alkali feld	66.37	0.01	19.21	0.11	0.01	0.00	0.29	8.20	3.87	98.08	12.36	2.344	66.36	31.3
DB-9 #14 Plag 1a	orthoclase	62.90	0.00	19.92	0.01	0.00	0.00	0.02	0.40	15.04	98.30	15.47	0.161	2.616	97.22
DB-9 #14 Orth 1b	albite	66.32	0.00	19.19	0.05	0.00	0.00	0.23	11.05	0.17	97.01	11.45	2.035	96.45	1.515
DB-9 #14 Feld 1c	albite	68.50	0.00	19.48	0.41	0.01	0.00	0.19	11.49	0.26	100.35	11.94	1.586	96.22	2.191
DB-9 #14 Feld 1d	orthoclase	64.39	0.00	19.47	0.20	0.00	0.17	0.02	0.89	14.93	100.07	15.84	0.1	5.612	94.29
DB-9 #14 Feld 1e	alkali feld	71.72	0.00	16.62	0.02	0.03	0.00	0.10	8.49	3.46	100.45	12.05	0.847	70.46	28.69

Feldspars cont.

DB-1 K1	plag	65.80	0.01	23.59	0.17	0.00	0.05	3.45	9.16	1.13	103.35	13.74	25.1	66.67	8.23
DB-1 K2	plag	62.87	0.00	23.50	0.05	0.00	0.05	4.16	8.72	0.90	100.31	13.78	30.17	63.26	6.563
DB-1 K1*	plag	64.62	0.00	22.90	0.18	0.00	0.04	3.16	8.48	1.22	100.61	12.86	24.58	65.94	9.477
DB-1 Plag 1	plag	63.86	0.00	22.64	0.12	0.00	0.05	3.20	8.77	1.09	99.72	13.05	24.49	67.19	8.327
DB-1 GM 2	albite	68.55	0.00	20.14	0.08	0.00	0.05	0.31	10.90	0.43	100.46	11.64	2.685	93.65	3.667
DB-1 GM 3	albite	68.20	0.01	20.03	0.09	0.00	0.04	0.22	11.60	0.22	100.42	12.04	1.843	96.33	1.832
DB-1 Plag 2	plag	62.31	0.01	23.69	0.17	0.00	0.05	4.19	8.54	0.88	99.84	13.61	30.8	62.73	6.463
DB-1 Plag 3	plag	62.82	0.00	23.13	0.19	0.01	0.04	3.74	8.65	0.98	99.55	13.37	27.94	64.69	7.363
DB-1 Plag 3b	alkali feld	64.69	0.00	19.58	0.16	0.00	0.06	0.00	4.98	8.99	98.46	13.97	0	35.67	64.33
DB-1 Plag 3c	alkali feld	64.49	0.01	20.85	0.47	0.00	0.06	1.32	8.26	3.80	99.25	13.38	9.895	61.74	28.37
DB-1 Plag 3d	albite	67.36	0.01	20.12	0.00	0.00	0.05	0.19	11.54	0.57	99.84	12.30	1.563	93.82	4.619
DB-1 Plag 5	plag	63.93	0.01	22.09	0.13	0.00	0.05	2.58	9.39	1.19	99.37	13.16	19.63	71.35	9.013
SB-10 Plag 1a	plag	58.38	0.00	26.34	0.23	0.01	0.05	7.22	6.82	0.58	99.63	14.63	49.4	46.65	3.952
SB-10 Plag 1b	plag	59.69	0.00	25.54	0.22	0.00	0.05	6.54	7.14	0.58	99.76	14.27	45.84	50.08	4.079
SB-10 Plag 1c	plag	59.38	0.00	25.17	0.22	0.00	0.05	6.12	7.32	0.79	99.04	14.23	43.03	51.42	5.547
SB-10 Plag 1d	plag	64.43	0.00	22.13	0.15	0.00	0.05	2.98	9.24	0.99	99.98	13.22	22.55	69.92	7.525
SB-10 GM 4	alkali feld	65.24	0.00	19.47	0.27	0.00	0.06	0.14	4.42	10.29	99.89	14.85	0.932	29.77	69.3
SB-10 GM 5	plag	66.02	0.00	21.49	0.10	0.02	0.05	1.86	10.17	0.42	100.14	12.46	14.97	81.65	3.384
SB-10 GM 6	plag	66.18	0.01	20.70	0.19	0.00	0.04	1.29	9.39	2.04	99.84	12.72	10.14	73.85	16.02
SB-10 GM 7	plag	62.50	0.01	22.58	0.62	0.00	0.09	3.46	8.80	0.94	99.01	13.20	26.23	66.65	7.12
SB-10 GM 8	plag	64.81	0.02	21.75	0.28	0.00	0.05	2.49	8.98	1.47	99.87	12.95	19.26	69.35	11.39
SB-10 GM 9	alkali feld	63.78	0.02	19.26	0.75	0.00	0.06	0.07	5.17	8.50	97.59	13.74	0.51	37.65	61.85
SB-10 GM 10	alkali feld	66.94	0.01	19.86	0.14	0.01	0.06	0.00	7.40	5.04	99.46	12.44	0.00	59.50	40.50

Appendix VI cont.

Amphiboles

	oxide weight percent										
	SiO ₂	(TiO ₂	Al ₂ O ₃	FeO	MnO	MgO	CaO	Na ₂ O	K ₂ O	Oxide Totals	Fe/Mg
SB-6 #8 1a	39.65	1.84	11.88	17.82	0.29	9.43	11.33	2.07	1.71	96.03	1.89
SB-6 #8 1b	40.53	1.87	11.94	17.69	0.27	9.85	11.51	2.18	1.74	97.58	1.80
SB-6 #8 1c	39.62	1.90	12.17	18.35	0.32	9.41	11.51	2.11	1.76	97.16	1.95
SB-6 #8 1d	38.99	1.91	12.40	21.73	0.45	6.92	11.16	2.31	1.45	97.32	3.14
SB-6 #8 1e	38.90	1.97	11.67	20.40	0.51	7.99	11.43	2.15	1.65	96.68	2.55
SB-6 #9 1a	39.82	2.02	11.87	17.86	0.45	9.45	11.51	2.17	1.47	96.61	1.89
SB-6 #9 1b	40.00	2.03	11.73	17.93	0.35	9.62	11.45	2.27	1.58	96.97	1.86
SB-6 #9 1c	39.70	2.00	11.77	19.31	0.46	8.98	11.44	2.37	1.62	97.65	2.15
SB-6 #9 1d	39.72	1.93	11.23	18.77	0.41	9.30	11.37	2.25	1.65	96.64	2.02
SB-6 #9 1e	38.51	2.06	12.09	21.15	0.52	7.54	11.34	2.17	1.76	97.14	2.80
SB-6 #11 1a	38.22	1.99	11.36	21.40	0.52	7.40	11.37	2.03	1.65	95.94	2.89
SB-6 #11 1b	38.58	2.04	11.84	21.25	0.46	7.66	11.40	2.23	1.70	97.16	2.77
SB-6 #11 1c	38.09	2.05	11.26	20.90	0.55	7.29	11.50	2.02	1.67	95.33	2.87
SB-6 #11 1d	39.26	1.98	11.86	20.89	0.47	7.52	11.39	2.17	1.71	97.24	2.78
SB-6 #11 1e	38.70	1.99	11.99	20.85	0.50	7.38	11.41	2.20	1.67	96.70	2.83
SB-6 #13 1a	39.60	2.01	12.02	19.67	0.43	8.46	11.24	2.14	1.83	97.40	2.33
SB-6 #13 1b	40.17	1.87	11.58	19.13	0.47	9.19	11.28	2.14	1.69	97.52	2.08
SB-6 #13 1c	41.28	1.91	11.43	17.31	0.39	10.47	11.55	2.31	1.52	98.15	1.65
SB-6 #13 1d	40.31	1.86	11.92	18.91	0.40	8.80	11.25	2.23	1.71	97.40	2.15
SB-6 #13 1e	39.89	1.87	11.27	19.19	0.44	9.01	11.49	2.25	1.55	96.95	2.13
SB-11 #39 Hb 1a	40.22	1.71	12.23	17.73	0.30	9.88	11.35	2.23	1.64	97.29	1.80
SB-11 #39 Hb 1b	37.27	1.98	13.05	21.93	0.49	6.13	11.26	1.97	1.80	95.90	3.58
SB-11 #39 Hb 1c	38.85	2.07	12.48	20.26	0.45	7.92	11.34	2.15	1.68	97.20	2.56
SB-11 #39 Hb 1d	42.91	0.66	13.56	20.39	0.21	2.75	2.94	6.72	0.44	90.58	7.43
SB-11 #39 Hb 1e	38.82	1.82	11.47	20.73	0.62	7.92	11.28	2.05	1.67	96.39	2.62
SB-10 Hb 1	39.10	1.88	12.28	19.85	0.44	8.61	11.03	2.20	1.85	97.25	2.31
SB-10 Hb 2	40.29	1.94	11.92	19.03	0.43	8.77	10.89	2.21	1.74	97.23	2.17
SB-10 Hb 3	39.48	1.98	12.16	19.60	0.45	8.75	11.06	2.12	1.86	97.45	2.24
SB-10 Hb 4a	41.15	1.94	11.51	18.11	0.40	10.03	11.31	2.15	1.50	98.11	1.81
SB-10 Hb 4b	41.85	1.87	11.17	16.78	0.35	11.00	11.29	2.21	1.51	98.03	1.52
SB-10 Hb 4c	40.23	1.85	11.53	16.62	0.34	11.07	12.08	2.36	1.46	97.53	1.50
SB-10 Hb 4d	40.35	1.92	11.64	19.75	0.45	9.13	11.05	2.17	1.55	98.01	2.16

Amphiboles cont.

Normalized

oxide weight percent

	SiO2	TiO2	Al2O3	Fe2O3	FeO	MnO	MgO	CaO	Na2O	K2O	Total	Fe/Mg
SB-6 #8 1a	39.65	1.84	11.88	4.08	14.15	0.29	9.43	11.33	2.07	1.71	96.44	1.93
SB-6 #8 1b	40.53	1.87	11.94	3.73	14.33	0.27	9.85	11.51	2.18	1.74	97.95	1.83
SB-6 #8 1c	39.62	1.90	12.17	4.53	14.28	0.32	9.41	11.51	2.11	1.76	97.61	2.00
SB-6 #8 1d	38.99	1.91	12.40	4.47	17.71	0.45	6.92	11.16	2.31	1.45	97.77	3.21
SB-6 #8 1e	38.90	1.97	11.67	4.29	16.54	0.51	7.99	11.43	2.15	1.65	97.11	2.61
SB-6 #9 1a	39.82	2.02	11.87	3.92	14.33	0.45	9.45	11.51	2.17	1.47	97.01	1.93
SB-6 #9 1b	40.00	2.03	11.73	3.88	14.44	0.35	9.62	11.45	2.27	1.58	97.36	1.90
SB-6 #9 1c	39.70	2.00	11.77	4.43	15.33	0.46	8.98	11.44	2.37	1.62	98.09	2.20
SB-6 #9 1d	39.72	1.93	11.23	4.39	14.82	0.41	9.30	11.37	2.25	1.65	97.08	2.06
SB-6 #9 1e	38.51	2.06	12.09	4.81	16.82	0.52	7.54	11.34	2.17	1.76	97.62	2.87
SB-6 #11 1a	38.22	1.99	11.36	4.85	17.04	0.52	7.40	11.37	2.03	1.65	96.43	2.96
SB-6 #11 1b	38.58	2.04	11.84	4.78	16.95	0.46	7.66	11.40	2.23	1.70	97.64	2.84
SB-6 #11 1c	38.09	2.05	11.26	3.31	17.92	0.55	7.29	11.50	2.02	1.67	95.66	2.91
SB-6 #11 1d	39.26	1.98	11.86	3.55	17.70	0.47	7.52	11.39	2.17	1.71	97.60	2.82
SB-6 #11 1e	38.70	1.99	11.99	3.48	17.72	0.50	7.38	11.41	2.20	1.67	97.05	2.87
SB-6 #13 1a	39.60	2.01	12.02	4.48	15.65	0.43	8.46	11.24	2.14	1.83	97.85	2.38
SB-6 #13 1b	40.17	1.87	11.58	5.30	14.37	0.47	9.19	11.28	2.14	1.69	98.06	2.14
SB-6 #13 1c	41.28	1.91	11.43	4.21	13.52	0.39	10.47	11.55	2.31	1.52	98.58	1.69
SB-6 #13 1d	40.31	1.86	11.92	3.65	15.63	0.40	8.80	11.25	2.23	1.71	97.77	2.19
SB-6 #13 1e	39.89	1.87	11.27	4.02	15.57	0.44	9.01	11.49	2.25	1.55	97.36	2.18
SB-11 #39 Hb 1a	40.22	1.71	12.23	4.94	13.29	0.30	9.88	11.35	2.23	1.64	97.79	1.85
SB-11 #39 Hb 1b	37.27	1.98	13.05	4.08	18.26	0.49	6.13	11.26	1.97	1.80	96.31	3.64
SB-11 #39 Hb 1c	38.85	2.07	12.48	4.59	16.14	0.45	7.92	11.34	2.15	1.68	97.66	2.62

Appendix VI cont.

Fe-Oxides

ilmenite

oxide weight percent

	SiO2	TiO2	Al2O3	Fe2O3	FeO	MnO	MgO	CaO	Na2O	K2O	Totals
Un 31 DB-1 FeO 1	0.14	43.31	0.04	16.09	33.49	5.24	0.11	0.46	0.02	0.01	98.89

$$\text{Fe+3}=(\text{totFe}+\text{Mn}+\text{Mg})-(\text{Ti}+0.5*\text{Al}+0.5*\text{Cr})$$

titano-magnetite

oxide weight percent

	SiO2	TiO2	Al2O3	Fe2O3	FeO	MnO	MgO	CaO	Na2O	K2O	Totals
Un 32 DB-1 FeO 2	0.09	4.72	0.64	57.27	33.82	0.21	0.37	0.02	0.01	0.01	97.16
Un 33 DB-1 FeO 3	0.09	3.25	0.37	61.67	33.38	0.16	0.17	0.00	0.02	0.02	99.13
Un 39 SB-10 FeO 1	0.72	7.25	0.95	50.73	35.88	0.45	0.10	0.23	0.04	0.01	96.35
Un 40 SB-10 FeO 2	0.13	12.12	1.42	43.06	40.40	1.21	0.30	0.10	0.00	0.03	98.74
Un 44 SB-10 FeO 3	0.09	8.10	1.95	50.38	37.86	0.52	0.12	0.02	0.03	0.00	99.07
Un 45 SB-10 FeO 4	1.10	5.94	0.69	53.06	34.23	0.69	0.06	0.16	0.01	0.00	95.94
Un 46 SB-10 FeO 5	5.78	10.66	3.19	37.86	37.50	0.56	0.21	0.25	2.08	0.03	98.11
Un 51 SB-10 FeO 6	0.12	10.83	0.63	46.43	39.69	0.82	0.15	0.01	0.00	0.01	98.68
Un 52 SB-10 FeO 7	0.09	10.51	0.57	47.10	39.19	1.07	0.12	0.13	0.01	0.01	98.81
Un 53 SB-10 FeO 8	16.04	8.71	7.99	31.31	32.80	0.45	1.19	0.47	5.02	0.05	104.04

$$\text{Fe+3}=\frac{2}{3}(\text{totFe}+\text{Mn}+\text{Mg})-\frac{1}{3}(4*\text{Ti}+\text{Al}+\text{Cr})$$

Appendix VII

Sample locations and descriptions

Type: TS=Thin Section; Ref.= Referenced hand sample; WR=Whole rock analyses; EM=Electron Microprobe; (I)=Whole rock analyses of inclusion; Photo=Photo
 Rock: Tlp=Tertiary latite porphyry; Tlhf=Tertiary latite (hornblende + feldspar phenocrysts); Tlb=Tertiary latite (biotite phenocrysts); Tlh=Tertiary latite (hornblende

Sample	Type	Rock	Quadrangle	Location	Description of sample location
DB-R	TS, WR, I, EM	Tlbf	Rattlesnake 15	"Deer Butte"; SWNE 34 T28N R20E	SW Suction Creek Co. road, heading SE out of Cleveland
DB-1	TS, WR, EM	Tlbf	Rattlesnake 15	"Deer Butte"; SWNE 34 T28N R20E	SW Suction Creek Co. road, heading SE out of Cleveland
DB-2	TS, I	Tlbf	Rattlesnake 15	"Deer Butte"; SWNE 34 T28N R20E	SW Suction Creek Co. road, heading SE out of Cleveland
DB-3	TS, WR, I	Tlbf	Rattlesnake 15	"Deer Butte"; SWNE 34 T28N R20E	SW Suction Creek Co. road, heading SE out of Cleveland
DB-4	TS, WR	Tlbf	Rattlesnake 15	"Deer Butte"; SWNE 34 T28N R20E	SW Suction Creek Co. road, heading SE out of Cleveland
DB-5	TS, WR, EM	Tlbf	Rattlesnake 15	"Deer Butte"; SWNE 34 T28N R20E	SW Suction Creek Co. road, heading SE out of Cleveland
DB-6	Ref, WR, I	Tlbf	Rattlesnake 15	"Deer Butte"; SWNE 34 T28N R20E	W of Suction Creek Co. road, top of 1st knoll west from rd
DB-7	WR	Tlbf	Rattlesnake 15	"Deer Butte"; SWNE 34 T28N R20E	W/NW talus slope of deer butte east of canyon road
DB-8	WR	Tlbf	Rattlesnake 15	"Deer Butte"; SWNE 34 T28N R20E	W/NW talus slope of deer butte east of canyon road
DB-9	EM	Tlbf	Rattlesnake 15	"Deer Butte"; SWNE 34 T28N R20E	W/NW talus slope of deer butte east of canyon road
DB-10	WR	Tlbf	Rattlesnake 15	"Deer Butte"; NENE 34 T28N R20E	South side of 2nd outcrop from west at the top
DB-11	WR, I	Tlbf	Rattlesnake 15	"Deer Butte"; SWNW 35 T28N R20E	in 2nd canyon south of butte top, slick outcrop surface
DB-12	Ref	Tlbf	Rattlesnake 15	"Deer Butte"; SWNW 35 T28N R20E	in 2nd canyon south of butte top, slick outcrop surface
DB-13	WR, EM	Tlbf	Rattlesnake 15	"Deer Butte"; SWNW 35 T28N R20E	in 2nd canyon south of butte top, slick outcrop surface
DB-14		Tlbf	Rattlesnake 15	"Deer Butte"; SWNE 34 T28N R20E	SW Suction Creek Co. road, heading SE out of Cleveland
DB-15	WR	Tlbf	Rattlesnake 15	"Deer Butte"; SWNE 34 T28N R20E	SW Suction Creek Co. road, heading SE out of Cleveland
DB-16		Tlbf	Rattlesnake 15	"Deer Butte"; SWNE 34 T28N R20E	SW Suction Creek Co. road, heading SE out of Cleveland
DB-17	WR	Tlbf	Rattlesnake 15	"Deer Butte"; SWNE 34 T28N R20E	SW Suction Creek Co. road, heading SE out of Cleveland
DB-18		Tlbf	Rattlesnake 15	"Deer Butte"; SWNE 34 T28N R20E	SW Suction Creek Co. road, heading SE out of Cleveland
DB-19	WR	Tlbf	Rattlesnake 15	"Deer Butte"; SWNE 34 T28N R20E	W/NW talus slope of deer butte east of canyon road
DB-20	WR	Tlbf	Rattlesnake 15	"Deer Butte"; SWNE 34 T28N R20E	W/NW talus slope of deer butte east of canyon road
DB-21		Tlbf	Rattlesnake 15	"Deer Butte"; SWNE 34 T28N R20E	W/NW talus slope of deer butte east of canyon road
DB-22	WR	Tlbf	Rattlesnake 15	"Deer Butte"; NENE 34 T28N R20E	South side of 2nd outcrop from west at the top
DB-23	WR	Tlbf	Rattlesnake 15	"Deer Butte"; NENE 34 T28N R20E	South side of 2nd outcrop from west at the top
DB-24		Tlbf	Rattlesnake 15	"Deer Butte"; NENE 34 T28N R20E	South side of 3rd outcrop from west at the top
DB-25	WR	Tlbf	Rattlesnake 15	"Deer Butte"; NENE 34 T28N R20E	South side of 4th outcrop from west at the top
DB-26		Tlbf	Rattlesnake 15	"Deer Butte"; SESESE 34 T28N R20E	South side of 5th outcrop from west at the top
DB-27		Tlbf	Rattlesnake 15	"Deer Butte"; SESESE 34 T28N R20E	South side of 6th outcrop from west at the top
DB-28	WR	Tlbf	Rattlesnake 15	"Deer Butte"; SWNW 35 T28N R20E	In creek bed, 100ft.W from N60W trending turn

DB-29		Tlbf	Rattlesnake 15	"Deer Butte"; SWNW 35 T28N R20E	float, 30 feet west from DB-28, 140 yards from road
DB-30	WR	Tlbf	Rattlesnake 15	"Deer Butte"; SWNW 35 T28N R20E	In canyon floor, 20 feet E/SE from DB-m pt. Count locality
DB-31		Tlbf	Rattlesnake 15	"Deer Butte"; SWNW 35 T28N R20E	N slope of 2nd canyon S of butte top, around first bend
DB-32	WR	Tlbf	Rattlesnake 15	"Deer Butte"; SENE 34 T28N R20E	south slope of canyon, 100 yards from the road
DB-33		Tlbf	Rattlesnake 15	"Deer Butte"; SENE 34 T28N R20E	N slope of 2nd canyon S of butte top, 20 yards from rd
DB-34		Tlbf	Rattlesnake 15	"Deer Butte"; SENE 34 T28N R20E	N slope of 2nd canyon S of butte top, 20 yards from rd
SB-R	TS, WR, I	Tlh	Rattlesnake 15	Suction Butte; SWSW 12 T28N R20E	fresh exposure in the middle of the talus slope
SB-1	WR	Tlh	Rattlesnake 15	Suction Butte; SWSW 12 T28N R20E	talus and weathering dome rock on eastern flank
SB-2	TS, Ref, WR	Tlh	Rattlesnake 15	Suction Butte; SWSW 12 T28N R20E	talus and weathering dome rock on eastern flank
SB-3	Ref	Tlh	Rattlesnake 15	Suction Butte; SWSW 12 T28N R20E	talus and weathering dome rock on eastern flank
SB-4		Tlh	Rattlesnake 15	Suction Butte; SWSW 12 T28N R20E	talus and weathering dome rock on eastern flank
SB-5		Tlh	Rattlesnake 15	Suction Butte; SWSW 12 T28N R20E	talus and weathering dome rock on eastern flank
SB-6	WR, EM	Tlh	Rattlesnake 15	Suction Butte; SWSW 12 T28N R20E	large outcrop and weathering dome rock on eastern flank
SB-7		Tlh	Rattlesnake 15	Suction Butte; SWSW 12 T28N R20E	large outcrop and weathering dome rock on eastern flank
SB-8	TS, WR	Tlh	Rattlesnake 15	Suction Butte; SWSW 12 T28N R20E	large outcrop and weathering dome rock on eastern flank
SB-9	WR	Tlh	Rattlesnake 15	Suction Butte; SWSW 12 T28N R20E	large outcrop and weathering dome rock on eastern flank
SB-10	TS, WR, EM	Tlh	Rattlesnake 15	Suction Butte; SWSW 12 T28N R20E	large outcrop and weathering dome rock on eastern flank
SB-11	TS, WR, EM	Tlh	Rattlesnake 15	Suction Butte; SWSW 12 T28N R20E	large outcrop and weathering dome rock on eastern flank
SB-12		Tlh	Rattlesnake 15	Suction Butte; NWSE 11 T28N R20E	huge talus slope on NW side of butte
SB-13	WR	Tlh	Rattlesnake 15	Suction Butte; NWSE 11 T28N R20E	huge talus slope on NW side of butte
SB-14	WR	Tlh	Rattlesnake 15	Suction Butte; SWSW 12 T28N R20E	large outcrop and weathering dome rock on eastern flank
SB-15	Ref	Tlh	Rattlesnake 15	Suction Butte; SWSW 12 T28N R20E	talus and weathering dome rock on eastern flank
SB-16	Ref, WR	Tlh	Rattlesnake 15	Suction Butte; SWSW 12 T28N R20E	talus and weathering dome rock on eastern flank
SB-17	Ref	Tlh	Rattlesnake 15	Suction Butte; SWSW 12 T28N R20E	large outcrop and weathering dome rock on eastern flank
SB-18	Ref	Tlh	Rattlesnake 15	Suction Butte; SWSW 12 T28N R20E	large outcrop and weathering dome rock on eastern flank
SB-19	Ref	Tlh	Rattlesnake 15	Suction Butte; SWSW 12 T28N R20E	large outcrop and weathering dome rock on eastern flank
SB-20		Tlh	Rattlesnake 15	Suction Butte; SWSW 12 T28N R20E	E talus slope, 40yds. from outcrop, 220 yds from contact gully
SB-21		Tlh	Rattlesnake 15	Suction Butte; SWSW 12 T28N R20E	E talus slope, 40yds. from outcrop, 200 yds from contact gully
SB-22		Tlh	Rattlesnake 15	Suction Butte; SWSW 12 T28N R20E	outcrop 40 yds. from contact gully
SB-23		Tlh	Rattlesnake 15	Suction Butte; SWSW 12 T28N R20E	E talus slope, 15 yds from treeline, 35 yds from contact gully
SB-24		Tlh	Rattlesnake 15	Suction Butte; SWSW 12 T28N R20E	E talus slope, 15 yds from treeline, 20yds out from tree line
SB-25		Tlh	Rattlesnake 15	Suction Butte; SWSW 12 T28N R20E	outcrop 200 yds from contact gully
SB-26		Tlh	Rattlesnake 15	Suction Butte; SWSW 12 T28N R20E	outcrop 220 yds from contact gully
SB-27		Tlh	Rattlesnake 15	Suction Butte; SWSW 12 T28N R20E	eastern talus slope, 40 yds out from cliff, just N of talus slope
SB-28		Tlh	Rattlesnake 15	Suction Butte; SWSW 12 T28N R20E	up. talus slope, 30 yds below upper cliffs, 100 yds from N end
SB-29		Tlh	Rattlesnake 15	Suction Butte; SESE 11 T28N R20E	up. talus slope, 30 yds below upper cliffs, 100 yds from N end
SB-30		Tlh	Rattlesnake 15	Suction Butte; NWSE 11 T28N R20E	up. talus slope, 30 yds below upper cliffs, 100 yds from N end

SB-30a		Tlh	Rattlesnake 15	Suction Butte; NWSE 11 T28N R20E	group collected from forest along E slope above outcrops
SB-31		Tlh	Rattlesnake 15	Suction Butte; NWSE 11 T28N R20E	talus from NW slope towards the top of butte
SB-32		Tlh	Rattlesnake 15	Suction Butte; NWSE 11 T28N R20E	talus from NW slope towards the top of butte
SB-33		Tlh	Rattlesnake 15	Suction Butte; NESE 11 T28N R20E	talus from NW slope towards the top of butte
SB-34		Tlh	Rattlesnake 15	Suction Butte; NESE 11 T28N R20E	talus from NW slope, 20 ft below outcrop
SB-35		Tlh	Rattlesnake 15	Suction Butte; NESE 11 T28N R20E	NW slope, underneath outcrop; adjacent to SB-o
SB-36		Tlh	Rattlesnake 15	Suction Butte; NESE 11 T28N R20E	NW slope, 50 ft. underneath outcrop; adjacent to SB-o
SB-37		Tlh	Rattlesnake 15	Suction Butte; NESE 11 T28N R20E	North talus slope of Suction Butte
SB-38		Tlh	Rattlesnake 15	Suction Butte; NESE 11 T28N R20E	NE talus slope, 30 ft from tree line crest (hi pt. In tree line)
SB-39		Tlh	Rattlesnake 15	Suction Butte; NESE 11 T28N R20E	NE talus slope, 30 ft from tree line crest (hi pt. In tree line)
SB-40		Tlh	Rattlesnake 15	Suction Butte; NESE 11 T28N R20E	NE talus slope, 30 ft from tree line crest (hi pt. In tree line)
SB-41		Tlh	Rattlesnake 15	Suction Butte; NESE 11 T28N R20E	NE talus slope, 30 ft from tree line crest (hi pt. In tree line)
SB-42		Tlh	Rattlesnake 15	Suction Butte; NESE 11 T28N R20E	NE talus slope, 30 ft from tree line crest (hi pt. In tree line)
BT-1	TS	Tlhf	Rattlesnake 15	BigTimber Butte; NWNE 27 T29N R19E	BTA waypoint; two outcrops+talus on SW flank of intrusion
BT-2		Tlhf	Rattlesnake 15	BigTimber Butte; NWNE 27 T29N R19E	BTA waypoint; two outcrops+talus on SW flank of intrusion
BT-3		Tlhf	Rattlesnake 15	BigTimber Butte; NWNE 27 T29N R19E	BTA waypoint; two outcrops+talus on SW flank of intrusion
BT-4		Tlhf	Rattlesnake 15	BigTimber Butte; NWNE 27 T29N R19E	BTA waypoint; two outcrops+talus on SW flank of intrusion
BT-5		Tlhf	Rattlesnake 15	BigTimber Butte; NWNE 27 T29N R19E	BTA waypoint; two outcrops+talus on SW flank of intrusion
BT-6		Tlhf	Rattlesnake 15	BigTimber Butte; NWNE 27 T29N R19E	BTA waypoint; two outcrops+talus on SW flank of intrusion
BT-7		Tlhf	Rattlesnake 15	BigTimber Butte; NWNE 27 T29N R19E	blanketing butte, found adjacent to rd on SW and W sides
BT-8		Tlhf	Rattlesnake 15	BigTimber Butte; NWNE 27 T29N R19E	blanketing butte, found adjacent to rd on SW and W sides
BT-9	TS	Tlhf	Rattlesnake 15	BigTimber Butte; NWNE 27 T29N R19E	blanketing butte, found adjacent to rd on SW and W sides
BT-10		Tlhf	Rattlesnake 15	BigTimber Butte; NWNE 27 T29N R19E	blanketing butte, found adjacent to rd on SW and W sides
BT-11	Ref	Tlhf	Rattlesnake 15	BigTimber Butte; NWNE 27 T29N R19E	blanketing butte, found adjacent to rd on SW and W sides
BT-12	TS	Tlhf	Rattlesnake 15	BigTimber Butte; NWNE 27 T29N R19E	blanketing butte, found adjacent to rd on SW and W sides
BT-13	TS	Tlhf	Rattlesnake 15	BigTimber Butte; NWNE 27 T29N R19E	blanketing butte, found adjacent to rd on SW and W sides
BT-14		Tlhf	Rattlesnake 15	BigTimber Butte; SENW 26 T29N R19E	top of the bench, chipped off weathering outcrop
BT-15		Tlhf	Rattlesnake 15	BigTimber Butte; SENW 26 T29N R19E	found at the top of the bench
BT-16		Tlhf	Rattlesnake 15	BigTimber Butte; NWNW 26 T29N R19E	20ft S of sandstone outcrop at base of butte (local float)
BT-17		Tlhf	Rattlesnake 15	BigTimber Butte; NWNW 26 T29N R19E	20ft S of sandstone outcrop at base of butte (local float)
BT-18		Tlhf	Rattlesnake 15	BigTimber Butte; NWNW 26 T29N R19E	30 yards east of western sandstone outcrop
BT-19		Tlhf	Rattlesnake 15	BigTimber Butte; SENE 26 T29N R19E	200 feet below tree line, 350 yds from end of canyon
ST-1		Tlhf	Rattlesnake 15	Star Butte; SWSE 10 T28N R20E	outcrop on SW side of butte near the top
ST-2	TS	Tlhf	Rattlesnake 15	Star Butte; SWSE 10 T28N R20E	outcrop on SW side of butte near the top
ST-3		Tlhf	Rattlesnake 15	Star Butte; SWSE 10 T28N R20E	outcrop on SW side of butte near the top
ST-4		Tlhf	Rattlesnake 15	Star Butte; SWSE 10 T28N R20E	outcrop on SW side of butte near the top
ST-5	Ref	Tlhf	Rattlesnake 15	Star Butte; SWSE 10 T28N R20E	outcrop on SW side of butte near the top

ST-6	TS	TIhf	Rattlesnake 15'	Star Butte; SWSE 10 T28N R20E	outcrop on SW side of butte near the top
ST-7	Ref	TIhf	Rattlesnake 15'	Star Butte; SWSE 10 T28N R20E	outcrop on SW side of butte near the top
ST-8	Ref	TIhf	Rattlesnake 15'	Star Butte; SWSE 10 T28N R20E	outcrop on SW side of butte near the top
ST-9		TIhf	Rattlesnake 15'	Star Butte; SWSE 10 T28N R20E	outcrop on SW side of butte near the top
ST-10		TIhf	Rattlesnake 15'	Star Butte; SWSE 10 T28N R20E	S slope of butte, 100 yds or less from contact w/ country rx
ST-11		TIhf	Rattlesnake 15'	Star Butte; SWSE 10 T28N R20E	S slope of butte, 100 yds or less from contact w/ country rx
ST-12		TIhf	Rattlesnake 15'	Star Butte; SWSE 10 T28N R20E	S slope of butte, 100 yds or less from contact w/ country rx
ST-13		TIhf	Rattlesnake 15'	Star Butte; SWSE 10 T28N R20E	S slope of butte, 100 yds or less from contact w/ country rx
ST-14		TIhf	Rattlesnake 15'	Star Butte; SWSE 10 T28N R20E	S slope of butte, 100 yds or less from contact w/ country rx
ST-15		TIhf	Rattlesnake 15'	Star Butte; SWSE 10 T28N R20E	S slope of butte, 100 yds or less from contact w/ country rx
ST-16		TIhf	Rattlesnake 15'	Star Butte; SWSE 10 T28N R20E	western slope of butte, 15 yds from the top
MC-1	TS	TIp	Cleveland 15'	McCann Butte; SW 6 T29N R20E	western slope; majority from outcrop weathering into talus
MC-2	TS	TIp	Cleveland 15'	McCann Butte; SW 6 T29N R20E	western slope; majority from outcrop weathering into talus
MC-3	Ref	TIp	Cleveland 15'	McCann Butte; SW 6 T29N R20E	western slope; majority from outcrop weathering into talus
MC-4	Ref	TIp	Cleveland 15'	McCann Butte; SW 6 T29N R20E	western slope; majority from outcrop weathering into talus
MC-5	Ref	TIp	Cleveland 15'	McCann Butte; SW 6 T29N R20E	MCA waypoint on GPS, 2/3 of the way up on W slope
MC-6		TIp	Cleveland 15'	McCann Butte; SW 6 T29N R20E	1/2 way up on western slope
MC-7		TIp	Cleveland 15'	McCann Butte; SENE 6 T29N R20E	2/3 way up northern slope in outcrop ridge
MC-8		TIp	Cleveland 15'	McCann Butte; SENE 6 T29N R20E	2/3 way up northern slope in outcrop ridge
MC-9		TIp	Cleveland 15'	McCann Butte; SENE 6 T29N R20E	2/3 way up northern slope in outcrop ridge
MC-10		TIp	Cleveland 15'	McCann Butte; SENE 6 T29N R20E	3/4 way up northern slope in outcrop ridge
MC-11		TIp	Cleveland 15'	McCann Butte; NESW 6 T29N R20E	NW side of the top of the butte, amidst large boulders
MC-12		TIp	Cleveland 15'	McCann Butte; NESW 6 T29N R20E	200 ft from top on SE slope
MC-13		TIp	Cleveland 15'	McCann Butte; NESW 6 T29N R20E	200 ft from top on SE slope
MC-14		TIp	Cleveland 15'	McCann Butte; NESW 6 T29N R20E	between large boulders on S side of peak
MC-15		TIp	Cleveland 15'	McCann Butte; NESW 6 T29N R20E	next to eagle perch/Indian relict
MC-16		TIp	Cleveland 15'	McCann Butte; NESW 6 T29N R20E	top of the butte
MC-17		TIp	Cleveland 15'	McCann Butte; NESW 6 T29N R20E	top of the butte
MC-18		TIp	Cleveland 15'	McCann Butte; NESW 6 T29N R20E	south edge of boulder field
MC-19		TIp	Cleveland 15'	McCann Butte; NESW 6 T29N R20E	Indian relict
MC-20		TIp	Cleveland 15'	McCann Butte; NESW 6 T29N R20E	south edge of boulder field
CB-1		TIhf	Rattlesnake 15'	"Cairns Butte"; NESW 34 T28N R20E	last knoll before steep incline to peak
CB-2		TIhf	Rattlesnake 15'	"Cairns Butte"; NESW 34 T28N R20E	exposed SW trending canyon, 1/3 of the way to peak
CB-3		TIhf	Rattlesnake 15'	"Cairns Butte"; NESW 34 T28N R20E	top of butte, from among dispersed talus
CB-4		TIhf	Rattlesnake 15'	"Cairns Butte"; NESW 34 T28N R20E	top of butte, from among dispersed talus
CB-5		TIhf	Rattlesnake 15'	"Cairns Butte"; NESW 34 T28N R20E	2/3 to top on NE side of butte
FD-1		TIp	Cleveland 15'	"Faber Dike"; SWSE 16 T28N R20E	dike rock on north side of dam on Faber Reservoir

FD-2		Tip	Cleveland 15'	"Faber Dike"; SWSE 16 T28N R20E	dike rock on north side of dam on Faber Reservoir
FD-3		Tip	Cleveland 15'	"Faber Dike"; SWSE 16 T28N R20E	dike rock on north side of dam on Faber Reservoir
FD-4		Tip	Cleveland 15'	"Faber Dike"; SWSE 16 T28N R20E	dike rock on north side of dam on Faber Reservoir
FD-5		Tip	Cleveland 15'	"Faber Dike"; SWSE 16 T28N R20E	dike rock on north side of dam on Faber Reservoir
FD-6		Tip	Cleveland 15'	"Faber Dike"; SWSE 16 T28N R20E	dike rock on north side of dam on Faber Reservoir
FD-7	Ref	Tip	Cleveland 15'	"Faber Dike"; SWSE 16 T28N R20E	dike rock on north side of dam on Faber Reservoir
FD-8		Tip	Cleveland 15'	"Faber Dike"; SWSE 16 T28N R20E	dike rock on north side of dam on Faber Reservoir
MB-1		Tib/TIhf	Rattlesnake 15'	Myrtle Butte; NENE 36 T28N R20E	western slope of butte in what looks like a dike
MB-2		Tib/TIhf	Rattlesnake 15'	Myrtle Butte; NENE 36 T28N R20E	western slope of butte in what looks like a dike
MB-3		Tib/TIhf	Rattlesnake 15'	Myrtle Butte; NENE 36 T28N R20E	MBA waypoint of decent outcrop on western slope
MB-4		Tib/TIhf	Rattlesnake 15'	Myrtle Butte; NENE 36 T28N R20E	east-west trending dike extending away from butte
MB-5		Tib/TIhf	Rattlesnake 15'	Myrtle Butte; NWNW 31 T28N R21E	top of myrtle butte
MB-6		Tib/TIhf	Rattlesnake 15'	Myrtle Butte; NWNW 31 T28N R21E	top of myrtle butte
MB-7		Tib/TIhf	Rattlesnake 15'	Myrtle Butte; NENW 31 T28N R21E	south talus slope
WB-1		TIhf	Rattlesnake 15'	Wilson Butte; NW 25 T27N R20E	top of the butte, amidst talus pile
WB-2		TIhf	Rattlesnake 15'	Wilson Butte; NW 25 T27N R20E	top of the butte, amidst talus pile
WB-3		TIhf	Rattlesnake 15'	Wilson Butte; NW 25 T27N R20E	top of the butte, amidst talus pile
SS-1		TIhf	Rattlesnake 15'	"South Suction"; SESW 13 T28N R20E	large outcrop/alterd dome rock on SW flank of Suction
SS-2		TIhf	Rattlesnake 15'	"South Suction"; SESW 13 T28N R20E	large outcrop/alterd dome rock on SW flank of Suction
SS-3		TIhf	Rattlesnake 15'	"South Suction"; SESW 13 T28N R20E	large outcrop/alterd dome rock on SW flank of Suction
SS-4		TIhf	Rattlesnake 15'	"South Suction"; SESW 13 T28N R20E	large outcrop/alterd dome rock on SW flank of Suction
HB-1		TIhf	Rattlesnake 15'	Hansen Butte; NESW 16 T28N R20E	relat.unweathered talus at peak of 3rd knob from the S
HB-2		TIhf	Rattlesnake 15'	Hansen Butte; NESW 16 T28N R20E	relat.unweathered talus at peak of 3rd knob from the S
HB-3	TS	TIhf	Rattlesnake 15'	Hansen Butte; NESW 16 T28N R20E	relat.unweathered talus at peak of 3rd knob from the S
HB-4	TS	TIhf	Rattlesnake 15'	Hansen Butte; NESW 16 T28N R20E	relat.unweathered talus at peak of 3rd knob from the S
HB-5		TIhf	Rattlesnake 15'	Hansen Butte; NESW 16 T28N R20E	relat.unweathered talus at peak of 3rd knob from the S
HB-6		TIhf	Rattlesnake 15'	Hansen Butte; NESW 16 T28N R20E	relat.unweathered talus at peak of 3rd knob from the S
HB-7		TIhf	Rattlesnake 15'	Hansen Butte; NESW 16 T28N R20E	relat.unweathered talus at peak of 3rd knob from the S
HB-8	TS	TIhf	Rattlesnake 15'	Hansen Butte; NESW 16 T28N R20E	relat.unweathered talus at peak of 3rd knob from the S
HB-9		TIhf	Rattlesnake 15'	Hansen Butte; NESW 16 T28N R20E	relat.unweathered talus at peak of 3rd knob from the S
HB-10	TS	TIhf	Rattlesnake 15'	Hansen Butte; NESW 16 T28N R20E	relat.unweathered talus at peak of 3rd knob from the S
HB-11	Ref	TIhf	Rattlesnake 15'	Hansen Butte; NWNE 16 T28N R20E	NW trending dike extending out of Hansen butte
HB-12		TIhf	Rattlesnake 15'	Hansen Butte; SWSE 9 T28N R20E	4th knob of HB
HB-13		TIhf	Rattlesnake 15'	Hansen Butte; SWSE 9 T28N R20E	5th knob of HB
JB-1		TIhf	Rattlesnake 15'	Johnson Butte; SENE 17 T28N R20E	only JB outcrop; small knob SE of the main butte
JB-2		TIhf	Rattlesnake 15'	Johnson Butte; SENE 17 T28N R20E	only JB outcrop; small knob SE of the main butte
JB-3	TS	TIhf	Rattlesnake 15'	Johnson Butte; SENE 17 T28N R20E	only JB outcrop; small knob SE of the main butte

JB-4		Tlhf	Rattlesnake 15'	Johnson Butte; SENE 17 T28N R20E	only JB outcrop; small knob SE of the main butte
JB-5		Tlhf	Rattlesnake 15'	Johnson Butte; SENE 17 T28N R20E	only JB outcrop; small knob SE of the main butte
JB-6		Tlhf	Rattlesnake 15'	Johnson Butte; SENE 17 T28N R20E	only JB outcrop; small knob SE of the main butte
JB-7		Tlhf	Rattlesnake 15'	Johnson Butte; SENE 17 T28N R20E	only JB outcrop; small knob SE of the main butte
JB-8		Tlhf	Rattlesnake 15'	Johnson Butte; SENE 17 T28N R20E	only JB outcrop; small knob SE of the main butte
CC-1	TS	Pyroclastic	Maddux 15'	"Happy Hollow"; NESE 23 T27N R17E	6 miles S on Clear Creek rd. from Hungry Hollow Rd., E side
CC-2		Pyroclastic	Maddux 15'	"Happy Hollow"; NESE 23 T27N R17E	7 miles S on Clear Creek rd. from Hungry Hollow Rd., E side
CC-3		Pyroclastic	Maddux 15'	"Happy Hollow"; NESE 23 T27N R17E	8 miles S on Clear Creek rd. from Hungry Hollow Rd., E side
SC-1	Ref	Tlbf	Rattlesnake 15'	Scotty Butte; SWNE 13 T28N R19E	talus above large outcrop near top of butte, NW flank
SC-2	Ref	Tlbf	Rattlesnake 15'	Scotty Butte; SWNE 13 T28N R19E	talus above large outcrop near top of butte, NW flank
SC-3	TS	Tlbf	Rattlesnake 15'	Scotty Butte; SWNE 13 T28N R19E	talus above large outcrop near top of butte, NW flank
BB-1		Tlhf	Rattlesnake 15'	Black Butte; SWNE 6 T28N R20E	talus on western slope
BB-2		Tlhf	Rattlesnake 15'	Black Butte; SWNE 6 T28N R20E	talus on western slope
BB-3		Tlhf	Rattlesnake 15'	Black Butte; SWNE 6 T28N R20E	talus on western slope
BB-4	Ref	Tlhf	Rattlesnake 15'	Black Butte; SENE 6 T28N R20E	talus at north end of the summit
BB-5		Tlhf	Rattlesnake 15'	Black Butte; SENE 6 T28N R20E	talus at north end of the summit
BB-6		Tlhf	Rattlesnake 15'	Black Butte; SENE 6 T28N R20E	talus at north end of the summit
BB-7		Tlhf	Rattlesnake 15'	Black Butte; SENE 6 T28N R20E	talus at north end of the summit
TB-1		Tlh	Rattlesnake 15'	Taylor Butte; NWNW 12 T28N R19E	large outcrop on western flank of summit
TB-2		Tlh	Rattlesnake 15'	Taylor Butte; NWNW 12 T28N R19E	large outcrop on western flank of summit
ETA	TS, Ref	tuff-breccia	Maddux 15'	"Extrusive Top"; NWNE 5 T27N R19E	6.5 miles S of People's Creek turnoff, on W side of road
ET-2		tuff-breccia	Maddux 15'	"Extrusive Top"; NWNE 5 T27N R19E	6.5 miles S of People's Creek turnoff, on W side of road
ET-3	Ref	Tfpv	Maddux 15'	"Extrusive Top"; NWNE 5 T27N R19E	6.5 miles S of People's Creek turnoff, on W side of road
ET-3A	TS	Tfpv	Maddux 15'	"Extrusive Top"; NWNE 5 T27N R19E	6.5 miles S of People's Creek turnoff, on W side of road
ET-4		Tfpv	Maddux 15'	"Extrusive Top"; NWNE 5 T27N R19E	6.5 miles S of People's Creek turnoff, on W side of road
ET-4A		Tfpv	Maddux 15'	"Extrusive Top"; NWNE 5 T27N R19E	6.5 miles S of People's Creek turnoff, on W side of road
ET-5		tuff-breccia	Maddux 15'	"Extrusive Top"; NWNE 5 T27N R19E	6.5 miles S of People's Creek turnoff, on W side of road
ET-6		ash/tuff-brec	Maddux 15'	"Extrusive Top"; NWNE 5 T27N R19E	6.5 miles S of People's Creek turnoff, on W side of road
ET-6A	TS	ash/tuff-brec	Maddux 15'	"Extrusive Top"; NWNE 5 T27N R19E	6.5 miles S of People's Creek turnoff, on W side of road
ET-7	TS	ash	Maddux 15'	"Extrusive Top"; NWNE 5 T27N R19E	6.5 miles S of People's Creek turnoff, on W side of road
ET-8	TS	ash	Maddux 15'	"Extrusive Top"; NWNE 5 T27N R19E	6.5 miles S of People's Creek turnoff, on W side of road
ET-9	Ref	ash	Maddux 15'	"Extrusive Top"; NWNE 5 T27N R19E	6.5 miles S of People's Creek turnoff, on W side of road
ET-10	Ref	tuff-breccia	Maddux 15'	"Extrusive Top"; NWNE 5 T27N R19E	6.5 miles S of People's Creek turnoff, on W side of road
ET-11	TS	tuff-breccia	Maddux 15'	"Extrusive Top"; NWNE 5 T27N R19E	6.5 miles S of People's Creek turnoff, on W side of road
ET-12		tuff-breccia	Maddux 15'	"Extrusive Top"; NWNE 5 T27N R19E	6.5 miles S of People's Creek turnoff, on W side of road
ET-13		ash	Maddux 15'	"Extrusive Top"; NWNE 5 T27N R19E	6.5 miles S of People's Creek turnoff, on W side of road
ET-14		ash	Maddux 15'	"Extrusive Top"; NWNE 5 T27N R19E	6.5 miles S of People's Creek turnoff, on W side of road

ET-15		latite block	Maddux 15'	"Extrusive Top"; NWNE 5 T27N R19E	6.5 miles S of People's Creek turnoff, on W side of road
ET-16		ash	Maddux 15'	"Extrusive Top"; NWNE 5 T27N R19E	6.5 miles S of People's Creek turnoff, on W side of road
ET-17		ash	Maddux 15'	"Extrusive Top"; NWNE 5 T27N R19E	6.5 miles S of People's Creek turnoff, on W side of road
ET-18		wall rock?	Maddux 15'	"Extrusive Top"; NWNE 5 T27N R19E	6.5 miles S of People's Creek turnoff, on W side of road
VC-1		ash	Maddux 15'	"Volcano Canyon"; SENW 29 T26N R18E	exposed sequentially in deep ravines, 1 mile S of road
VC-2	Ref	ash	Maddux 15'	"Volcano Canyon"; SENW 29 T26N R18E	exposed sequentially in deep ravines, 1 mile S of road
VC-3	Ref	ash	Maddux 15'	"Volcano Canyon"; SENW 29 T26N R18E	exposed sequentially in deep ravines, 1 mile S of road
VC-4		latite block	Maddux 15'	"Volcano Canyon"; NWNW 33 T26N R19E	exposed sequence facing SE, app.50-100 ft from fault
VC-5		latite block	Maddux 15'	"Volcano Canyon"; NWNW 33 T26N R19E	exposed sequence facing SE, app.50-100 ft from fault
VC-6		latite block	Maddux 15'	"Volcano Canyon"; NWNW 33 T26N R19E	exposed sequence facing SE, app.50-100 ft from fault
VC-7		inclusion	Maddux 15'	"Volcano Canyon"; NWNW 33 T26N R19E	exposed sequence facing SE, app.50-100 ft from fault
VC-7a		inclusion	Maddux 15'	"Volcano Canyon"; NWNW 33 T26N R19E	exposed sequence facing SE, app.50-100 ft from fault
VC-8		latite block	Maddux 15'	"Volcano Canyon"; NWNW 33 T26N R19E	exposed sequence facing SE, app.50-100 ft from fault
VC-9		latite block	Maddux 15'	"Volcano Canyon"; SESE 29 T26N R19E	ridgetop exposure of ash, due east of intermittent coulee
VC-10		latite block	Maddux 15'	"Volcano Canyon"; SESE 29 T26N R19E	ridgetop exposure of ash, due east of intermittent coulee
VC-11		ash	Maddux 15'	"Volcano Canyon"; SESE 29 T26N R19E	ridgetop exposure of ash, due east of intermittent coulee

Appendix VIII

Orientation of Hornblende Crystals at Star Butte

Location 1					2					3		
Count #	Quad.Tr.	Quad. Pl.	Azim.	Tr. Plunge	Count #	Quad.Tr.	Quad. Pl.	Azim.	Tr. Plunge	Count #	Quad.Tr.	Quad. Pl.
1	N25W	16W	335	16	1	N36W	23W	324	23	1	N18W	15W
2	N22W	21W	338	21	2	N27W	12W	333	12	2	N22E	15E
3	N18W	8W	342	8	3	N38W	16W	322	16	3	N16W	20W
4	N20W	18W	340	18	4	N48W	15W	312	15	4	N25W	20W
5	N22W	28W	338	28	5	N36W	2W	334	2	5	N12E	21E
6	N21W	15W	339	15	6	N55W	18W	305	18	6	N17E	23E
7	N25W	10W	335	10	7	N59W	15W	301	15	7	N21E	12E
8	N25W	10W	335	10	8	N37W	26W	323	26	8	N8W	14W
9	N9W	2W	351	2	9	N23W	23W	337	23	9	N12W	25W
10	N24W	16W	336	16	10	N12W	18W	348	28	10	N98W	32NE
11	N3W	10W	357	10	11	N2E	22NE	2	22	11	N19W	32W
12	N22W	11W	338	11	12	N18W	11W	342	11	12	N28W	3W
13	N23W	8W	337	8	13	N25W	18W	335	18	13	N9W	12W
14	N21W	18W	339	18	14	N47W	8W	313	8	14	N44W	30W
15	N21W	24W	339	24	15	N60W	51W	300	51	15	N18W	27W
16	N24W	36W	336	36	16	N47W	30W	313	30	16	N75E	37E
17	N34W	26W	326	26	17	N82E	32SW	262	32	17	N9W	16W
18	N32W	44W	328	44	18	N11E	7E	11	7	18	N12W	13W
19	N10E	5E	10	5	19	N37W	22W	323	22	19	N0W	10N
20	N31W	6W	329	6	20	N6W	14W	354	14	20	N38W	13W
21	N24W	23W	336	23	21	N31W	13W	329	13	21	N45W	38W
22	N11W	2W	349	2	22	N12E	12E	12	12	22	N7E	29E
23	N38W	34W	322	34	23	N44W	3W	316	3	23	N6W	22W
24	N37W	18W	323	18	24	N34W	7W	326	7	24	N56W	28W
25	N16W	25W	344	25	25	N37W	14W	323	14	25	N84W	21SE
	Mean		324.08	17.36		Mean		284	17.68		Mean	

4					5					6		
Count #	Quad.Tr.	Quad. Pl.	Azim. Tr.	Plunge	Count #	Quad.Tr.	Quad. Pl.	Azim. Tr.	Plunge	Count #	Quad.Tr.	Quad. Pl.
1	N88W	3W	272	3	1	N72W	27NW	288	27	1	N78W	12NW
2	N45W	9W	315	9	2	N78W	26NW	282	26	2	N43W	5SE
3	N82E	22SW	262	22	3	N40W	2NW	320	2	3	N68W	4NW
4	N68W	4W	292	4	4	S	50S	180	50	4	N36W	34SE
5	N47E	13SW	227	13	5	N8W	50S	172	50	5	N81W	20NW
6	N18W	28SE	162	28	6	N36W	9NW	324	9	6	N74E	29SW
7	N38W	2NW	322	2	7	N58W	24NW	302	24	7	N55W	3NW
8	N10W	6SE	170	6	8	N82E	31NE	82	31	8	N62W	12NW
9	N58E	21SW	238	21	9	N83E	40SW	263	40	9	N67E	26SW
10	N7E	23SW	187	23	10	N72E	23SW	252	23	10	N16E	22SW
11	N3W	36NW	357	36	11	N73W	35NW	287	35	11	N38W	1SE
12	N67E	12SW	247	12	12	N23W	ON	337	0	12	N23W	13NW
13	N28E	43SW	208	43	13	N67W	25NW	293	25	13	N81W	17NW
14	N38W	10SE	142	10	14	N6W	12SE	177	12	14	N88W	29NW
15	N23W	16NW	337	16	15	N74W	4NW	286	4	15	N72E	33SW
16	N62E	3NE	62	3	16	N27E	45SW	207	45	16	N82W	31NW
17	N68W	11NW	292	11	17	N58W	22NW	302	22	17	N73W	23NW
18	N78W	6NW	282	6	18	N72E	38SW	252	38	18	N20E	21SW
19	N5W	19SE	175	19	19	N53W	12NW	307	12	19	N62W	33NW
20	N44W	5NW	316	5	20	N50E	12NE	50	12	20	N53W	16NW
21	N27W	18SE	153	18	21	N53W	9NW	307	9	21	N18W	20SE
22	N66W	4NW	294	4	22	N36W	15NW	324	15	22	N72W	16NW
23	N46W	20W	314	20	23	N17E	35SW	197	35	23	N15W	20SE
24	N1W	8SE	179	8	24	N42E	33SW	222	33	24	N64E	25SW
25	N73W	16NW	287	16	25	N90W	28NW	270	28	25	N71W	24NW
	Mean		243.68	14.32		Mean		251.32	24.28		Mean	

7					8					9				
Count #	Quad.Tr.	Quad. Pl.	Azim.	Tr.	Plunge	Count #	Quad.Tr.	Quad. Pl.	Azim.	Tr.	Plunge	Count #	Quad.Tr.	Quad. Pl.
1	N87E	26SW	267		26	1	N78W	22NW	282		22	1	N38W	6NW
2	N74W	14NW	286		14	2	N43W	15NW	317		15	2	N10W	19NW
3	N74E	23NW	254		23	3	N33W	8NW	327		8	3	N73W	12SE
4	N42E	47SW	222		47	4	N42W	11NW	318		11	4	N35W	6SW
5	N62E	15SW	242		15	5	N40W	4NW	320		4	5	N46W	3SE
6	N74W	14NW	286		14	6	N84W	28NW	276		28	6	N68W	13SE
7	N83W	26NW	277		26	7	N70W	20NW	290		20	7	N72W	16SE
8	N87E	18SW	267		18	8	N76W	15NW	284		15	8	N62W	11SE
9	N72E	20SW	252		20	9	N72W	27NW	288		27	9	N28W	26NW
10	N66W	0N	296		0	10	N42E	14SW	222		14	10	N30W	9NW
11	N79E	15SW	259		15	11	N78W	19NW	282		19	11	N56W	16SE
12	N84W	24NW	276		24	12	N72W	6NW	288		6	12	N78W	6SE
13	N5E	40NE	5		40	13	N68W	20NW	292		20	13	N43W	5SE
14	N89E	14W	269		14	14	N46W	5SE	134		5	14	N58W	12SE
15	N83W	5SE	97		5	15	N60W	26NW	300		26	15	N19E	6NE
16	N66W	11NW	294		11	16	N48W	11NW	312		11	16	N40E	12NE
17	N66W	11NW	294		11	17	N81W	27NW	279		27	17	N28W	2SE
18	N57E	23NW	237		23	18	N80W	27NW	280		27	18	N78W	13SE
19	N78W	65NW	282		65	19	N81W	27NW	279		27	19	N19E	24NE
20	N87E	11SW	267		11	20	N76W	37NW	284		37	20	N7E	30NE
21	N82E	26SW	262		26	21	N51W	16NW	309		16	21	N30W	12NW
22	N27E	57SW	207		57	22	N78W	9NW	282		9	22	N83W	20SE
23	N83W	11NW	277		11	23	N75W	9SE	105		9	23	N78W	14SE
24	N11W	24NE	169		24	24	N66W	12NW	294		12	24	N34W	2SE
25	N33W	2NW	327		2	25	N82E	13SW	262		13	25	N70W	4SE
		Mean	246.84		21.68			Mean	276.24		17.12			Mean

10					11				
Count #	Quad.Tr.	Quad. Pl.	Azim. Tr.	Plunge	Count #	Quad.Tr.	Quad. Pl.	Azim. Tr.	Plunge
1	N82E	52NE	82	52	1	N58W	12NW	302	12
2	N60E	48NE	60	48	2	N56W	5NW	304	5
3	N32E	40NE	32	40	3	N36W	12NW	334	12
4	N19E	42NE	19	42	4	N76W	37NW	284	37
5	N53E	22NE	53	22	5	N32W	9NW	328	9
6	N37E	29NE	37	29	6	N6W	14NW	354	14
7	N56W	35NW	304	35	7	N23E	15SW	203	15
8	N51E	51NE	51	51	8	N26W	ONW	334	0
9	N15E	19NE	15	19	9	N27W	10NW	333	10
10	N58E	46NE	58	46	10	N20E	9SW	200	9
11	N62E	33NE	62	33	11	N17E	14NE	17	14
12	N57E	31NE	57	31	12	N26W	19NW	334	19
13	N28W	34NW	332	34	13	N21E	22SW	201	22
14	N18W	16NW	342	16	14	N30E	8SW	210	8
15	N41E	28NE	41	28	15	N78W	9NW	282	9
16	N43W	53SE	137	53	16	N68W	24NW	292	24
17	N35E	32NE	35	32	17	N2E	7NE	2	7
18	N82E	11NE	82	11	18	N63W	16NW	297	16
19	N52E	8NE	52	8	19	N63W	20NW	297	20
20	N37E	57NE	37	57	20	N72E	19SW	252	19
21	N54E	26NE	54	26	21	N30W	2NW	330	2
22	N81E	24NE	81	24	22	N53W	5NW	307	5
23	N82E	11NE	82	11	23	N4E	7NE	4	7
24	N89W	7E	91	7	24	N52E	215W	232	215
25	N56W	19NW	304	19	25	N60W	22NW	300	22
	Mean		100	30.96		Mean		253.32	21.28